BROADLINE ^{1}H AND ^{2}H NUCLEAR MAGNETIC RESONANCE STUDIES OF BINARY LIPID MIXTURES CONTAINING DOCOSAHEXAENOIC ACID.

James Lloyd-Smith

B. Sc. Hons. (Physics & Chemistry) Queen's University, 1996

A THESIS SUBMITTED IN PARTIAL FULFILLMENT OF

THE REQUIREMENTS FOR THE DEGREE OF

MASTER OF SCIENCE

in

THE FACULTY OF GRADUATE STUDIES

DEPARTMENT OF PHYSICS & ASTRONOMY

We accept this thesis as conforming

to the required standard

THE UNIVERSITY OF BRITISH COLUMBIA

August 1999

In presenting this thesis in partial fulfilment of the requirements for an advanced degree at the University of British Columbia, I agree that the Library shall make it freely available for reference and study. I further agree that permission for extensive copying of this thesis for scholarly purposes may be granted by the head of my department or by his or her representatives. It is understood that copying or publication of this thesis for financial gain shall not be allowed without my written permission.

Department of Physics & Astronomy
The University of British Columbia
1956 Main Mall
Vancouver, Canada

Date: AUGUST 11, 1999

Abstract

Containing six double bonds, docosahexaenoic acid (DHA) is the most highly unsaturated acyl chain commonly found in biological membranes. It is present in large proportions in retinal and synaptic membranes and there is substantial evidence that specific DHA concentrations are required for proper function of some membrane proteins. A prevalent hypothesis attributes this functional influence to the supposed wedge shape of polyunsaturated lipid molecules, suggesting that lipids with DHA chains influence conformational changes of membrane proteins by exerting pressure laterally through the centre of the bilayer.

This model was tested using broadline ^{1}H- and ^{2}H-NMR techniques to study a series of binary lipid mixtures. The membrane systems were mixtures of monounsaturated 1-palmitoyl-d_{31}-2-oleoyl-phosphatidylcholine (POPC-d_{31}) and polyunsaturated 1-palmitoyl-d_0-2-docosahexaenoyl-phosphatidylcholine (PDPC-d_0) in varying proportions (from 0 mol% PDPC to 100 mol% PDPC), and were designed to be representative of membranes found in the brain. The deuterated POPC acted as a reporter molecule in ^{2}H-NMR experiments, giving a clear picture of the effects of increasing DHA content on the surrounding lipid matrix. The ^{1}H-NMR signal included contributions from both lipid species, and yielded information regarding general properties of the membrane. Spectroscopic measurements were made and analyzed in terms of orientational order parameters of the lipid acyl chains, and relaxation experiments yielded further information on membrane dynamics at a range of timescales. All experiments were conducted at 10^o C, 25^o C, and 37^o C.

The order parameter measurements showed remarkably little change across the full range of membrane compositions. As PDPC content increased, the residual second moment (which is proportional to a mean-squared orientational order parameter) of the proton spectrum increased slightly, while that of the deuterium line showed a small decrease. We infer that the average chain length and order of PDPC molecules is similar to that of POPC-d_{31}, and possibly that species-enriched microdomains may have formed which isolated POPC from the effects of increasing polyunsaturation. The ^{2}H-NMR order parameter profiles demonstrated clearly that the addition of PDPC influenced the conformational freedom of POPC-d_{31}'s perdeuterated chain. A slight decrease in orientational order was observed in the lower half of this chain, indicating greater mobility in that region. This is the first direct measurement of the effect of DHA-bearing lipids on the the chain order of other, less unsaturated lipids in the membrane, and is *not* consistent with the prediction of the "wedge model" that lateral pressure increases in the centre of the bilayer. To explain this observation, it is suggested that the DHA chains spend slightly more time doubled back towards the lipid-water interface, vacating space deep in the bilayer which is occupied by other acyl chains.

T_{1z} values for both ^{1}H- and ^{2}H-NMR were found to rise significantly as PDPC was added to the membrane. Since T_{1z} also increased with temperature, this is deduced to result from a decrease in the correlation times of very fast motions. A likely example, which is consistent with the above model for DHA's motions, would be speeding up of the *trans-gauche* isomerizations of the acyl chains. Finally, T_2^{qe} values for POPC-d_{31}'s perdeuterated chain were found to decrease markedly as PDPC was added, dropping by almost a factor of two between the 0% and 75% PDPC samples. T_2^{qe} relaxation processes are determined to arise from thermally-activated collective motions of the bilayer, and the primary mechanism is proposed to be membrane surface undulations. If the twofold change in T_2^{qe} resulted entirely from increased amplitude of these fluctuations, then the

membrane curvature energy κ_c has been reduced by almost 50% by the addition of 75 mol% PDPC to the POPC-d_{31} membrane; the real effect is expected to be somewhat smaller, since other processes doubtless contributed to the observed change.

The relation of the order parameter measurements to the proposed decrease in curvature energy is considered, and the implications of these results for DHA's role in membrane function are discussed. While significant effects can be postulated for increased flexibility or altered chain packing, no explanation has emerged for the extreme specificity with which nature chooses DHA for certain important systems.

Table of Contents

List of Tables

List of Figures

Abbreviations

K_a Membrane Area Compressibility Modulus.

κ_c Membrane Curvature Energy.

CPMG Carr-Purcell-Meiboom-Gill.

CXP Bruker Spectrometer Model Number.

DHA Docosahexaenoic Acid.

DPPC Di-Palmitoyl-Phosphatidylcholine.

EFA Essential Fatty Acid.

FID Free Induction Decay.

FRAP Fluorescence Recovery After Photobleaching.

LTD Long Term Depression.

LTP Long Term Potentiation.

MAS-NOESY Magic Angle Spinning-Nuclear Overhauser Effect Spectroscopy.

MII Metarhodopsin-II.

MI Metarhodopsin-I.

MLV Multi-Lamellar Vesicle.

NMDA N-Methyl-D-Aspartate.

NMR Nuclear Magnetic Resonance.

PC Phosphatidylcholine.

PDPC 1-Palmitoyl-2-Docosahexaenoyl-Phosphatidylcholine.

PE Phosphatidylethanolamine.

PKC Protein Kinase C.

POPC 1-Palmitoyl-2-Arachadonoyl-Phosphatidylcholine.

POPC 1-Palmitoyl-2-Oleoyl-Phosphatidylcholine.

PS Phosphatidylserine.

PUFA Polyunsaturated Fatty Acid.

ROS Rod Outer Segment.

SNR Signal-to-Noise Ratio.

sn-1, sn-2 Binding sites for acyl chains on glycerol backbone.

sn-3 Binding site for headgroup on glycerol backbone.

Acknowledgement

I have much to be grateful for as this project winds up, many friends both old and new to thank. They have given freely of laughter and friendship, knowledge and new ideas, and they have made my time at UBC enriching and joyful.

I would like to thank Dr. Myer Bloom, my supervisor, for the many lessons of science and of life which he has taught by his example. It has been a privilege to learn about the philosophies and the culture of research from such a master of the trade. Equally deep thanks are due to Dr. Frank Linseisen, whose broad knowledge and great generosity – with time and with the hard-won fruits of experience – have supported me through the setbacks and triumphs of the past few years. I am also grateful to Dr. Jenifer Thewalt for her advice throughout the project and her formal participation at the end, as well as for the wonderful social influence she has exerted on our lab.

I thank everyone in Room 100 for the happy hours, days, and years; such a convivial and stimulating workplace will be hard to replace. I thank my friends in Vancouver for enhancing my world with soccer, red wine and other fine things (and for their on-going efforts with swimming and olives), and for nourishing my body and soul. I thank Yulia, who from far away has helped me through good times and bad by knowing me as no one else does. Finally I thank my family, for their unwavering faith in me and for their trust and full support through the tough decisions of recent times.

I would also like to acknowledge financial support from the Natural Science and Engineering Research Council of Canada.

Chapter 1

Introduction

1.1 Biological Membranes

The lipid bilayer is a fundamental element of eukaryote biology, serving to enclose and compartmentalize the contents of the cell. As depicted in Figure 1.1, biological membranes are a heterogeneous mixture of lipids, proteins and carbohydrates, held together by non-covalent forces. The bilayer structure is a continuous double layer of amphiphilic lipid molecules, with "integral membrane proteins" embedded through it and "membrane-associated proteins" (including elements of the cytoskeleton) and carbohydrates (including the glycocalyx) associated with its surface. The thickness of the bilayer is typically 40-50 Å.

Biological membranes are highly dynamic, fluid structures, characterized by a broad range of molecular motions, rapid lateral diffusion of protein and lipid constituents, and the absence of shear forces between the monolayers. This fluidity is thought to be essential to various functions of the membrane, allowing conformational changes of membrane proteins and selective permeation of water-soluble molecules.

1.1.1 Lipids

Lipid molecules typically constitute roughly 50% of eukaryotic membranes, by weight. They are divided into three main classes – phospholipids, sterols (particularly cholesterol) and glycolipids. Phospholipids are the most abundant element, and comprise the matrix

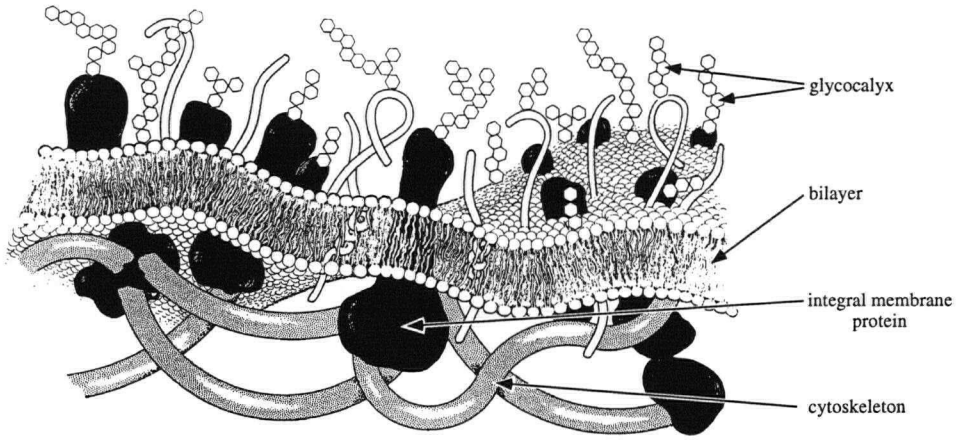

Figure 1.1: Schematic diagram of a biological membrane, showing the phospholipid bilayer "matrix", as well as integral membrane proteins, associated carbohydrates such as the glycocalyx, and connections to the cytoskeleton. Figure borrowed from [1].

of the bilayer.

The structure of a phospholipid molecule is shown schematically in Figure 1.2. A hydrophilic headgroup is connected to two hydrophobic acyl chains by the glycerol backbone; the resulting amphiphilic character of the molecule provides the driving force for assembly into bilayers (or other phases) in aqueous environments, due to the so-called "hydrophobic effect". As shown, the acyl chains are labelled *sn-1* and *sn-2* – these are actually the names of their binding sites on the glycerol backbone, and the headgroup occupies the *sn-3* site.

Different species of phospholipid are defined by their headgroup and acyl chain composition. Acyl chains are fatty acid molecules, and are defined by their chain length, degree of unsaturation, and position of the first double bond. (These three parameters are summarized by a common notation, *e.g.* the 18:1*n-9* chain has 18 carbon atoms and 1 double bond, with the first double bond beginning on the ninth carbon from the methyl end[1]. Acyl chains with no double bonds are termed "saturated", those with one double

[1]This notation is extended in several ways throughout this thesis. "Perdeuterated" chains, on which the hydrogen atoms have been replaced by deuterons, are denoted like 16:0-d_{31} (for a 16:0 chain with

bond are "mono-unsaturated", etc. "Polyunsaturated" acyl chains (*i.e.* those with three or more double bonds) are the major focus of this thesis – particularly docosahexaenoic acid (DHA, or 22:6*n-3*), which with 6 double bonds in its 22-carbon length is the most highly unsaturated chain commonly used by nature .

1.2 Biological Motivation to Study DHA

(Section 1.2 has been modified from a section of an earlier paper [1], written by JL-S.)

1.2.1 Membrane Lipid Composition and Polyunsaturation

The conventional view of lipid bilayers in the cell has been that they serve simply as physical and electrical barriers (both to the external environment and between internal compartments), and as inert substrates upon which membrane proteins carry out their functions. While these roles are clearly very important, there has been a growing appreciation in recent years that lipids have more subtle and wide-ranging functions (*e.g.* [2]). These may be due to properties of the bilayer alone, such as permeability to water or ions, or to interactions with the proteins associated with the membrane, such as matching of hydrophobic thickness as mentioned earlier. For different biological systems, these properties are determined (and presumably optimized, as discussed in [3]) by characteristic lipid compositions, encompassing variation in phospholipid head groups and acyl chains as well as in proportions of other lipids.

The human brain has made a striking choice in favour of polyunsaturated lipids (*i.e.* phospholipids with polyunsaturated acyl chains), and particularly of lipids containing

all 31 protons replaced). Also, the chain notation will be compounded to describe the composition of phospholipid molecules – *e.g.* 16:0/18:1-PC indicates 1-palmitoyl-2-oleoyl-phosphatidylcholine, a lipid with a phosphatidylcholine (PC) headgroup, a palmitoyl chain (16:0) at the *sn-1* site, and an oleoyl chain (18:1) at *sn-2*.

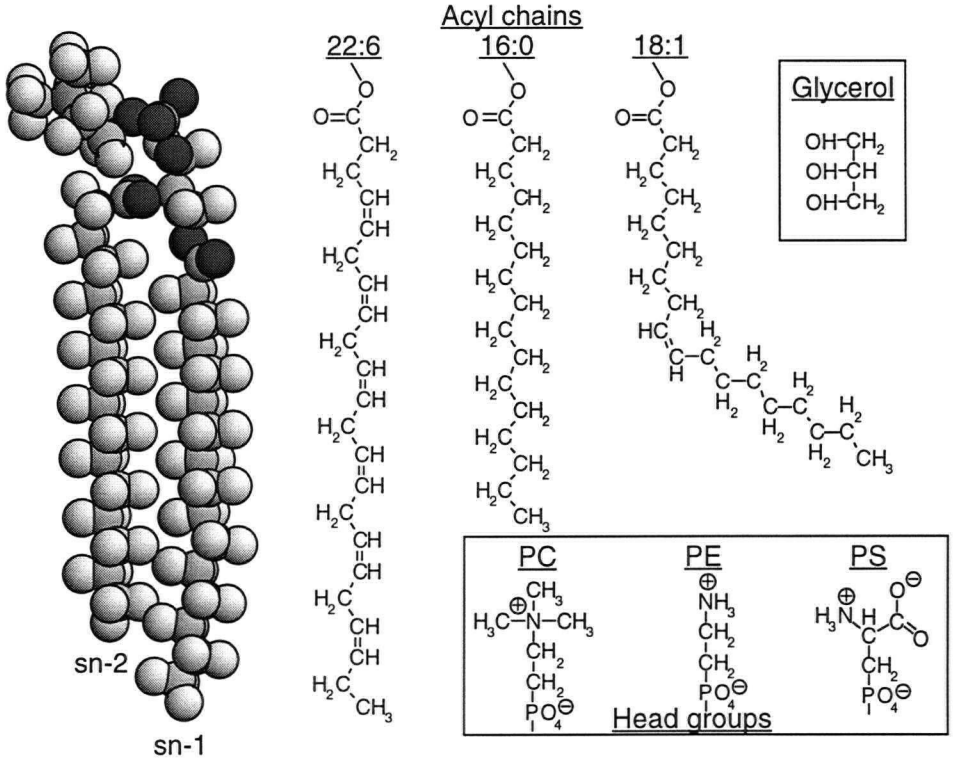

Figure 1.2: A space-filling diagram of a phospholipid molecule is shown on the left, depicting the hydrophilic headgroup (top) and two hydrophobic acyl chains (bottom) connected by the glycerol backbone. The acyl chains used in this study are shown, representing three important classes: the polyunsaturated docosahexaenoyl chain, or DHA (22:6), is on the left; the mono-unsaturated oleoyl chain (18:1) is on the right; in the middle is a saturated palmitoyl chain (16:0). Each of these chains can bind to the glycerol backbone (shown, top right) at the *sn-1* or *sn-2* site, as described in the text. The three most common phospholipid headgroups are shown in the bottom right box – they are phosphatidylcholine (PC), which is used in the experiments described in this thesis, phosphatidylethanolamine (PE), and phosphatidylserine (PS). Figure borrowed from [1].

DHA – so much that it is often called "cervonic acid". While DHA levels in most membranes range from 1-6 mol%, values of about 15 mol%, and as high as 25-35 mol% for certain head groups, are reported in brain grey matter and synaptic membranes [4, 5]. More remarkable still are the outer segment disk membranes of the rod photoreceptor cells of the retina, with DHA comprising roughly 50 mol% of the total fatty acid complement [6]. These exquisitely specialized neurons (see Figure 1.3), which convert photons into electrical signals, thus have among the most highly unsaturated membranes of all vertebrate systems.

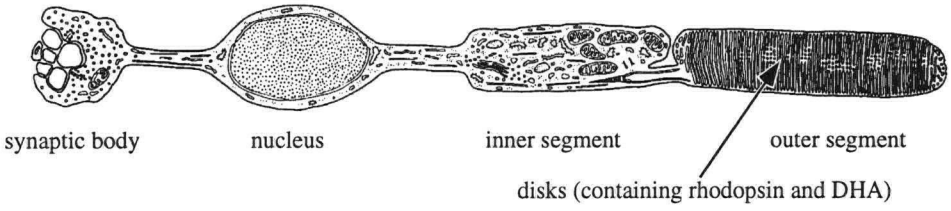

Figure 1.3: Schematic representation of a retinal rod cell (taken from Alberts *et al.* [7]). The stacked membranous disks of the rod outer segment (ROS) contain 50 mol% DHA and are densely packed with rhodopsin molecules.

Maintaining polyunsaturated membranes, however, presents two serious challenges to mammalian cells. First, mammals lack the enzymes required to synthesize DHA (22:6*n-3*) or arachadonic acid (20:4*n-6*) from scratch, and therefore must obtain the associated essential fatty acid (EFA) precursors (18:3*n-3* and 18:2*n-6*, respectively) from their diet, and convert them by a series of elongation and desaturation reactions [8]. Not only does this render the supply of polyunsaturated fatty acids (PUFAs) dependent on the supply of dietary precursors (and hence on environmental factors), but the conversion process is indirect and time-consuming. In fact, in very fast-growing animals (such as cattle), these enzymatic reactions are unable to keep up with bodily growth, resulting in decreased DHA levels and increased content of metabolic intermediates such as 22:5*n-3* [9]. Second, polyunsaturated lipids are extremely vulnerable to oxidation, and large

quantities of anti-oxidant agents (such as vitamin E) must be present to protect them [10]. DHA is the most highly unsaturated of all fatty acids commonly used by nature and is particularly unstable, degrading almost ten times faster than 18:3*n-3* [11].

In short, polyunsaturated lipids are very difficult for the human body to produce and to maintain, and their prevalence in such vital systems as the brain and the eye poses a fascinating evolutionary puzzle. Nor can this be explained as a "fluke" occurrence - Nature's enigmatic choice of high DHA levels for neural membranes is conserved across an extremely broad range of species (including mammals, fish, reptiles and even the photosynthetic "eye-spots" of unicellular dinoflagellates), in stark contrast to the wide inter-species variability in lipid make-up of other tissues [12]. What advantage does this lipid bring which would have caused evolution to select it despite the substantial problems involved in doing so? What function could it possibly have, which could not be fulfilled by some more convenient alternative?

1.2.2 Evidence for a Functional Role of DHA

A strong argument can be made that DHA plays a functional role in the visual system, and evidence is mounting that it is important for higher brain function as well. Due to the direct link between proper nutrition and adequate supply of PUFAs, any such correlations between lipid polyunsaturation and neural function have very significant social implications. A great effort is underway by many groups to elucidate this relationship, and a parallel line of inquiry is examining issues related to dietary supplementation.

An indirect argument for the importance of PUFAs arises from the remarkable lengths to which neural cells will go to maintain their membrane polyunsaturation. The extraordinarily high DHA content in the rod outer segment (ROS) disks is retained tenaciously during dietary deficiencies of its EFA precursor (18:3*n-3*), and radiographic studies have revealed an elaborate recycling mechanism which minimizes its loss [13]. Membranes of

the brain similarly resist loss of DHA, but under conditions of extreme EFA deficiency substantial decreases have been observed. Such changes are often accompanied by increases in concentration of 22:5*n-6*, the closest structural match to DHA outside the *n-3* family [14, 15].

Dietary EFA depletion during pregnancy and infancy, while the brain and nervous system are undergoing rapid development, has been shown to lead to decreased DHA levels and to impaired visual function in rats [16], rhesus monkeys [17] and human premature infants [18]. The latter studies have led to pre-formed DHA being declared provisionally essential for human infants, presumably due to the heavy needs of the developing nervous system; very high levels of DHA are also found in human placental blood and breast milk, and faced with dietary deficiency the mother's body will sacrifice its own needs to ensure that the baby receives an adequate supply of PUFAs [12]. Similar studies have concluded that *n-3* deficiency leads to reduced learning ability and psychomotor development in animals and human infants [16, 19]. One relatively recent, very lucid review of the field emphasizes the need for caution in drawing conclusions linking EFA deficiency to intellectual or cognitive deficits [20], but sufficient evidence has arisen in subsequent years to firmly establish that learning is affected (at least in rats) [15, 21, 22, 23]. Such effects of *n-3* deficiency have even been associated with morphological changes in synapses; intriguingly, these changes are observed only in animals which have been challenged with learning tests [15, 21].

A different source of evidence for the link between PUFAs and neural function comes from a number of congenital diseases in which abnormal membrane composition is associated with visual or mental impairment. For example, retinitis pigmentosa, an eye disease leading to night blindness and visual field constriction, is correlated with low DHA levels in the retina [18]. Zellweger syndrome, a disorder of the peroxisomes (cellular centres of lipid metabolism, involved in synthesis of DHA), is characterized by extremely low levels

of DHA [24]. Infants suffering from this disease are born with severe psychomotor retardation, become blind and deaf shortly after birth, and usually die within their first year. Preliminary results indicate that DHA supplementation can lead to clear improvements in the normal development and clinical outcome of afflicted patients [25, 26]. Finally, a recent study of the brains of individuals with Alzheimer's disease has identified significantly decreased levels of DHA in the phosphatidylethanolamine (PE) phospholipids; such changes were not observed in the brains of normally aging patients [27].

These observations have motivated many experiments into how polyunsaturation affects the physical properties of membranes, and particularly into the role of DHA in the retina. The photoreceptor has been the favoured experimental paradigm since the visual system is much more tractable (less complex, more accessible to experiment, and much more easily quantified) than the brain and its higher functions. Furthermore, the studies on vision have been greatly aided by the enormous strides taken by the biochemistry community during the 1980s, which have led to a near-quantitative understanding of the molecular basis of photoreceptor activity [7, 28]. This has allowed experiments to be devised which focus on the specific molecular processes where DHA may exert its influence.

1.2.3 Possible Roles for DHA at the Molecular Level

Phototransduction, the process of translating a visual stimulus into an electrical signal, takes place in the outer segments of rod and cone photoreceptor cells in the retina. Most experimentation has dealt with the highly sensitive, monochromatic rod cells, whose outer segments contain stacks of membranous disks, as shown in Figure 1.3. These ROS disk membranes, the site of high DHA content in the rods, in turn are densely packed with the integral membrane protein rhodopsin. Rhodopsin initiates the light response by absorbing a photon and undergoing a series of rapid conformational changes.

After passing through a number of unstable intermediate states within microseconds, rhodopsin is transformed into metarhodopsin-I (MI). The next reaction is an acid-base equilibrium, in which MI can be protonated to become metarhodopsin-II (MII). MII is the enzymatically active form of rhodopsin, and catalyzes the G-protein transducin to trigger a cascade of biochemical reactions which results in the closure of ion channels in the rod plasma membrane, and subsequent hyperpolarization of the cell. Significant formation of MII is clearly critical to the transmission of the visual signal, and modulation of the MI/MII equilibrium (which of course takes place embedded in the disk membrane) seems a plausible way for membrane composition to exert its functional influence. Indeed, MII formation has been shown to be diminished considerably in model membranes with lower-than-physiological levels of DHA [6]; these experiments and others which address possible mechanisms for this effect will be discussed in Section 1.3.

Though the retina is an extension of the brain and thus photoreceptors are in fact highly specialized central neurons, it is unclear whether such specific experiments have any relevance to the high DHA content observed in the synapses and grey matter of the brain. It is a distinct possibility, however, that DHA's putative interactions with rhodopsin could be generalized to the large family of G-protein linked receptors (of which rhodopsin is a member), all of which share very similar structure particularly in their transmembrane domains [7]. This could certainly extend DHA's role throughout the nervous system, since G-proteins are involved in many signal transduction pathways in the brain, and quite possibly beyond into other systems of the body.

Recent studies have also revealed a host of other membrane proteins upon which DHA exerts specific functional influences. Na^+-K^+-ATPase, an ion pump critical to maintaining the ionic concentration gradients which subserve all of neuronal signalling, suffers reductions in activity of up to 45% in the absence of physiological DHA levels [4]. Several voltage-gated ion channels have been shown to be blocked by free DHA in solution

(*i.e.* the fatty acid form; physiologically, DHA can be freed from the membrane by the actions of several common enzymes) [29, 30], and activation of acetylcholine pathways has been demonstrated to selectively increase uptake of DHA by the membrane, suggesting "a primary role for DHA in phospholipid mediated signal transduction" at cholinergic synapses [31]. Even more intriguing, DHA levels in the membrane affect activity of protein kinase C (PKC) [32], and free DHA increases the channel-open probability for the NMDA-type glutamate receptor [33]. These molecules (PKC and NMDA receptors) are thought to be critical factors underlying the phenomena of long term potentiation (LTP) and long term depression (LTD), which are leading topics of investigation into the molecular basis of learning and memory. Indeed, a very recent study has demonstrated a direct relationship between DHA levels in solution and the suppression of LTD [34]; together with the above results, this could be interpreted as the first concrete indication of a molecular site of action for DHA's effects on cognitive function. Taken together, the above results (most of which date only from the last few years) suggest a role for DHA in brain function which is significant and wide-ranging. It seems reasonable to expect this rapid growth of knowledge to continue, resulting in a much fuller appreciation of the influences of this extraordinary lipid on the brain.

1.3 Physical Properties of Polyunsaturated Lipids

The desire to understand the role of DHA in membrane function has drawn researchers from many fields, and the pace of investigation (and progress) has increased greatly in recent years. Much of this effort has focused on the "non-specific" physical and mechanical properties (as opposed to "specific" chemical interactions, some of which are described above) imparted by DHA to lipid membranes. A summary of relevant results in this field is presented here; for further details, there are two recent, comprehensive reviews of the

subject [1, 35].

1.3.1 Early Work – Molecular Shape and Spontaneous Curvature

The work of Brown on DHA's interaction with rhodopsin [6] highlights several key points. Using optical spectroscopy to measure the success of rhodopsin's crucial MI-MII transition as a function of membrane composition, he confirmed the importance of polyunsaturated lipids for MII formation. Testing other lipid species, he found that those with bulky acyl chains and small headgroups could also produce the favourable effect. From these observations, Brown concludes (i) that a bulk property of the membrane must underlie the effect, rather than a DHA-specific chemical interaction, and (ii) that this property is "negative spontaneous curvature", the tendency of a lipid monolayer to curve in a concave manner at the lipid-water interface. A model of the interaction with rhodopsin is suggested, in which this curvature stabilizes a purported increase in hydrophobic thickness as MI changes to MII[2].

The role of DHA-bearing lipids in rhodopsin function is thus proposed to arise from their molecular "shape", which is related to the range of conformations assumed by the acyl chains. At the time of Brown's studies, preliminary work had indicated that polyunsaturated chains might be unexpectedly flexible. Applegate & Glomset performed the first computer-modelling of static DHA chain conformations [37, 38, 39]. In addition to defining certain zero-energy states, their work indicated that the C-C single bonds in DHA were remarkably free to rotate – the energy barriers to bond rotation were much lower than those of a saturated chain. Early NMR work by Baenziger *et al.* complemented

[2]A recent theoretical study has explored the possibility of such coupling between protein conformational changes and resultant membrane deformations [36]. Contributions due to hydrophobic mismatch, "splay-deformation" of the membrane protein (*e.g.* changing from cylindrical to conical, and thus affecting the orientation of neighbouring lipid molecules), and surface tension are modelled explicitly, and the former two mechanisms are predicted to be capable of exerting significant influences on conformational equilibria (and hence on function).

this result, using site-specific deuteration on a di-unsaturated lipid (16:0/18:2-PC) to reveal surprisingly low orientational order for the carbon between the two double bonds [40, 41]. These results challenged the intuitive view that DHA's many double bonds would render the chain rigid.

1.3.2 Later Work – Molecular Order and Lateral Organization

The first definitive work on the influence of polyunsaturation on membrane orientational order was conducted by Holte *et al.* [42], in the Gawrisch laboratory. They used deuterium NMR to study a series of one-component membranes, consisting of PC phospholipids with a perdeuterated stearoyl chain at the *sn-1* site, and a series of progressively more unsaturated chains at *sn-2* (*i.e.* 18:0-d_{35}/*X*-PC, where *X* is 18:1*n-9*, 18:2*n-6*, 18:3*n-3*, 20:4*n-6*, 20:5*n-3*, or 22:6*n-3* (DHA)). From smoothed order parameter profiles, which give a measure of local orientational order for each carbon on a perdeuterated lipid chain, they found that polyunsaturation causes decreased order in the lower half of the saturated chain (*i.e.* the end nearer to the middle of the bilayer). The largest changes were seen between the lipids with 1, 2 and 3 double bonds – little difference was found in going from 3 to 6 unsaturations.

This localized disorder is consistent with the 18:0-d_{35} chain becoming more "wedge-shaped" with increasing *sn-2* unsaturation. In subsequent discussions, though, the entire polyunsaturated lipid molecule is depicted as a wedge, and the authors speculate about its possible interactions with membrane proteins (see Figure 1.4) [42, 43]. This is strongly reminiscent of Brown's hypothesis of negative spontaneous curvature, caused by acyl chains bulkier than their headgroups – indeed Holte *et al.* refer to the "curvature stress" experienced by such membranes when confined to the lamellar state. It must be emphasized, however, that Holte's measurements were sensitive only to the order of the deuterated 18:0 chain, and that great caution must be exercised in extending them to

the molecule as a whole.

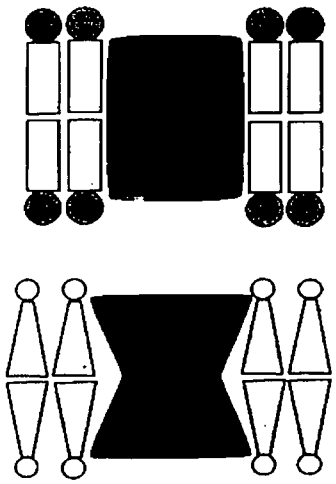

Figure 1.4: Lipids with polyunsaturated chains are shown to occupy wedge-shaped volumes in the bilayer in this figure taken from the literature [43]. Relative to neatly-packing saturated chains *(above)*, lipid molecules with small headgroups and polyunsaturated chains *(below)* are proposed to accommodate certain protein transitions because of their wedge-like shape.

The Gawrisch group has continued to make substantial contributions. Combining deuterium NMR and X-ray diffraction techniques, they determined that lipids bearing DHA chains have much greater lateral compressibilities than saturates or monounsaturates; the same study revealed significantly higher cross-sectional areas for the polyunsaturated membranes [44]. The compressibility was proposed to facilitate conformational changes involving lateral expansion of transmembrane proteins, while the greater area is again consistent with the wedge-shaped hypothesis.

Another recent study, which combined ^{1}H- (MAS-NOESY) and ^{2}H-NMR techniques, showed that cholesterol interacts preferentially with saturated chains in mixed-chain lipids [45]. Polyunsaturation (as well as headgroup composition) was suggested to affect lateral organization of lipid molecules, perhaps leading to the formation of transient "microdomains" in the presence of cholesterol. This conclusion is foreshadowed in the

work of Mitchell & Litman, who used fluorescence depolarization methods to examine the effects of "free volume" (ensemble-averaged voids in lipid packing) on the MI-MII equilibrium (reviewed in [46, 35]). They proposed that polyunsaturated lipids form dynamic lateral clusters which exclude cholesterol and hence mitigate its inhibitory effect on MII formation – further experiments have indicated that di-DHA-PC is especially effective at buffering cholesterol's influence in this way [47]. Smaby *et al.* report results consistent with this model, and hypothesize that the *cis*-unsaturated "kinks" of the polyunsaturated chains interfere with favourable van der Waals interactions between the chains and the smooth ring structure of cholesterol [48].

1.3.3 The Wedge Model and the Lateral Pressure Profile

Proposed explanations for the role of DHA in membrane function are cast in terms of decreased acyl chain order and disrupted lipid packing. (Even hypotheses like domain formation have their bases in these experimentally accessible parameters.) Encouraged by Brown's findings and the order parameter profiles of Holte *et al.*, a model arose in which polyunsaturated lipid molecules occupy wedge-shaped volumes which cause the monolayers to want to curve (in a concave manner) about their headgroups. When confined to a lamellar bilayer (due to the hydrophobic effect which dominates lipid-water interactions), such lipids would lead to packing irregularities near the lipid-water interface and crowding in the hydrophobic interior of the membrane. This "curvature stress" could influence protein conformational changes, essentially by exerting pressure laterally through the lipid bilayer.

A fascinating theoretical study examining this "lateral pressure profile" as a function of lipid composition has just been published by Cantor [49]. Using mean-field statistical thermodynamics[3], the author finds that highly unsaturated chains such as DHA shift

[3]The configurational entropy of the acyl chains is calculated using a mean-field approximation of

lateral pressure *away* from the bilayer interior – exactly contrary to what the wedge model would predict. The model shows an increase in pressure near the lipid-water interface, which is offset by decreased crowding in the interior such that the membrane thickness (also calculated) is minimally affected. (Note that the calculations impose a constant density condition on the hydrophobic region, such that free volume cannot exist. In the worst case, this could seriously skew the results by eliminating a key contribution to the real physical effect.) Cantor concludes that the functional role of polyunsaturated lipids in membranes is to redistribute lateral pressures – thus influencing membrane protein conformation, as argued in an earlier work [50] – while maintaining constant thickness to facilitate hydrophobic matching. These results, which appear only as this report is being written, provide a welcome new perspective on the DHA question.

1.4 Motivation and Summary of Experiments

The basis for DHA's observed influences on membrane function is not yet understood. As described above, a prevalent hypothesis suggests that polyunsaturated lipids occupy wedge-shaped spaces in the membrane, affecting protein conformation via lateral pressure through the bilayer. Such a shape has never been directly demonstrated, however. ^{2}H-NMR measurements on mixed-chain lipids (*e.g.* 18:0-d_{35}/22:6-PC) have indicated that the *saturated* chain occupies a wedge-shaped cloud of conformations, but the relation of this result to the shape of the DHA chain, or that of the entire lipid molecule, is ambiguous.

Furthermore the majority of experiments have been conducted in single-component model bilayers, very dissimilar to the complex mixtures of lipid (and protein) species

excluded volume which accounts for bond orientational correlations. The bilayer free energy is estimated, and the negative of its derivative with area determines the lateral pressure; the pressure profile is derived from values of this derivative at different layers in the cubic lattice used for the calculations.

invariably found in physiological membranes. It is conceivable that exceptional properties of polyunsaturated lipids might be expressed through their interaction with other membrane constituents; clearly the single-species experiments would not be sensitive to such effects.

This study addresses the above issues by examining the effects of increasing acyl chain polyunsaturation in binary lipid mixtures. The phospholipid species used were monounsaturated 1-palmitoyl-d_{31}-2-oleoyl-phosphatidylcholine (POPC-d_{31}, or 16:0-d_{31}/18:1-PC) and polyunsaturated 1-palmitoyl-d_0-2-docosahexaenoyl-phosphatidylcholine (PDPC-d_0 or 16:0/22:6-PC), in proportions ranging from 0 to 100 mol% PDPC. These molecules, shown in Figure 1.2, were chosen to crudely approximate the lipid composition of neural membranes [51], where DHA exerts its functional role[4]. Varying the concentrations allows for the possibility of anomalous behaviour arising from particular molar ratios of the lipid species.

The POPC-d_{31}/PDPC mixtures were studied using broadline ^{1}H- and ^{2}H-NMR techniques. Since only POPC has a deuterated portion, all ^{2}H-NMR results report directly and exclusively on POPC's 16:0-d_{31} chain. The deuterium signal thus provides an unambiguous report of the effect of increasing PDPC concentration (*i.e.* of greater polyunsaturation) on other membrane components, and will directly test for the lateral pressure predicted by the wedge model. Meanwhile, ^{1}H-NMR lends an independent and complementary assessment of conditions in the rest of the membrane.

In addition to standard spectroscopic measurements, which yield information on orientational order and fast motions of the lipid molecules, relaxation measurements were performed to learn more about lipid dynamics. T_1 experiments provide further insight

[4]Phosphatidylcholine (PC) headgroups were selected for consistency with earlier work in the field. Polyunsaturated chains are often associated with phosphatidylethanolamine (PE) headgroups in physiological membranes, and it would be of great interest to conduct a parallel series of experiments using PE lipids.

into very fast molecular motions, while T_2 can describe slower, collective modes of the membrane. Since in-depth relaxation studies have not yet been reported for polyunsaturated membranes, these experiments are a foray into relatively uncharted territory. All measurements were conducted at 10^o C, 25^o C, and 37^o C.

This thesis addresses the following questions:

1. What mechanical effects do polyunsaturated lipids (and particularly those bearing DHA chains) have on other bilayer components?

2. Does a bilayer with acyl chain composition closer to that found in neural membranes have special properties? Is there a concentration-dependent "magic mixture" effect?

3. Can new insights be gained into the role of DHA in membranes by probing unexplored timescales (and hence distance scales)?

1.5 Overview of Thesis

The thesis is organized largely in a conventional manner. In Chapter 2, the NMR theory relevant to the experiments and their interpretation is summarized. A significant part of this summary (included as Appendix A) was borrowed from the proceedings of the 1998 Fermi School of Physics [1]. Chapter 3 outlines the details of experimental techniques and analysis. The results are presented in Chapter 4, with accompanying discussion; the chapter concludes with suggested extensions of the study, and the relevance of the findings to the biological question is assessed. Chapter 5 is a brief concluding statement.

Appendix A is the background theory described above. Certain preliminary NMR experiments are described in Appendix B. Appendix C includes tabulated numerical results, as well as several figures not presented in Chapter 4.

Chapter 2

NMR Theory

2.1 Broad-line NMR Spectroscopy of Lipid Membranes

The reader is referred to Appendix A for a general overview of broadline NMR spectroscopy of lipid membranes. Written by Professor Myer Bloom, it is an excerpt from a paper entitled "Insights from NMR on the functional role of polyunsaturated lipids in the brain", from the proceedings of the 1998 Fermi School of Physics [1]. Throughout the text results will be cited freely from this summary, with comments added as required. The following two sections extend discussions from the appendix on topics of particular relevance to this study.

2.1.1 Ranges of Correlation Times

In Section A.2, the complex spectrum of correlation times associated with various motions in a fluid bilayer is discussed, and examples are given of motions at a few ranges of τ_c. Section A.3 goes on to classify these motions as "slow" or "fast", depending on their relation to the spectroscopic time scale τ_s, where $\tau_s \approx 1/\Delta\omega$. The definition of $\Delta\omega$ will vary with circumstance, but a working definition is $\Delta\omega = (M_2)^{-\frac{1}{2}}$, where M_2 is the second moment (or residual second moment) appropriate for the question being considered. Within this classification, "fast" motions give rise to narrower spectral features by motional averaging, while "slow" motions do not appreciably affect the lineshape.

It is useful to introduce a further discrimination between ranges of correlation times,

relevant to T_1 and T_2 relaxation processes. Motions for which $\omega_o\tau_c \gg 1$ (including the "slow" and a subset of the "fast" motions defined above) will be denoted "adiabatic", using the word in the sense described by Abragam [52]. The remaining "non-adiabatic" motions, for which $\omega_o\tau_c \ll 1$, will be labelled "very fast". Timescales of interest will thus be divided into three regimes: slow adiabatic, fast adiabatic, and very fast non-adiabatic, as shown in Figure 2.1. The NMR parameters affected by motions in the three ranges are also shown, as well as representative motions present in fluid bilayers.

2.1.2 Moments of NMR Spectra

The study of spectral moments is of considerable importance in broadline NMR. At their simplest, moments provide a quantitative measure of the "shape" of an NMR absorption line, which proves useful for study of complex or featureless spectra (like the deuterium and proton spectra derived from lipid samples; see Figures 3.3 and A.1). In certain instances spectral moments can be related rigorously to theory, which allows their value to be related to real physical parameters.

The n^{th} moment of a lineshape function $f(\omega)$ can be defined as

$$M_n = \frac{\int_{-\infty}^{+\infty} |\omega - \omega_o|^n f(\omega) d\omega}{\int_{-\infty}^{+\infty} f(\omega) d\omega} \tag{2.1}$$

where ω_o is the Larmor frequency. The second moment, when $n = 2$, gives the mean-squared frequency splitting $\langle(\Delta\omega)^2\rangle$ and is of particular interest in NMR studies. While the true value of the second moment (M_2) never changes, the presence of fast motions with correlation times $\tau_c \ll (M_2)^{-\frac{1}{2}}$ will cause narrowing of the absorption line as described above. The experimentally-measured second moment is then less than M_2, and is termed the *residual* second moment M_{2r}.

Since it is related to fast molecular motions, the reduction in M_2 can be interpreted

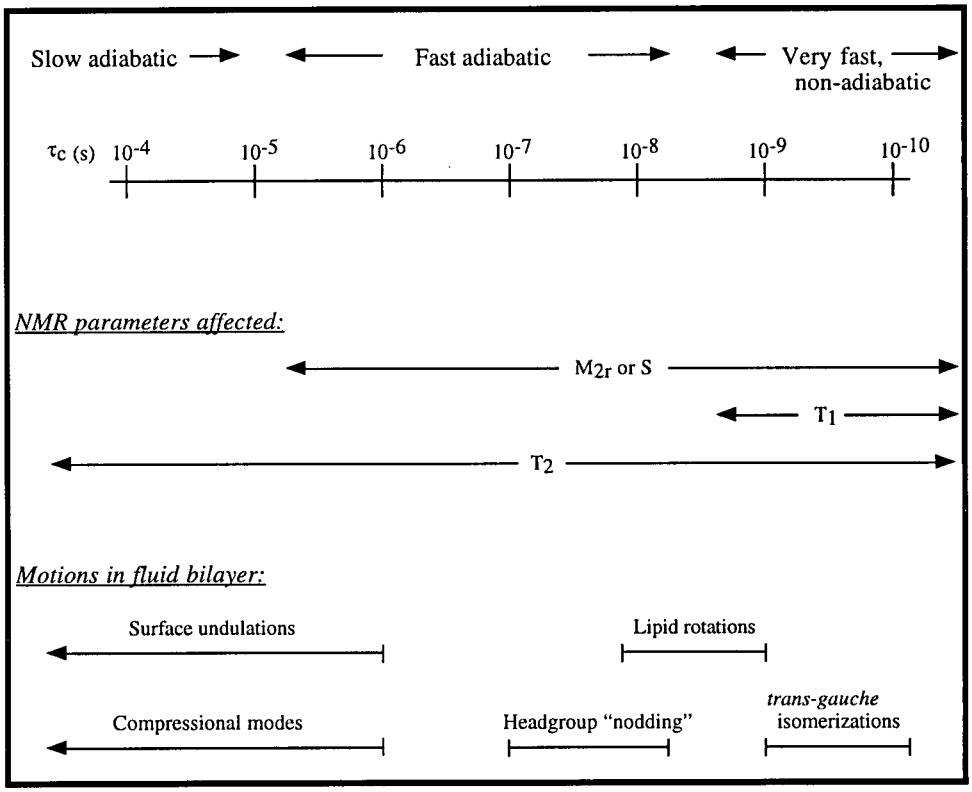

Figure 2.1: Summary of important timescales in NMR experiments, showing the three regimes of motion as defined in the text. Note that the precise boundaries will be determined by the field strength (influencing $1/\omega_o$ and thus the limit of "adiabatic" times) and the spectroscopic timescale (τ_s, assumed here to be roughly 10^{-5} s, which defines the boundary of the motional narrowing regime as discussed in Section A.3). Beneath the bar showing τ_c values, selected NMR parameters are shown along with the range of timescales to which they are sensitive. At the bottom, representative motions present in fluid bilayers are shown, along with estimated ranges of their correlation times [1, 53, 54].

in terms of "order parameters". These unitless parameters, denoted S, describe the orientational order of a molecular system. Ideally they take on a value from 0 to 1, where $S = 0$ indicates total isotropic disorder and $S = 1$ indicates absolute orientational order.

The Proton Second Moment and Pseudo-Order Parameter

The well-known Van Vleck formula gives the dipolar second moment for a rigid lattice of identical nuclei (with spin I and gyromagnetic ratio γ) [52],

$$M_2 = \frac{3}{4}\gamma^4\hbar^2 I(I+1)\sum_B \frac{(1-3\cos^2\theta_{AB})^2}{R_{AB}^6} \tag{2.2}$$

where R_{AB} is the distance between dipolar coupled spins A and B and θ_{AB} is the angle between $\vec{R}_{AB}$ and the external magnetic field, $\vec{B}_o$. In systems of protons, the dipolar interaction dominates and Equation 2.2 applies in principle.

For lipid molecules in fluid membranes, this value is reduced by several factors, including lateral diffusion of the lipids, rapid rotation of the molecules about the bilayer normal, and a random "powder" distribution of orientations of the normal. The resulting relation between M_2 and M_{2r} is discussed in depth by Bloom *et al.* [55, 56], who obtain

$$M_{2r} = M_2\left\langle|S_{AB}|^2\right\rangle = \frac{1}{N}\sum_{A=1}^{N}\sum_{B\neq A} M_2^{A,B}S_{AB}^2 \tag{2.3}$$

where $M_2^{A,B}$ is the contribution of spins A and B to the second moment, and $S_{AB} = \langle P_2(\cos\theta_{AB})/r_{AB}^3\rangle$ is the proton dipolar pseudo-order parameter, as mentioned in Section A.6. The prefix "pseudo-" is used because $|S_{AB}|$ depends on the length of the vector joining the interacting spins as well as its orientation.

If the ground-state geometry of the molecule is known, M_2 can be calculated from Equation 2.2. Experimental measurement of M_{2r} then allows determination of $\left\langle|S_{AB}|^2\right\rangle$. If M_2 is not known, changes in M_{2r} can still provide a relative measure of order. In either

case, caution must be exercised in interpreting the results due to the possible influence of the inter-proton distance on $|S_{AB}|$.

The Moment Expansion of the Free Induction Decay

In broadline ^{1}H-NMR experiments, the beginning of the FID is usually lost during the recovery time of the receiver (unlike ^{2}H-NMR, it is not simple to refocus the proton signal). In order to Fourier transform the data this lost signal must be extrapolated, making it difficult to reliably determine M_{2r} in the frequency domain.

Under certain circumstances (the FID is properly phased and collected on-resonance), it is possible to obtain the residual M_2 (and other moments) directly from the real part of the FID, $F(t)$, by means of the "moment expansion". By Taylor expanding $F(t)$ and applying the definitions of the Fourier transform and of spectral moments, one obtains:

$$F(t) = \sum_{n=0}^{\infty} \frac{(-1)^n}{(2n)!} M_{2n} t^{2n}. \tag{2.4}$$

By truncating this expression and performing a polynomial fit in t^2, the residual values of M_{2n} can be obtained experimentally (as discussed in Section 3.3.1).

The Deuterium Second Moment

The order parameter $|S_{CD}|$ derived from ^{2}H-NMR measurements is discussed at length in Appendix A. Its interpretation is less complex than in the dipolar case, for two reasons: (i) it is a pure orientational order parameter, depending only on the orientation of the C-D bond in space, and (ii) the discrete nature of the quadrupolar splitting allows direct measurement of $|S_{CD}|$ from an oriented (or de-Paked) spectrum.

Since $|S_{CD}|$ is the factor by which the quadrupolar splitting is reduced by motion (see Section A.4), the residual second moment is proportional to its mean-squared value. For

a powder pattern of perdeuterated lipids in the fluid membrane, one obtains [57]:

$$M_{2r} = \frac{1}{5}\left(\frac{3}{4}\frac{e^2qQ}{h}\right)^2 \left\langle S_{CD}^2 \right\rangle \tag{2.5}$$

where e^2qQ/h is the quadrupolar coupling constant for a methylene C-D group. (Note that this expression neglects the much smaller contribution from dipolar interactions.) The deuterium M_{2r} is a useful index of molecular order in its own right, or in comparison with the proton M_{2r} in partially deuterated systems.

2.2 Relaxation

"Spin-lattice" (T_1) and "spin-spin" (T_2) relaxation studies are very important tools for investigating the dynamic properties of spin systems. NMR relaxation in membranes has been studied in considerable depth [58, 59, 60, 61, 62, 63, 64], and has contributed greatly to our understanding of the wide spectrum of motions present in this complex system.

Experiments described in this thesis deal exclusively with T_{1z}, the relaxation time of the Zeeman polarization, and T_2^{qe}, the transverse relaxation time of a spin 1 system as measured by a two-pulse quadrupolar echo sequence. (Experimental details are described in Sections 3.2.2 and 3.2.3.) Comments below pertain to these parameters only, though many of the principles extend to other relaxation times. For ease of reading the notations T_1 and T_2 will be used throughout, except in a few statements where greater precision is required.

T_1 relaxation describes the return of an excited system to thermal equilibrium, as the spins re-align with the external magnetic field. T_2 relaxation is concerned with the loss of phase coherence of the transverse components of the nuclear magnetization. The general theory of spin relaxation [52] describes how these processes arise from fluctuations in NMR interactions. The fluctuations are due to various motions present in the system,

and are characterized by their correlation times, τ_c. Describing the motions in terms of their "reduced spectral densities", $j(\omega)$, the following expressions (valid for fluctuations with $\tau_c \ll \tau_s$) are obtained:

$$\frac{1}{T_1} = C_1 \left[a_1 \, j(\omega_o) + a_2 \, j(2\omega_o) \right] \tag{2.6}$$

$$\frac{1}{T_2} = C_2 \left[b_0 \, j(0) + b_1 \, j(\omega_o) + b_2 \, j(2\omega_o) \right] \tag{2.7}$$

where C_1 and C_2 are coupling constants for the interaction in question and a_i, b_i are proportional to the mean-squared amplitude of the fluctuations at the appropriate frequencies. ω_o is the Larmor frequency for the particular nucleus and field strength.

It is evident from Equation 2.6 that T_1 processes are sensitive to fluctuations at $\omega = \omega_o$ and $\omega = 2\omega_o$; this is because T_1 relaxation involves exchange of one or two quanta of Zeeman energy between the spin system and the lattice[1]. Spin-spin relaxation requires no such exchange, so the T_2 rate receives contributions from a zero-frequency spectral density $j(0)$ as well as $j(\omega_o)$ and $j(2\omega_o)$.

This additional term in $1/T_2$ has profound consequences: not only is $T_2 \leq T_1$ always satisfied, but also $T_2 \ll T_1$ in the presence of slower "adiabatic" motions. The difference in sensitivity of T_1 and T_2 to motions with different τ_c greatly expands the power of relaxation techniques to study dynamics. Systematic variation of parameters like field strength (and hence ω_o) and temperature or pressure (and hence τ_c) allows the "spectrum" of correlation times to be studied through a great range of amplitudes. Studies of this nature have been the source of much of our current knowledge regarding molecular motions in membranes.

[1]The surroundings of the spins are collectively called "the lattice", and are assumed to be an infinite heat bath.

2.2.1 Effects of Temperature on T_1 and T_2

Raising the temperature of the sample can affect the spin system in several ways. The first, of particular interest for T_1 relaxation, is that correlation times can shorten as molecular motions become more rapid [52, 65]. The second, important for T_2 processes dominated by adiabatic motions, is that thermally-activated modes can increase in amplitude [63, 66]. Obviously a third class of effect would be observed if the system were to undergo a phase transition, but this is outside the current discussion.

To understand the effects of these changes on relaxation times, it is useful to give functional form to the equations shown above. In the case of truly random fluctuations, τ_c will be the time constant of an exponentially decaying correlation function. The spectral density (related by a Fourier transform) will then take on a Lorentzian lineshape, $j(\omega) = \frac{\tau_c}{1+\omega^2\tau_c^2}$. It is important to note that the area under the spectral density curve is fixed for all τ_c, and that the amplitude of $j(\omega)$ is roughly constant for $\omega < 1/\tau_c$, beyond which it drops rapidly towards zero (see Figure 2.2a).

Decreasing τ_c (as when temperature is raised) thus causes the spectral density to become broader and flatter. The value of $j(\omega)$ at a specific ω (say ω_o) will rise and then fall as the shoulder of the lineshape (at $\omega \sim 1/\tau_c$) passes through that frequency. Correspondingly, as motions accelerate and τ_c decreases, we see from Equation 2.6 that the value of $1/T_1$ will first increase (while $1/\tau_c < \omega_o$) then decrease (when $1/\tau_c > \omega_o$). The plot of T_1 versus $1/\tau_c$ thus features two roughly linear portions and a minimum at $\tau_c \sim 1/\omega_o$, as shown in Figure 2.2b.

While these effects apply equally to the $j(\omega_o)$ and $j(2\omega_o)$ terms of the $1/T_2$ expression, in the presence of adiabatic motions these terms are swamped out by $j(0)$. In membrane NMR, relaxation in the T_2^{qe} experiment is caused primarily by "thermally driven fluctuations in the quadrupolar splittings" [67]. These fluctuations, the causes of which are

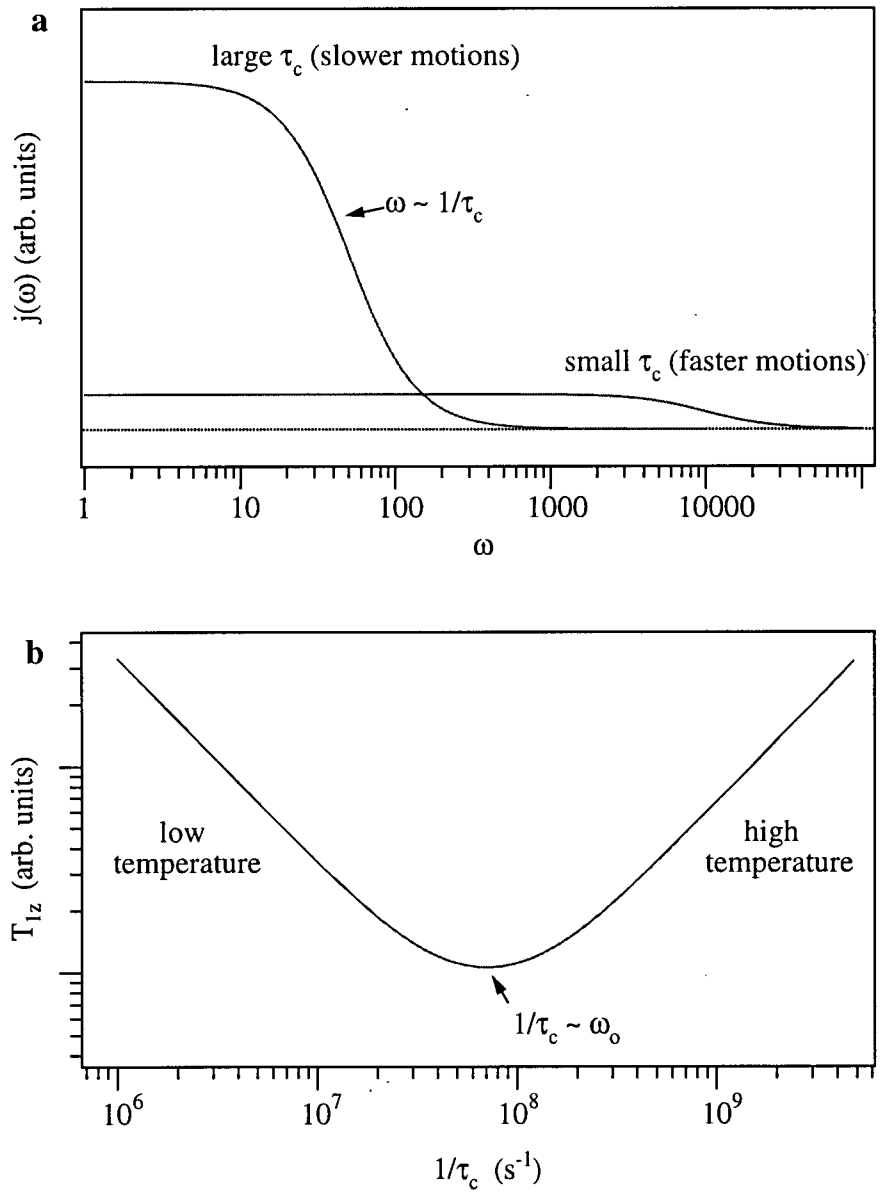

Figure 2.2: **(a)** The reduced spectral density, $j(\omega)$, corresponding to different values of τ_c. As described in the text, $|j(\omega)|$ is roughly constant for $\omega < 1/\tau_c$, then rapidly approaches zero; since it is normalized, this causes the maximum value of $|j(\omega)|$ to vary greatly as a function of τ_c. **(b)** The plot of T_{1z} as a function of $1/\tau_c$ (or equivalently of temperature) goes through a minimum near $1/\tau_c \sim \omega_o$.

discussed in the following section, have mean-squared amplitudes (b_0 in Equation 2.7) proportional to k_BT, such that raising the temperature leads to increases in the T_2 rate. A direct linear relationship is not assured due to possible temperature-dependence of material properties which also influence the amplitudes.

Of course, temperature can also affect the correlation times of these adiabatic modes and motions. If $\langle(\delta\omega)^2\rangle$ represents the contribution to the second moment from the fluctuating interaction responsible for relaxation, then $\tau_s = \langle(\delta\omega)^2\rangle^{-1/2}$ is the relevant spectroscopic timescale. (A reasonable estimate of τ_s in fluid bilayers with perdeuterated chains is 10^{-5}s [61].) For fast adiabatic motions (*i.e.* $1/\omega_o \ll \tau_c \ll \tau_s$) which give rise to uncorrelated fluctuations, Equation 2.7 yields the classic result:

$$\frac{1}{T_2^{qe}} = \left\langle(\delta\omega)^2\right\rangle \tau_c \tag{2.8}$$

In the limit of slow motions (*i.e.* $\tau_c \gg \tau_s$), the dependence of T_2^{qe} on τ_c is inverted [60]:

$$T_2^{qe} \propto \tau_c \tag{2.9}$$

As for T_1, the variation of T_2^{qe} with τ_c thus has a minimum in the neighbourhood of τ_s. Note however that this theory describes only a single contribution to transverse relaxation. In a system as complex as a perdeuterated membrane there will be many contributing processes, perhaps with a spectrum of τ_c's corresponding to each. If this τ_c spectrum is shifted significantly by temperature, then it may be expected that changes in T_2^{qe} due to motions on either side of the minimum will partially cancel out. It is also possible that the τ_c's will not shift, however, since for certain important mechanisms the range of τ_c is limited by physical constraints which do not vary significantly with temperature (*e.g.* surface undulations, discussed below).

The temperature-dependence of T_2^{qe} in membranes is thus difficult to predict *a priori* – the observed behaviour will be a complex superposition of effects, many of which are

not yet fully understood. Increases in the fluctuation amplitudes, however, will invariably make the relaxation processes more effective. If correlation time effects are assumed to balance out or to be negligible, then raising the temperature can be expected to decrease T_2^{qe}.

2.2.2 Orientation Dependence of T_2

The following is a brief summary of the dependence of deuterium T_2 relaxation rates on θ, the angle between the membrane surface normal and the external magnetic field. For details the reader is referred to the "phenomenological theory" by Bloom [68, 69].

From Section A.4 we learn that the quadrupolar splitting for a deuteron on an acyl chain is given by $\omega = \omega_Q P_2(\cos\theta) S_{CD}$. Since ω_Q is a constant, the adiabatic fluctuations which dominate T_2 relaxation in membranes can arise from motions which modulate either θ or S_{CD}. We assume these parameters to be independent, and define the motions by *effective* correlation times τ_θ and τ_a, respectively[2]. Changes in θ could arise from undulations of the membrane surface, while variation in S_{CD} corresponds via Equation A.3 to fluctuations in membrane thickness, or equivalently (assuming the bilayer to be an incompressible fluid) in membrane surface area a.

The mean-squared fluctuations $\langle(\delta\theta)^2\rangle$ and $\langle(\delta a)^2\rangle$ can be related to measurable material properties of membranes by thermodynamic considerations. Under appropriate conditions, the "curvature energy" κ_c [66] and the "isothermal area compressibility" $1/K_a$ [67] govern the two types of fluctuations, as follows:

$$\left\langle(\delta\theta)^2\right\rangle = \frac{k_B T}{4\pi\kappa_c} \ln\frac{\lambda_M}{\lambda_m} \tag{2.10}$$

$$\left\langle(\delta a)^2\right\rangle = \frac{k_B T}{K_a} \tag{2.11}$$

[2]Approaches to determination of these correlation times, a difficult problem not addressed here, are discussed in the literature [66, 63].

where λ_M and λ_m are the maximum and minimum wavelengths for membrane undulations. (Note that these limits on λ, which are based on geometrical considerations and are not expected to vary with temperature, define the range of correlation times τ_θ of undulational modes [66].) Another mechanism for fluctuations in θ could be diffusion of molecules on the curved surface of the vesicle, but this is discussed elsewhere and judged not to be a dominant effect in T_2^{qe} of membranes [63].

Assuming that the relevant correlation times satisfy $\tau_i \ll \langle(\delta\omega)^2\rangle^{-1/2}$, Equation 2.8 is used to assess the contributions of these fluctuations to T_2 relaxation. The T_2 rate due to adiabatic motions is:

$$\begin{aligned}\left(\frac{1}{T_2}\right)^{ad} &= \sum_i \left\langle(\delta\omega_i)^2\right\rangle \tau_i \\ &= \left(\frac{\delta\omega}{\delta\theta}\right)_a^2 \left\langle(\delta\theta)^2\right\rangle \tau_\theta + \left(\frac{\delta\omega}{\delta a}\right)_\theta^2 \left\langle(\delta a)^2\right\rangle \tau_a \\ &= B\sin^2\theta\cos^2\theta + C\left[P_2(\cos\theta)\right]^2 \end{aligned} \tag{2.12}$$

where the coefficients B and C are determined from Equations 2.10 and 2.11, the expression for the quadrupolar splitting, and estimates or models of the effective τ_i. When a constant term is added for the nearly isotropic contribution of fast motions, an orientation-dependence of the following form is expected:

$$\left(\frac{1}{T_2}\right) = A + B\sin^2\theta\cos^2\theta + C\left[P_2(\cos\theta)\right]^2 \tag{2.13}$$

This model may be tested by plotting experimentally-determined values of T_2 as a function of frequency for a Pake doublet spectrum, which represents a map of doublets for different local bilayer orientations θ.

Chapter 3

Experimental Methods

3.1 Sample Preparation

The perdeuterated lipid, 1-palmitoyl-2-oleoyl-phosphatidylcholine with deuterons substituted at all sites on the palmitoyl chain (POPC-d_{31}, or 16:0-d_{31}/18:1-PC), was purchased from Avanti Polar Lipids (Alabaster, AL). Protonated POPC-d_0 was obtained from Northern Lipids (Vancouver, BC). 1-palmitoyl-2-docosahexaenoyl-phosphatidylcholine (PDPC, or 16:0/22:6-PC) was purchased from Sigma (St. Louis, MO), as were the D_2O (<0.04 atom% ^1H) and phosphate buffer mixture (KH_2PO_4/K_2HPO_4 with added NaCl). Deuterium-depleted H_2O (<0.05 atom% ^2H) was supplied by Isotec (Miamisburg, OH).

Five samples were prepared, with molar concentrations of PDPC of 0%, 25%, 50%, 75% and 100%, as shown in Table 3.1. To attain constant signal-to-noise in the ^2H-NMR measurements, 40 mg of POPC-d_{31} were used in each sample and PDPC amounts were adjusted accordingly (except in the 75% PDPC sample, for reasons of expense). While the total amount of lipid thus varies between samples, in all cases the concentration is well within the dilute limit. (Phospholipids are fully hydrated for water concentrations greater than $\sim$ 40 wt% [70].) Throughout this thesis, samples will be referred to by their molar percentage of PDPC (*e.g.* "25% PDPC" refers to the sample which is 25% PDPC and 75% POPC-d_{31}; "0% PDPC" refers to the sample which is pure POPC-d_{31}).

For each lipid species, a stock solution was prepared in methylene chloride (CH_2Cl_2) and stored under argon at -20° C. Buffer solutions were prepared using deuterium-depleted

Table 3.1: Lipid composition of NMR samples.

Sample	Amount PDPC	Amount POPC-d_{31}
0% PDPC	0 mg	40 mg
25% PDPC	13 mg	40 mg
50% PDPC	40 mg	40 mg
75% PDPC	60 mg	20 mg
100% PDPC	40 mg	0 mg

water (or D_2O for some preparatory experiments), and adjusted to pH 7.4. These solutions contained 10 mM phosphate buffer (KH_2PO_4/K_2HPO_4) and 140 mM NaCl. To eliminate dissolved oxygen, buffers were degassed by bubbling argon through them for 15 minutes.

For each sample, stock solutions were mixed in appropriate proportions, the solvent was evaporated, and the samples were placed under vacuum overnight. The lipids were hydrated with an excess of deuterium-depleted buffer solution (500 μL) and vortexed for five minutes to create multilamellar vesicles (MLVs). The resulting dispersions were transferred into teflon sample tubes, and sealed under argon. All manipulations were carried out under a stream of argon, and shielded from light whenever possible; NMR measurements were conducted under a constant flow of dry nitrogen cooling gas, as described in Section 3.2.4.

A recent study by Drobnies *et al.* [71] examines the effects of lipid oxidation on membrane order, as measured using ^{2}H-NMR on MLVs composed of PAPC-d_{31} (16:0-d_{31}/20:4-PC). It is shown that 10% lipid oxidation produces drastic effects on the deuterium powder pattern, in which all sharp features of the spectrum are "blurred out", presumably by the presence of a range of slightly altered lipid species. Such blurring was not observed in any of the spectra collected in the present study, which instead were qualitatively similar to the results shown for 3% oxidation. We thus conclude tentatively that significant sample degradation has not occurred.

3.2 NMR Techniques

All NMR measurements were carried out using a Bruker CXP spectrometer with heteronuclear broadband capability, at a Larmor frequency of 200 MHz for protons and 30.7 MHz for deuterium. Proton and deuterium protocols, described in Sections 3.2.2 and 3.2.3, were implemented for each sample at temperatures of 10^o C, 25^o C and 37^o C.

3.2.1 Preparatory NMR Experiments

To minimize the risk of oxidative damage to the polyunsaturated lipids, it was desirable for all experiments on a given sample to be completed in as short a period as possible. It was thus necessary to limit the duration of the NMR experiments, and imperative that the experimental protocol be finalized before the first samples were prepared. (Samples frozen and later rethawed for further experiments would likely undergo chemical or physical changes. Certain NMR parameters, especially T_2^{qe}, are highly sensitive to such variations in sample handling and thermal history [69].) Many preliminary experiments were performed to address these challenges – experimental parameters were optimized to balance data quality with experiment duration, and possible systematic errors were examined and eliminated. This work is described in Appendix B.

3.2.2 ^{1}H-NMR Protocol

The ^{1}H-NMR experiments were conducted at 200 MHz. The duration of a 90^o pulse was 3 μs, and the recovery time for the receiver was approximately 8 μs. 2048 complex points were collected with a dwell-time of 2 μs, and the receiver filter width was 2 MHz. The repetition time was 2 s.

The proton FID was collected on-resonance to determine spectral moments. A "modified inversion recovery" scheme was used to reduce systematic noise from probe ringdown, in which the inverted signal following a 180^o pulse was subtracted from the signal from a single 90^o pulse. When both methods of water suppression were incorporated (see Appendix B), the basic pulse program was:

$$180_x - \tau_0 - 90_y - t - \tau_2 - 180_x - (\tau_3 - 180_x)_{16} \qquad (+)$$

$$180_x - \tau_0 - 180_x - \tau_1 - 90_y - t - \tau_2 - 180_x - (\tau_3 - 180_x)_{16} \qquad (-)$$

in which the signals collected during t are added and subtracted in computer memory (as indicated by (+) and (-), above) to yield the FID. The first 180^o pulse is the "pre-inversion" pulse for water suppression, and $\tau_0 = 2\,\mathrm{s}$ ($\approx \frac{T_{1z,water}}{\sqrt{2}}$) was selected to minimize the water contribution as described in Appendix B. $\tau_1 = 5\,\mathrm{ms}$ was chosen to satisfy $T_{2,lipid} \ll \tau_1 \ll T_{1z,lipid}$, in order to correct systematic errors without sacrificing signal-to-noise. τ_2 and τ_3 were selected ($200\,\mu\mathrm{s}$ and $400\,\mu\mathrm{s}$, respectively) to obtain a sufficient number of well-formed CPMG echoes to fit accurately. 128 scans were signal-averaged, with 8-CYCLOPS phase-cycling.

T_{1z} data were collected using the same modified inversion recovery sequence, which for relaxation studies has the added advantage of being insensitive to non-idealities in the 180^o pulse and yielding FID amplitudes which decay exponentially. Ten values of τ_1 were used, logarithmically spaced between 1 ms and 1000 ms. 16 scans were averaged for each value of τ_1, with 8-CYCLOPS phase-cycling. As is standard practice, τ values were interleaved in data collection to guard against instrumental drift.

3.2.3 ^{2}H-NMR Protocol

^{2}H-NMR measurements were conducted at 30.7 MHz, with a $4\,\mu\mathrm{s}$ 90^o pulse. The spectrometer was tuned to doped D_2O at 25^o C, and set on-resonance for lipids using the

chemical shift relation $\nu_{lipid} = \nu_{D_2O} - 142\,\text{Hz}$. The signal was detected in quadrature with phase cycling for all sequences, with 300 ms repetition time. 2048 complex points were collected with a dwell-time of $2\,\mu$s, and the receiver filter width was chosen to be 80 kHz.

The deuterium lineshape and quadrupolar echo spin-spin relaxation time, T_2^{qe}, were measured using the quadrupolar echo pulse sequence:

$$90_x - \tau - 90_y - t$$

For lineshape measurements, $\tau = 40\,\mu$s and 10,240 transients were averaged. Ten values of τ were used to measure T_2^{qe}, spaced logarithmically from $38\,\mu$s to $750\,\mu$s.

To measure the Zeeman spin-lattice relaxation time, T_{1z}, the quadrupolar echo sequence was combined with modified inversion recovery:

$$90_x - \tau - 90_y - t \qquad (+)$$

$$180_x - \tau_1 - 90_x - \tau - 90_y - t \qquad (-)$$

where the echoes collected during t were added and subtracted to yield a decaying exponential function of τ_1. τ was kept constant at $40\,\mu$s, while τ_1 was varied over ten logarithmically-spaced values between 1 ms and 150 ms. For both T_2^{qe} and T_{1z} measurements, delay values were interleaved, with 1024 scans collected for each value.

3.2.4 Temperature Control for NMR Experiments

Temperature was regulated using a Bruker BV-T1000 variable temperature unit, controlling an electric heating coil which warmed the nitrogen gas (boiled off from a dewar of liquid nitrogen) that blew constantly through the sample chamber. A copper-constantan (type T) thermocouple served as temperature sensor.

The spectrometer was tuned to each sample at 25° C, then experiments were conducted at 10° C, 25° C and 37° C. At each temperature change, the sample was allowed to equilibrate for 30 minutes after the establishment of the new temperature in the probe. This period was chosen after studying the moments of the deuterium spectrum for a POPC-d_{31} sample as a function of time following changes in temperature.

The temperature control system was calibrated immediately before data collection began; incorporating all sources of uncertainty, sample temperatures were constant and accurate during NMR experiments to within $\pm 0.5°$ C.

3.3 Analysis

3.3.1 Proton Moments

The proton residual second moments, $M_{2r,H}$, were obtained directly from the FID, in a process summarized in Figure 3.1. The proton signal was baseline corrected and a zeroeth order phase correction (a constant phase factor) was applied. The peaks of the CPMG echoes were fitted to a line, which was extrapolated to zero time and subtracted from the whole signal to eliminate the contribution from the water and buffer (see Appendix B).

For the moment expansion of Equation 2.4 to apply, it is necessary for the FID to be properly phased and on-resonance (*i.e.* the corresponding absorption line must be symmetric). The spectrometer was tuned to the signal from the entire sample, which is dominated by water. Subtraction of the slow-relaxing fraction has isolated the lipid signal, but still the FID was collected at the resonant frequency for the water-dominated sample. It is readily shown that an additive offset in the frequency domain corresponds to a linear phase shift in the time domain (*i.e.* $f(\omega + \delta\omega) = \int_{-\infty}^{+\infty} F(t)e^{i(\omega+\delta\omega)t}$), so a first-order phase correction must also be performed (*i.e.* $F(t)$ multiplied by $e^{-i(\delta\omega)t}$). The required frequency offset was determined to be 512 Hz, by taking the difference in

resonance frequencies between two POPC samples in H_2O and D_2O buffer solutions.

After these corrections, the FID was fitted to a truncated form of the moment expansion:

$$F(t) = F(0)\left(1 - \frac{M_{2r,H}t^2}{2!} + \frac{M_{4r,H}t^4}{4!} - \frac{M_{6r,H}t^6}{6!} + \ldots\right). \tag{3.1}$$

This is a polynomial in t^2 and could be solved routinely by a standard package (Igor v3.14; WaveMetrics, Lake Oswego, OR), using a linear matrix-solving algorithm.

A considerable effort was made to understand the effects of the fit parameters (such as the number of terms, the range of the FID which was fitted, and the precise placement of the origin) on the moment values obtained, in order to achieve accurate and stable solutions. A four-term fit was chosen (*i.e.* to order t^6), with the origin set to the centre of the 90^o pulse. The fit-range was chosen to begin 17 μs after the end of the pulse, to ensure that ring-down noise would not influence the result. As the range of data included in the fit was increased, $M_{2r,H}$ was found to vary widely at first, then to settle to a relatively stable value (see Figure 3.2). Balancing this stability against the increasing influence of higher-order terms at higher t, an end-point of 57 μs after the end of the pulse was selected for the final analysis. A representative fit is shown in Figure 3.1.

The uncertainties for the derived $M_{2r,H}$ values were generated by the fitting algorithm, and correspond to the diagonal elements of the covariance matrix for the fit. It should be noted that these errors do not contain information regarding the goodness-of-fit of the moment expansion to the FID, but instead are derived directly from the standard error values provided for the data. (For the parameters described above, the expansion always fitted the data adequately, such that $\chi^2 \leq \nu$ where ν is the number of degrees of freedom [72].) A second estimate of the uncertainty was obtained by analyzing three separate runs of the same sample (0% PDPC), and produced results of similar magnitude.

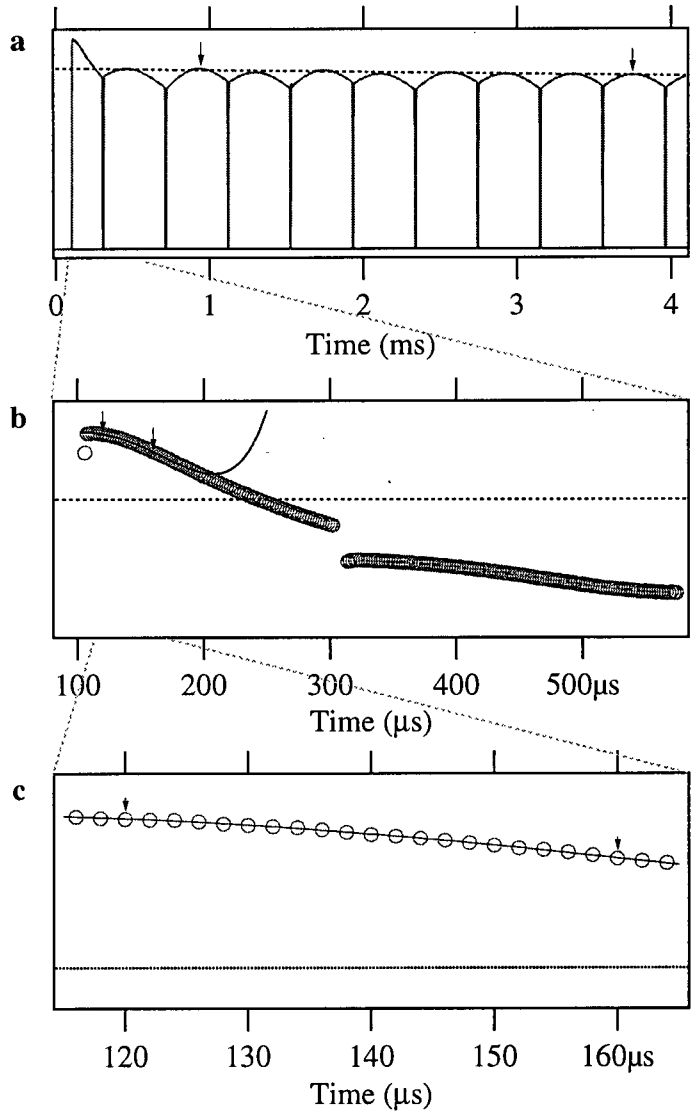

Figure 3.1: Analysis of the proton FID. **(a)** shows the FID as collected using the pulse sequence described in the text. The lipid signal is the small, fast-decaying component at the far left. The linear fit to the CPMG echo peaks is shown as a dotted line; the boundaries of this fit are marked by the arrows. **(b)** shows an expanded view of the lipid signal, after the slow-decaying signal is removed and the phase corrected. The solid curve shows the moment expansion fit-line corresponding to Equation 3.1; the arrows show the range fitted. (Note that the 90^o pulse began at $t = 100\mu$s on the time-scale shown.) **(c)** shows a further blow-up of the fit obtained using the moment expansion – again the fit-range limits are shown by the arrows. The fit-line matches the FID data well throughout the range fitted.

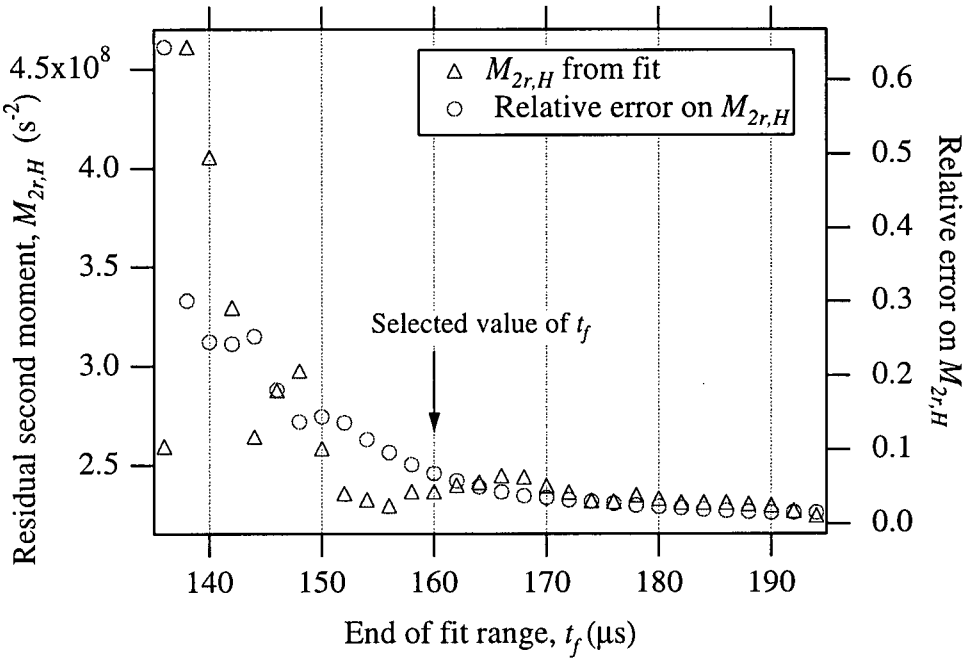

Figure 3.2: The calculated value of $M_{2r,H}$ and the statistical uncertainty derived from the fitting process are shown as a function of the end-point of the fit-range, t_f. (The results shown are for a four-term expansion (*i.e.* to order t^6) with the fit-range beginning at 120 μs. As in Figure 3.1, the excitation pulse began at $t = 100\,\mu$s, and is 3 μs long.) $M_{2r,H}$ varies wildly as the range is increased, then settles to a relatively constant value for $t_f > 150\,\mu$s. The relative error of the $M_{2r,H}$ value (scale shown on right axis) decreases almost monotonically, but as noted in the text it does not account for possible misfitting of the experimental data. $t_f = 160\mu$s was selected as the end-point for analysis which yielded the results presented in Section 4.2.1.

3.3.2 Deuterium Moments

Because the quadrupolar echo refocuses the signal well after the excitation pulses, no information is lost due to the receiver dead-time, and the time signal can be Fourier transformed to produce a complete spectrum. Before transforming, the signal was baseline corrected and phase-shifted so that the real channel had maximum amplitude. The peak of the echo was then symmetrized using a cubic spline fit [72], to avoid possible artifacts in the spectrum [58]. The out-of-phase channel was then zeroed, for a $\sqrt{2}$ gain in signal-to-noise (SNR), and the real signal was left-shifted to the peak of the echo and zero-filled.

The signals were then Fourier transformed, yielding the powder spectra shown in Figure 3.3. The residual second moments were obtained directly by integration, as described by Equation 2.1.

3.3.3 Order Parameter Profiles and Average Chain Length

The deuterium powder pattern spectra were de-Paked to give spectra equivalent to those of oriented samples, as described in Section A.4. The resulting spectra are shown in Figure 3.3. The smoothed order parameter profile, showing the approximate value of $|S_{CD}|$ for each carbon position on the deuterated chain, was obtained using the method of Lafleur *et al.* [73].

Seelig's method of determining the membrane thickness d from the average order parameter $\langle S \rangle$ is described in Section A.5. $\langle S \rangle$ was calculated from the $S(n)$ results, above (with $|S_{CD}|$ values for C1 and C16 derived from linear extrapolation of the neighbouring four and two points, respectively) [73], and the mean length of the perdeuterated chain was calculated using Equation A.3.

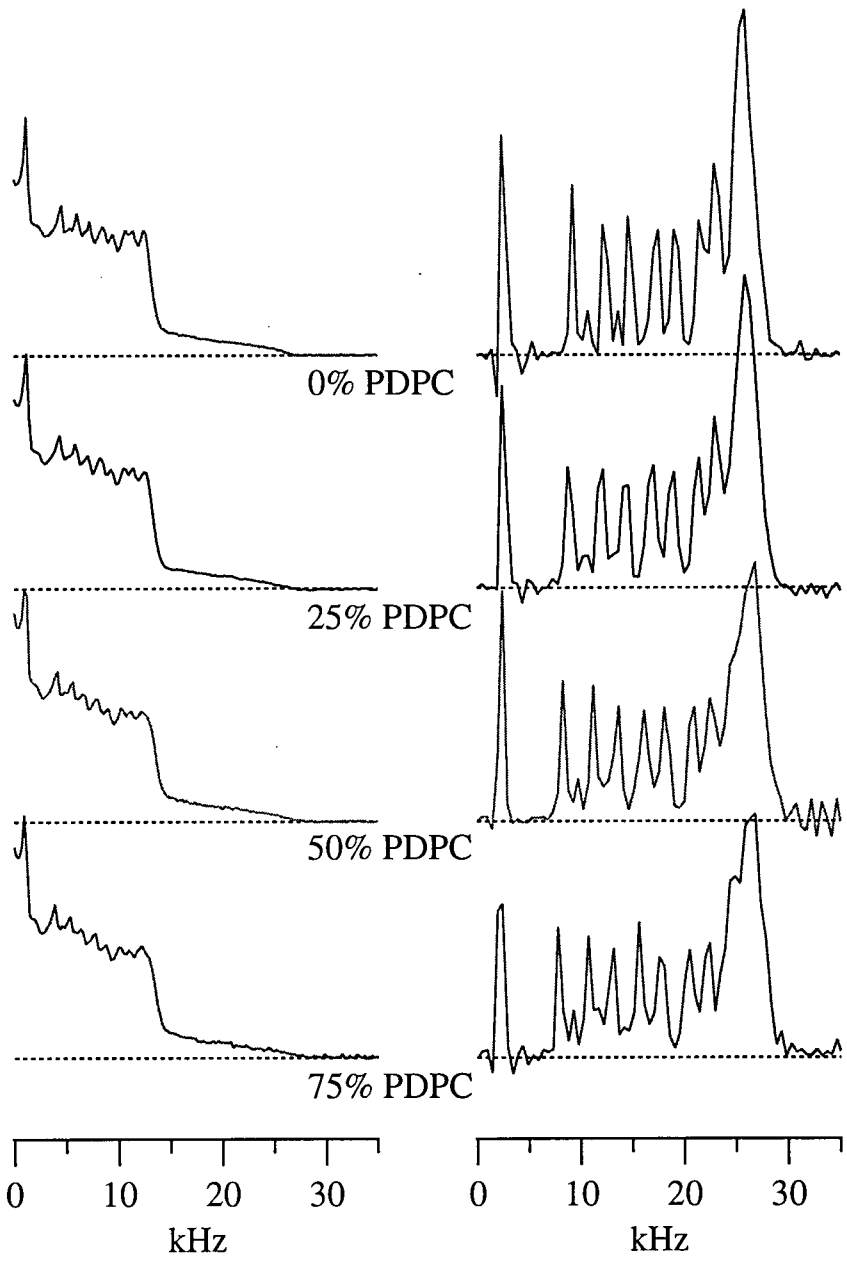

Figure 3.3: Deuterium spectra for the series of POPC-d_{31}/PDPC binary mixtures, collected at 25° C (and halved for display purposes). Powder patterns are shown on the left side; on the right are the de-Paked spectra used to obtain smoothed order parameter profiles.

3.3.4 Relaxation Analysis

Proton T_{1z}

For T_{1z} analysis, the FIDs were baseline- and phase-corrected, and the water signal was subtracted as described in Section 3.3.1. The amplitude of the FID (actually the mean value of 4 points, beginning 6 μs after the maximum to avoid dead-time artifacts) was recorded for each delay time τ_1.

The logarithm of these amplitudes was plotted versus τ_1, yielding a linear relationship for the shorter delay times. A linear fit was applied to the short-τ_1 points, and a T_{1z} value was obtained from its slope. Since the largest τ_1 value used in the fit (50 ms) is small relative to T_{1z}, this result can be shown rigorously to be the weighted average of all proton T_{1z} contributions in the sample (except the slow-relaxing water and buffer protons, of course, whose signal was removed earlier).

Deuterium T_{1z}

To obtain the average T_{1z} times from the deuterium experiments, the amplitude of the (baseline- and phase-corrected) quadrupolar echoes was measured for each delay time. Mean T_{1z} values were obtained from linear fitting of the short-τ data, as described above.

The variation of the relaxation times with chain position was a desirable complement to the order parameter profiles, but the data were too noisy to generate a full "oriented spectrum" of relaxation times by de-Paking the raw data and calculating T_{1z} point-by-point (or peak-by-peak). Instead, a coarser measure was obtained by taking Gaussian-weighted averages over three regions of the de-Paked spectra (shown in Figure 4.7), corresponding roughly to the plateau region (C2-C9), the middle of the chain (C10-C12), and the "tail" of the chain (C13-C15, *not* including the methyl protons). Mean T_{1z} values were calculated for each region, as above.

Note that uncertainties for these regional T_{1z}'s were calculated from the spread of values obtained for three determinations of the 0% PDPC sample, but do not account for certain errors inherent in the analysis. Since the three regions were defined using landmark features of the spectra, relative changes in $|S_{CD}|$ may have caused the peaks corresponding to certain carbon positions on the chain to move into or out of their ranges. This could systematically skew the relaxation results, particularly for the tail region where greater changes in peak position were observed in the $S(n)$ analysis.

Powder-pattern "T_{1z} spectra" were produced for these results as well, using the techniques described below for T_2^{qe}, but no noteworthy results were obtained.

Deuterium T_2^{qe} and Orientation-Dependence

The deuterium T_2^{qe} mean values and regional variation were determined exactly as for deuterium T_{1z}, above. In order to study the complex orientation-dependence of T_2^{qe}, a "T_2^{qe} spectrum" was also generated for each experiment [74]. To do this, the quadrupolar echo for each delay time was processed and Fourier transformed, yielding a series of powder spectra. For each frequency point in the spectra, the amplitudes for all values of τ were collected and a short-τ linear fit was performed. (Since the fitting procedure involves a logarithm, amplitudes which were negative due to random noise could not be processed. In these instances, which occurred only in the far shoulder and baseline of the spectra, the T_2^{qe} value was set to zero.) By plotting the calculated T_2^{qe} values as a function of frequency, a T_2^{qe} powder spectrum could be generated.

As described in Section 2.2.2, the orientation-dependence of deuterium T_2^{qe} in lipid vesicles is predicted by this equation:

$$\left(\frac{1}{T_2}\right) = A + B\sin^2\theta\cos^2\theta + C\left[P_2(\cos\theta)\right]^2 \tag{3.2}$$

Previous work on T_2^{qe} spectrum fitting [68] was restricted to a specifically deuterated

sample (*i.e.* deuterated at only one site, so the spectrum was a single Pake doublet), signal-averaged sufficiently that the entire T_2^{qe} spectrum was well-defined. Equation 3.2 was expressed in terms of orthogonal functions (Legendre polynomials) and the fitting coefficients were determined using the values at discrete points in the spectrum. The problem could be solved analytically, and quantitative results obtained.

The current study differs in several respects. The superposition of Pake doublets arising from the perdeuterated chain, combined with poor signal-to-noise due to the rigid constraints on experiment duration, prevent the application of such rigorous methods. Indeed, the T_2^{qe} spectra calculated from the data collected as described above were judged to be too complex and too noisy for meaningful results to be obtained from fitting them. Instead, to learn about T_2^{qe} mechanisms in POPC/PDPC mixtures in general, a higher SNR measurement (10,240 scans per τ value rather than 1024) was made for a representative sample (25% PDPC at 25^o C).

The resulting T_2^{qe} spectrum is shown in Figure 3.4. Even with the higher SNR, the T_2^{qe} values become quite erratic towards the edges of the spectrum. The Pearson's R coefficient (representing the strength of linear correlation of the fits from which the individual T_2^{qe} values were obtained [72]) was thus used to discriminate between data which were reliable and those which were too heavily influenced by noise. R was plotted across the spectrum – also shown in Figure 3.4 – and found to drop off rapidly in the outer region. A threshold of $R = 0.8$ was selected arbitrarily to define the "trustworthy" region of the T_2^{qe} spectrum.

The complexity of the spectrum, due to the superposition of Pake doublets from different sites on the chain, was a source of further difficulty. Since the problem of fitting the series of individual peaks was intractable, it was decided to focus solely on the large outer peaks corresponding to the plateau region of the chain (in which the contributions of roughly half the carbon sites are summed). The total range over which the T_2^{qe} spectrum

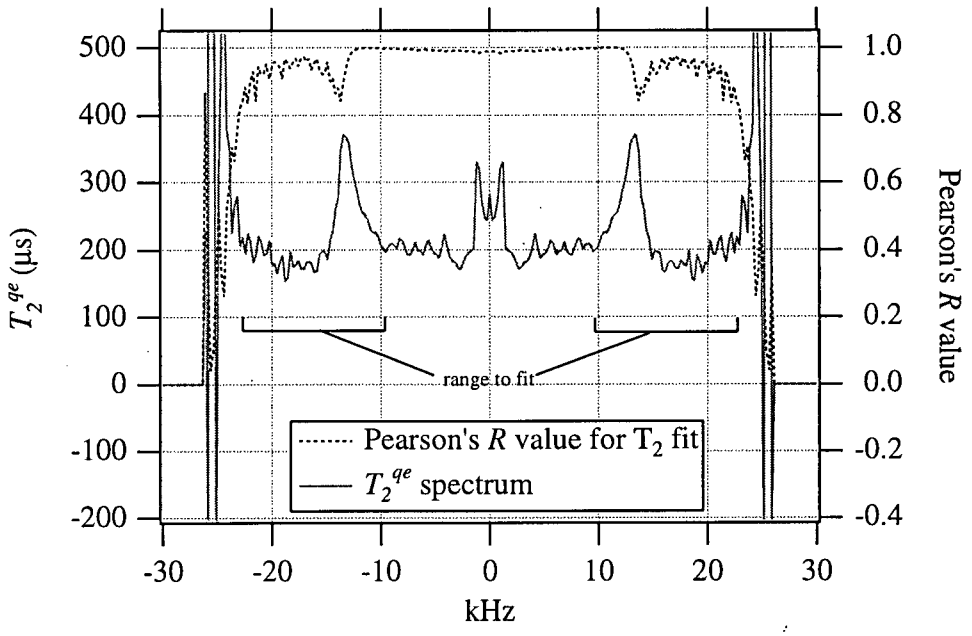

Figure 3.4: The "T_2^{qe} spectrum" for a representative sample (25% PDPC, at 25° C), showing values of T_2^{qe} for each frequency across the powder pattern. To determine the range of reliable data, the Pearson's R coefficients for the linear fit (performed to calculate a mean T_2^{qe} value) are plotted as a function of frequency. The R values drop off sharply beyond $\sim$ 22 kHz, defining the outer bound of the region to be fitted; the inner limit is defined by the edge of the large peak corresponding to the plateau carbons.

was fitted is thus as shown in Figure 3.4.

"Fitting" was carried out entirely by eye, and consisted of characterizing the effects of the three coefficients on the fit function, then honing in on the best solution for the region defined above. It must be emphasized that the terms in Equation 3.2 are not orthogonal, so this problem is fundamentally ill-posed. Because of this and the approximations made above, there is no pretense that quantitative conclusions can be drawn from these results. A satisfactory solution was obtained, however, and by varying the values of the coefficients the confidence limits could be estimated in an informal way.

Chapter 4

Results and Discussion

4.1 Preliminary Comments

As described in Section 3.1, the samples were binary mixtures of mono-unsaturated POPC-d_{31} and polyunsaturated PDPC. Samples will be referred to by their molar percentage of PDPC (*e.g.* "0% PDPC" refers to the 100% POPC-d_{31} sample, etc.).

Obviously, the composition of the samples must be borne in mind when interpreting the NMR results. The ^{1}H-NMR measurements include contributions from both POPC-d_{31} and PDPC, and indeed from headgroup and glycerol protons as well as from the acyl chains of both species. Changes in ^{1}H-NMR parameters observed upon increasing PDPC concentration may be due to its effect on the other lipid – and thus, presumably, on the membrane environment generally – or simply to an increasing proportion of PDPC's own distinctive contribution.

In contrast, all ^{2}H-NMR results come directly from the deuterium-labelled 16:0 chain of POPC-d_{31}. Therefore, any effects on ^{2}H-NMR measurements as PDPC concentration is raised are direct indications of the polyunsaturated lipid's effect on other components of the membrane.

Unless otherwise noted in the Analysis section, the uncertainties shown here were determined from the variation in results from several identical experiments (using the same sample or different samples with the same composition). They are thus functional measures of the experimental error, encompassing uncertainties from sample preparation

and oxidation as well as those inherent in the techniques of analysis.

Numerical results of curve-fitting are not shown below except when relevant to the discussion. They are included in Appendix C.

4.2 Moment Studies and Order Parameters

4.2.1 Proton Second Moment

The proton residual second moments, $M_{2r,H}$, are shown as a function of PDPC content in Figure 4.1. Considering the vast range of sample compositions, the values are remarkably constant. While a slight upward trend is apparent, only for the 25° C data did the slope of the least-squares fit line differ statistically from zero.

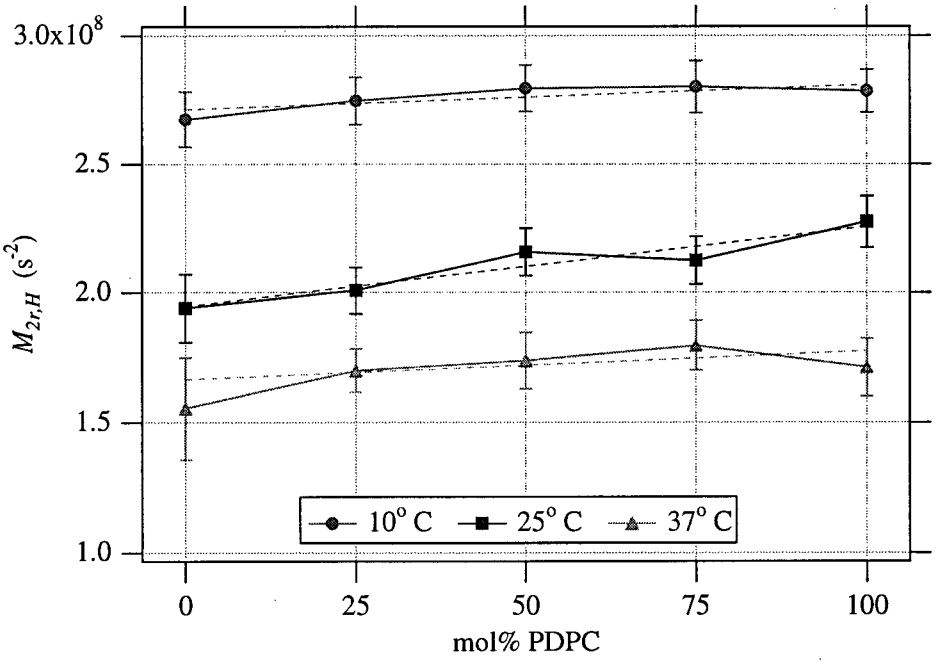

Figure 4.1: Residual proton second moments, $M_{2r,H}$, of binary mixtures of PDPC (16:0/22:6-PC) and POPC-d_{31} (16:0-d_{31}/18:1-PC), as a function of mol% PDPC and temperature. $M_{2r,H}$ values were determined directly from the proton FID using the moment expansion, as described in Section 3.3.1. Results of the least-squares linear fits to these data are included in Appendix C.

While this surprising lack of variation could be the net result of larger, offsetting changes, it seems that the two individual lipid species (POPC-d_{31} and PDPC) simply have very similar $M_{2r,H}$ values. Examination of the 0% PDPC and 100% PDPC data reveals that their $M_{2r,H}$ values differ by no more than 18% for any of the temperatures measured (*c.f.* the $\sim$ 500% change in $M_{2r,H}$ between gel and fluid phases of DPPC-d_0 [57]). Since the relationship at intermediate compositions is linear, it is impossible to distinguish whether the observed trend results from interactions between the two species, or simply from an increased weighting of PDPC's slightly greater intrinsic $M_{2r,H}$.

As described in Section 2.1.2, $M_{2r,H}$ is proportional to the mean-squared dipolar pseudo-order parameter. It is thus a function of the range of angles sampled (at a suitable speed) by all proton-proton vectors, and of the time-averaged distance between protons. (Note that in fluid membranes, intermolecular interactions are averaged to zero due to rapid lateral diffusion of lipid molecules. Since dipolar interactions fall off like $1/R^6$, each proton on the acyl chains "feels" the fields of only the four nearest CH_2 groups and roughly 50% of $M_{2r,H}$ arises from interactions between "geminal" protons bound to the same carbon atom [56, 57]. Since the distance between geminal protons is fixed – with apologies to infrared spectroscopists – this contribution will vary only with orientation.) The reduction of M_2 to M_{2r} arises from fast motions for which $\tau_c \ll \tau_s$, where $\tau_s = (M_2)^{-\frac{1}{2}}$. For intramolecular proton-proton dipolar interactions in typical phospholipids the proton $M_2 \approx 2 \times 10^{10} s^{-2}$ [57], so this condition requires $\tau_c \ll 10^{-5}$ s. Referring to Figure 2.1, we see that relevant motions would include *trans-gauche* isomerizations and rotational diffusion about the bilayer normal, as well as nodding motions of the phospholipid headgroup and the smallest-wavelength undulations.

To the extent that it is significant, the small increase observed in $M_{2r,H}$ indicates a net decrease in fast re-orientations or time-averaged inter-proton distances. Whether these changes occurred in the acyl chains or the lipid headgroups, and even whether they

result from interactions between the species or are simply properties of PDPC, cannot be stated from this evidence.

4.2.2 Deuterium Second Moment

Deuterium residual second moments ($M_{2r,D}$) were calculated directly from the powder patterns, as described in Section 3.3.2, and are summarized in Figure 4.2. As with the proton moments, there is no strong change in $M_{2r,D}$ as the proportion of PDPC increases. Least-squares linear fitting yielded only one slope which was significantly different from zero – that for 10° C, which shows a slight *decline* with increasing DHA content.

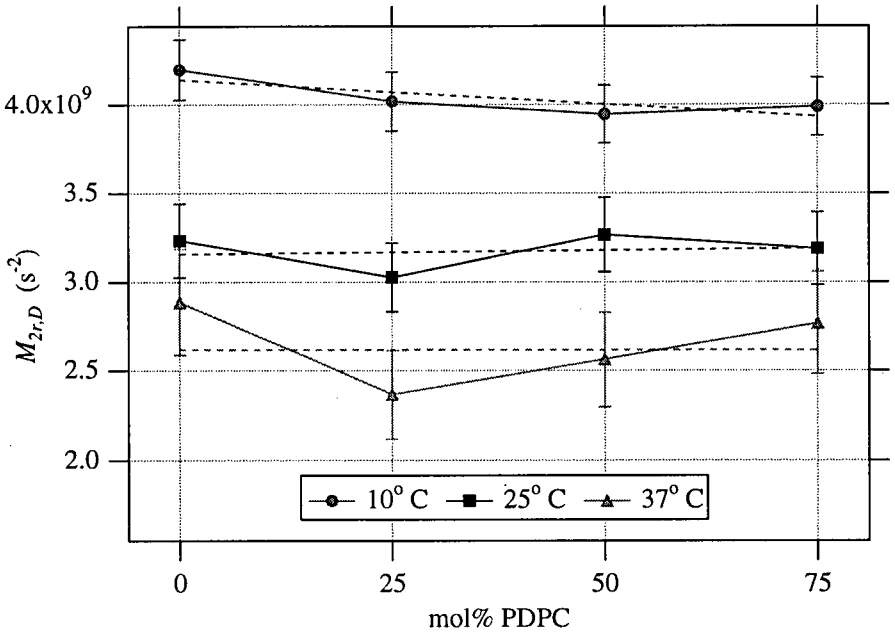

Figure 4.2: Residual second moment values, $M_{2r,D}$, of the deuterium spectrum arising from the 16:0-d_{31} chain of POPC-d_{31}. Fitting results are tabulated in Appendix C.

As discussed in Sections 2.1.2 and A.4, the residual second moment is proportional to $\langle S_{CD}^2 \rangle$, where $S_{CD} = \langle P_2(\cos\theta) \rangle$ is the orientational order parameter. Since $M_{2r,D}$ is relatively constant, we see that adding PDPC to the membrane has little net effect on the orientational order of the other lipid species (or, more specifically, on that of its

perdeuterated chain). Moving from a membrane which is composed entirely of POPC-d_{31} to one which is 75 mol% PDPC, the $M_{2r,D}$ of the deuterated chain changes by only $\sim 5\%$.

Again the effect is surprisingly small – this can be interpreted several ways. It could be that the two lipid species have such similar properties that addition of PDPC does not disturb POPC's state. This would seem to agree with the observation that the 0% PDPC and 100% PDPC samples had very similar values of $M_{2r,H}$. Another possibility is that the lipids are separating into species-enriched domains, so the perdeuterated 16:0 chains are largely isolated from the increasing proportion of PDPC in the membrane. While this is reminiscent of the dynamic clustering proposed by other investigators [46, 47], these domain models have been developed to explain DHA's lack of interaction with cholesterol and have not been extended to sterol-free membranes. Further insight into these questions is gained by consideration of the variation in $|S_{CD}|$ as a function of position on the acyl chain.

4.2.3 Deuterium Order Parameter Profiles

Smoothed order parameter profiles, obtained from de-Paked spectra using the method of Lafleur *et al.* [73], are shown in Figure 4.3. As PDPC is added, a progressive decrease in orientational order is observed in the lower half of POPC's perdeuterated 16:0 chain (*i.e.* in the half of the chain closer to the centre of the bilayer, from C9 to C15). This indicates that the 16:0-d_{31} chain is experiencing greater conformational freedom, corresponding to a slightly expanded "cloud of conformations" in this region. A concomitant, very slight increase in order is discernible in the plateau region of the profiles, though it barely exceeds the uncertainty of the measurement.

A general caveat must be stated with respect to the sensitivity of order parameter profile measurements to lipid oxidation. The recent study by Drobnies *et al.* [71] shows

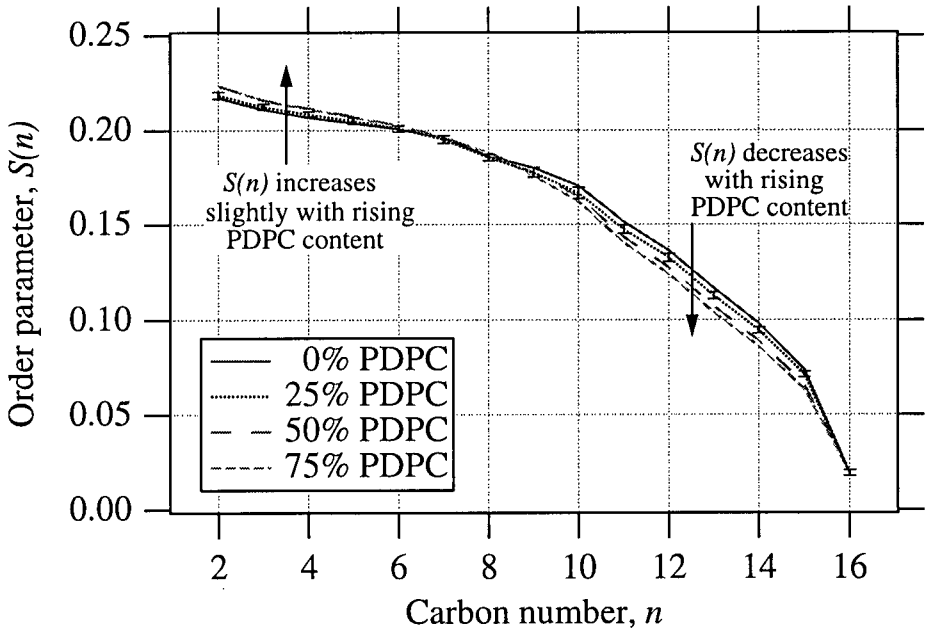

Figure 4.3: Smoothed order parameter profiles $S(n)$ for the series of lipid mixtures, calculated from the de-Paked ^{2}H spectra by the method of Lafleur *et al.* [73]. Representative error bars, derived from the variation in four separate measurements, are shown for the 25% PDPC profile. For clarity, only the results at $T = 25^o$ C are shown; the profiles for 10^o C and 37^o C, which show qualitatively similar results, are included in Appendix C.

that $|S_{CD}|$ varies significantly as oxidation of a polyunsaturated lipid (PAPC, or 16:0-d_{31}/20:4-PC, in their study) proceeds – changes of up to about 0.03 units for 10% oxidized lipids. While such an effect is certainly large enough to account for (or to overwhelm) the trends reported here, there is good reason to believe that oxidation has not progressed this far in any of the samples used (see Section 3.1). Furthermore, oxidation was shown to decrease $S(n)$ at all carbon sites on the chain, whereas Figure 4.3 distinctly shows regional variations as a function of PDPC content, and even slight increases in the plateau region. It should be noted, though, that in the Drobnies study the perdeuterated chain is on the same lipid molecule (at *sn-1*) as the polyunsaturated chain (at *sn-2*); the extension of these results to our two-species system is not obvious.

4.2.4 Average Chain Length

Figure 4.4 shows the average length, $\langle L \rangle$, of the perdeuterated acyl chain as a function of PDPC content. The chain length decreases (almost imperceptibly) as PDPC is added – the 75% PDPC membrane is $\sim$ 1% thinner than the 0% PDPC sample. In terms of the $S(n)$ profiles, the decreased order in the central region of the bilayer has "won out" over the slight rise in the plateau, leading to the slight thinning effect. In practical terms, however, this trend is so subtle that $\langle L \rangle$ can be considered constant for all samples studied.

4.2.5 Discussion of Moment and Order Parameter Results

The surprisingly small variation in the proton and deuterium M_{2r} results indicates that the lipid species are "well-matched" and do not perturb one another in the membrane, or perhaps that they separate into species-enriched microdomains. The order parameter profiles are more telling – there is a clear effect of increasing PDPC content on POPC's

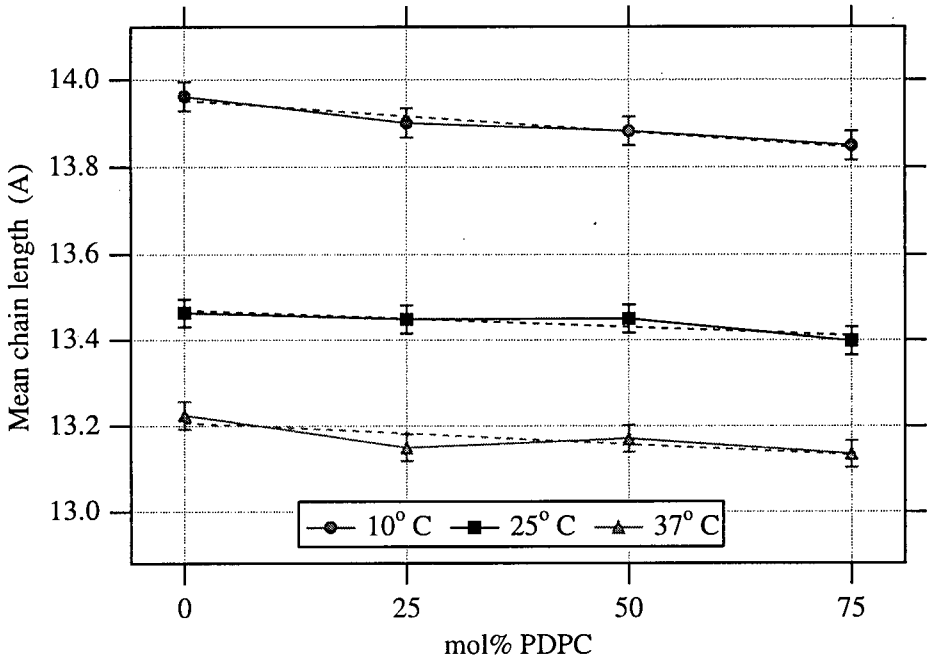

Figure 4.4: Average length $\langle L \rangle$ of the perdeuterated 16:0 chain of POPC-d_{31}, determined as described in Section 3.3.3. Fitting results are tabulated in Appendix C.

saturated chain, which allows us to address the question of DHA's effect on other constituents of the membrane.

The $S(n)$ results argue compellingly against the "wedge" model for polyunsaturation (described in Section 1.3). If it were true that lipids bearing DHA chains are wedge-shaped and exert lateral pressures through the middle region of the bilayer, then adding more PDPC should squeeze the other lipids in the membrane, reducing the conformational freedom of the lower half of their chains. Instead we saw that the perdeuterated chain on POPC-d_{31} *gained* conformational freedom as the proportion of polyunsaturated lipid increased. (Indeed we see that a perdeuterated chain on one lipid molecule responds to polyunsaturation on another much as the *sn-1* chain responded to polyunsaturation at *sn-2* in the earlier study [42].) Rather than forming wedge-shaped molecules which crowd the centre of the bilayer, it seems the DHA chain actually allows *more* space in this

region, so that all neighbouring chains (on the same or different molecules) have greater conformational freedom.

Inspired by several sources [37, 71, 75], we propose that the DHA chain is spending more time doubled back toward the lipid-water interface than do less unsaturated chains. This would account for the $S(n)$ results, since space is vacated (in a time-averaged sense) in the middle of the bilayer for the perdeuterated chains to occupy. Furthermore, it is consistent with the slight increase in $S(n)$ observed in the plateau region, as these sites are slightly crowded by the doubled-back DHA chains.

This model is being actively investigated by Gawrisch as a follow-up to the earlier $S(n)$ study, and as a possible explanation for DHA's known repulsion for cholesterol [75]. A similar "snorkelling" mechanism, in which polar oxidized sites on the chain tend to migrate to the lipid-water surface, was invoked to explain the effects of lipid oxidation on order profiles [71]. A related argument could be applied (though less convincingly) based on the slightly polarizable nature of DHA's many double bonds. Finally, in Applegate & Glomset's early work on computational modelling of DHA's ground state, a "hairpin" configuration was found to be the lowest-energy state but has been largely ignored due to presumed difficulties in packing [37].

The snorkelling model would also help explain why replacing the 18-carbon oleic acid of POPC with the 22-carbon DHA chain of PDPC leads to slight thinning of the membrane, since the longer chain would spend more time doubled up. Even the curious increase in $M_{2r,H}$, discussed in Section 4.2.1, can be explained: the hairpin conformation leads to smaller *intra*molecular inter-proton distances, increasing dipolar coupling and hence $M_{2r,H}$ as well.

4.3 Relaxation Studies

4.3.1 Proton Average T_{1z}

Average proton T_{1z} values were obtained by fitting the early points in the relaxation curve to a single exponential. The results are plotted in Figure 4.5, and exhibit a clear (20-25%) rise in T_{1z} as PDPC content is increased from 0 mol% to 75 mol%.

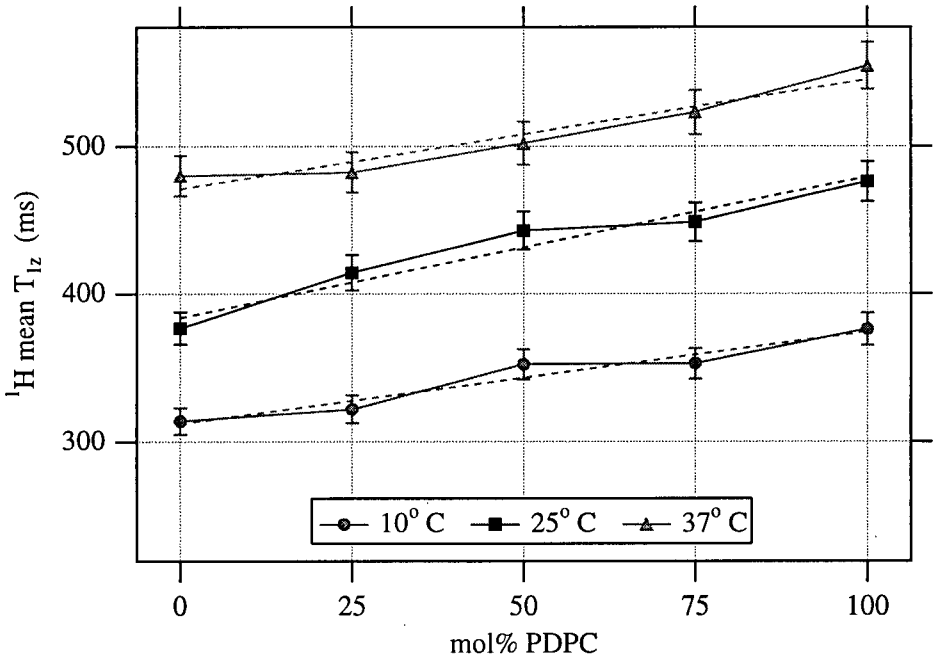

Figure 4.5: Mean value of T_{1z} for all lipid protons, determined from a single-exponential fit to short delay time data ($\tau_1 \ll T_{1z}$) collected with a modified inversion recovery pulse sequence (as described in Section 3.2.2). Fitting results are tabulated in Appendix C.

To understand these results, we must first determine the range of correlation times of the important T_{1z} relaxation processes. As shown in Figure 2.2, the fact that T_{1z} times increase with temperature indicates that the predominant mechanisms are motions for which $\omega_o\tau_c \ll 1$, and these "very fast" motions (such as *trans-gauche* isomerizations) get even faster as the temperature is raised.

This conclusion cannot automatically be extended, however, to explain the observed

increase in T_{1z} with PDPC content *at each temperature.* While speeding up the very fast motions is definitely a viable explanation, it is also conceivable that T_{1z} rates decrease due to a slowing down of certain motions (such that they become adiabatic and cease to contribute to $j(\omega_o)$), or that certain contributing modes are extinguished by increasing PDPC content.

To weigh these alternatives we appeal to the surprisingly small changes measured in $M_{2r,H}$ as PDPC was added. The very fast, non-adiabatic motions that underlie T_{1z} relaxation certainly satisfy the criterion $\tau_c \ll \tau_s$ for contributing to motional averaging; indeed rapid chain motions and rotational diffusion are commonly assumed to be the primary causes of line narrowing in lipid NMR. If these modes were extinguished in any appreciable number – or slowed such that $\tau_c \geq \tau_s$ – the loss of motional narrowing would cause a significant increase in $M_{2r,H}$, which was not observed. This does not rule out the possibility of motions being slowed from the very fast regime ($\tau_c \ll 1/\omega_o$) to the fast adiabatic regime ($\tau_s \ll \tau_c \ll 1/\omega_o$), but the likelihood of large classes of motions being slowed by 3 to 4 orders of magnitude seems small. Furthermore, the temperature dependence asserts that non-adiabatic motions are dominant over the full range of sample compositions.

The greater values of T_{1z} could also be due to decreases in the mean-squared fluctuation amplitudes of the relevant fluctuations (the constants a_1 and a_2 in Equation 2.6). However, the relationship between T_{1z} and lipid order is $1/T_{1z} \propto (1 - S^2)$ (for small S) [63]. If we generously approximate $\langle S \rangle \approx 0.2$, then $1 - \langle S^2 \rangle \approx 0.96$ and the observed 20% rise in T_{1z} requires a 120% increase in $\langle S \rangle$ (or a five-fold increase in $\langle S^2 \rangle$)! It is clear from the $M_{2r,H}$ results of Figure 4.1 that this is not the case.

A final alternative could involve spin exchange between the lipid and the surrounding water (since the experiments were carried out in H_2O buffer solutions). Bilayers composed of polyunsaturated lipids have been proposed to be highly permeable to water [76, 77],

which might be expected to influence T_{1z} if spin exchange is an important mechanism. This possibility was investigated by measuring average T_{1z} for POPC-d_0 in D_2O and H_2O buffer solutions. The results do not differ greatly, indicating that exchange processes do not contribute significantly to T_{1z} of these systems.

We thus conclude that the observed rise in average T_{1z} with increasing polyunsaturation results from decreasing correlation times for a class of very fast, non-adiabatic motions. We are once again unable, however, to distinguish whether this is due to PDPC's influence on POPC or simply from an increasing proportion of PDPC's contribution. (As with the $M_{2r,H}$ results, it is evident from the 100% PDPC sample that the mixture of lipids is not required to observe the effect.) Likewise, the average T_{1z} values entail contributions from all protons, so that chain, headgroup or backbone motions could underlie the changes.

4.3.2 Deuterium Average T_{1z}

Deuterium average T_{1z} values also increase as DHA-bearing lipid is added to the membrane, as shown in Figure 4.6. All the arguments of the proton case still apply, so again we interpret this as a decrease in correlation times for the very fast motions which dominate T_{1z} processes. The change is now localized, however, to the perdeuterated palmitoyl chain of POPC-d_{31}, indicating (i) that chain motions – likely *trans-gauche* isomerizations – underlie the effect, and (ii) that the effect can arise in POPC-d_{31} solely as a result of PDPC's influence. Combining these findings, we see that adding PDPC to the membrane somehow speeds the motions of POPC's saturated chain.

Attempting to further localize the effect, average T_{1z} values were determined for ranges of the de-Paked spectra, as described in Section 3.3.4. The results are shown in Figure 4.7. The 0% PDPC results agree generally with those obtained in detailed studies of T_{1z} as a function of chain position in oriented samples of POPC-d_{31} [62], lending confidence

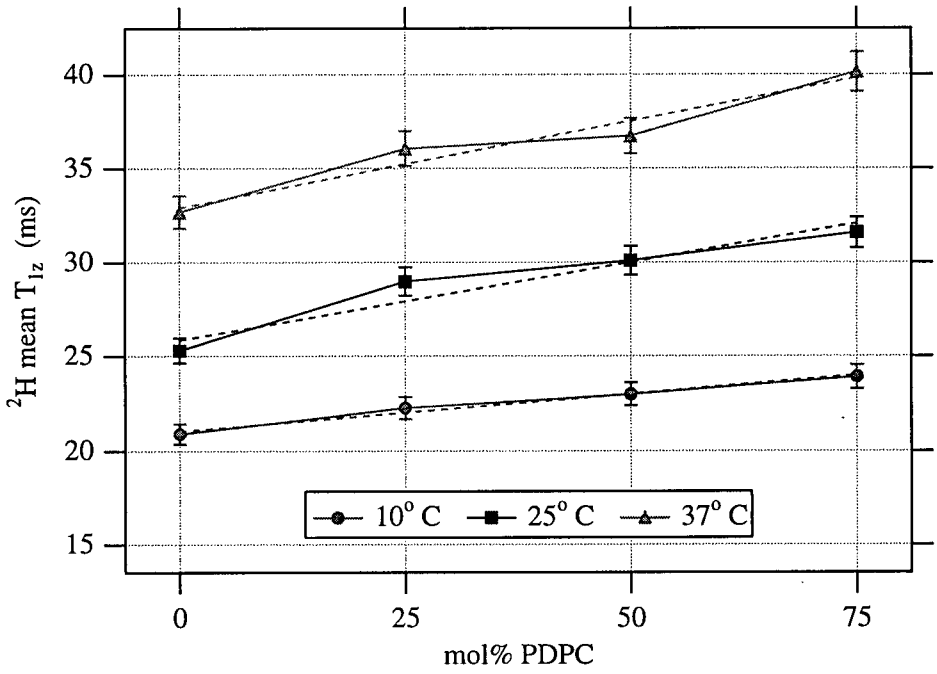

Figure 4.6: Average values of T_{1z} for the perdeuterated 16:0 chain of POPC-d_{31}, as determined from a single-exponential fit to short-τ data. Fitting results are tabulated in Appendix C.

in the analysis technique. As PDPC is added, clear increases in T_{1z} are visible in the plateau and middle regions of the chain. The results for the lower chain are more erratic, but as discussed in Section 3.3.4 there is reason to doubt their reliability even beyond the uncertainties shown. It is thus difficult to discern any further detail regarding the changes in the 16:0-d_{31} chain's motion – another study with better SNR would be required to learn more.

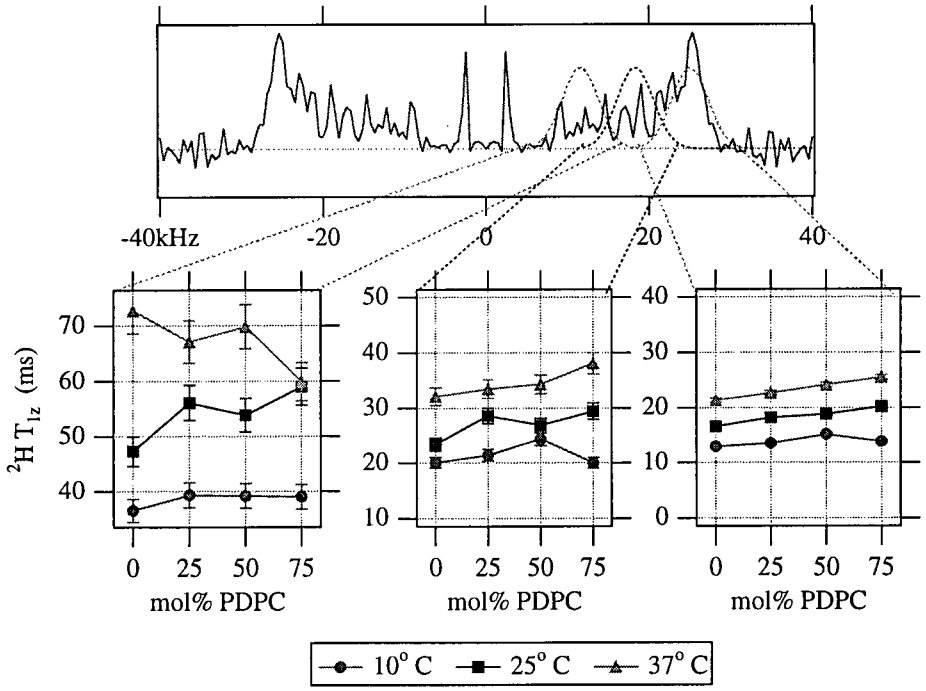

Figure 4.7: Average values of T_{1z} for different regions of the perdeuterated 16:0 chain of POPC-d_{31}. Gaussian-weighted integrals of the de-Paked spectrum isolated the signal from different parts of the chain (assuming a monotonic decrease in $|S_{CD}|$ with carbon number); a single-exponential fit yielded average T_{1z} for each series. From left to right, the plots correspond to the "tail" region of the chain (roughly C13-15), the middle of the chain (C10-12), and the plateau region (C2-9).

4.3.3 Deuterium Average T_2^{qe}

Addition of PDPC to the membrane had marked effects on the average T_2^{qe} of POPC's deuterated palmitoyl chain. As shown in Figure 4.8, T_2^{qe} decreases almost twofold going from 0% to 75% PDPC – the most striking change observed in any parameter in this study.

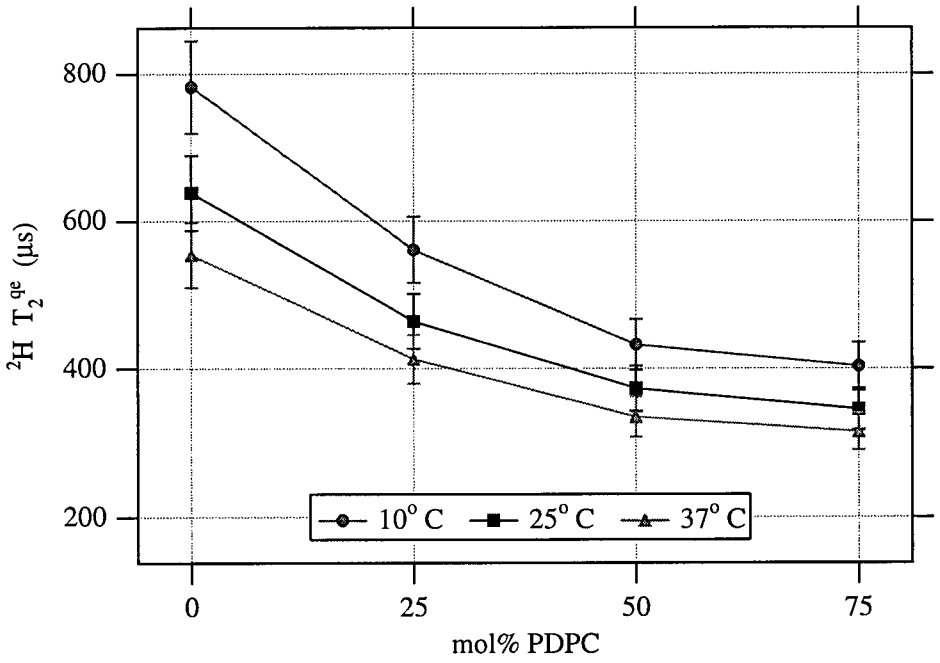

Figure 4.8: Average values of T_2^{qe} for the perdeuterated 16:0 chain of POPC-d_{31}, as calculated from a single-exponential fit to the peak amplitudes of the quadrupolar echoes for a range of delay times. A decrease of nearly 50% is observed in moving from 0%PDPC to 75% PDPC, the most striking effect observed in this study.

T_2^{qe} is much less than the deuterium T_{1z}, indicating that adiabatic motions are present and dominate transverse relaxation. This is expected from the complex nature of the membrane environment (as recognized by Davis [58]), and prior studies have concluded that T_2^{qe} relaxation in fluid membranes is due largely to thermally-activated adiabatic modes [63, 67]. This is consistent with the observed temperature dependence, as the decrease in T_2^{qe} as temperature rises could be due to increased efficacy of the thermal

mechanisms. Alternatively, though, this decrease could be explained in terms of shrinking correlation times, since for *very* slow motions $T_2^{qe} \propto \tau_c$ (see Section 2.2.1).

Since an understanding of the nature of the T_2^{qe} mechanisms is essential to intepreting this dramatic result, we will consider all available evidence to discriminate between these models. To begin, in Figure 4.9 we see the "regional" variation of average T_2^{qe} results. It is clear that the decreasing trend applies roughly equally to all regions of the perdeuterated chain, indicating that the T_2 processes may be dominated by "collective motions" of the membrane which affect each molecule as a whole, rather than by localized conformational changes. In addition, Figure 4.10 shows that the plot of T_2 rate versus temperature is almost perfectly linear, as predicted for thermally-activated mechanisms by Equations 2.10 and 2.11.

Furthermore, as noted in Section 2.2.2, the correlation times for certain adiabatic modes are not expected to vary greatly with temperature. (For membrane surface undulations, for instance, τ_c is thought to be determined largely by geometric considerations such as the thickness of the membrane and the separation between neighbouring bilayers in multi-lamellar vesicle (MLV) systems [67].) Finally, any shift of the τ_c spectrum in the vicinity of $\tau_c \approx \langle(\delta\omega)^2\rangle^{-\frac{1}{2}}$ will at least partially cancel itself out due to contributions from either side of the "T_2^{qe} minimum" (described in Section 2.2.1), making it difficult to obtain the large net effect which has been observed. It is thus unlikely that changes in correlation times underlie the significant dependence of T_2^{qe} on either temperature or PDPC content.

Orientation Dependence of Deuterium T_2^{qe}

All evidence is thus consistent with thermally-activated collective modes making the dominant contribution to T_2^{qe} relaxation. If this is the case, then the orientation-dependence of T_2^{qe} should be described by Equation 2.13, and should yield further details regarding

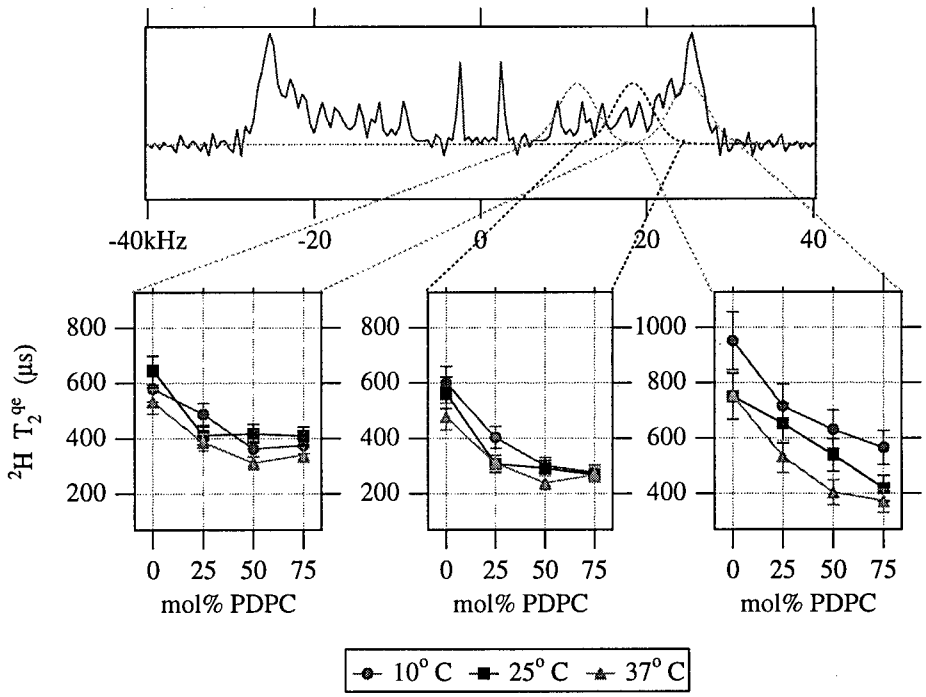

Figure 4.9: Regional dependence of mean T_2^{qe} values for the perdeuterated 16:0-d_{31} chain. As described in the caption for Figure 4.7, from left to right the plots correspond to the "tail" region of the chain (roughly C13-15), the middle of the chain (C10-12), and the plateau region (C2-9). The decrease in T_2^{qe} is seen clearly for all parts of the chain, indicating that the mechanism responsible for T_2^{qe} relaxation is probably a "collective motion" which affects each molecule as a whole.

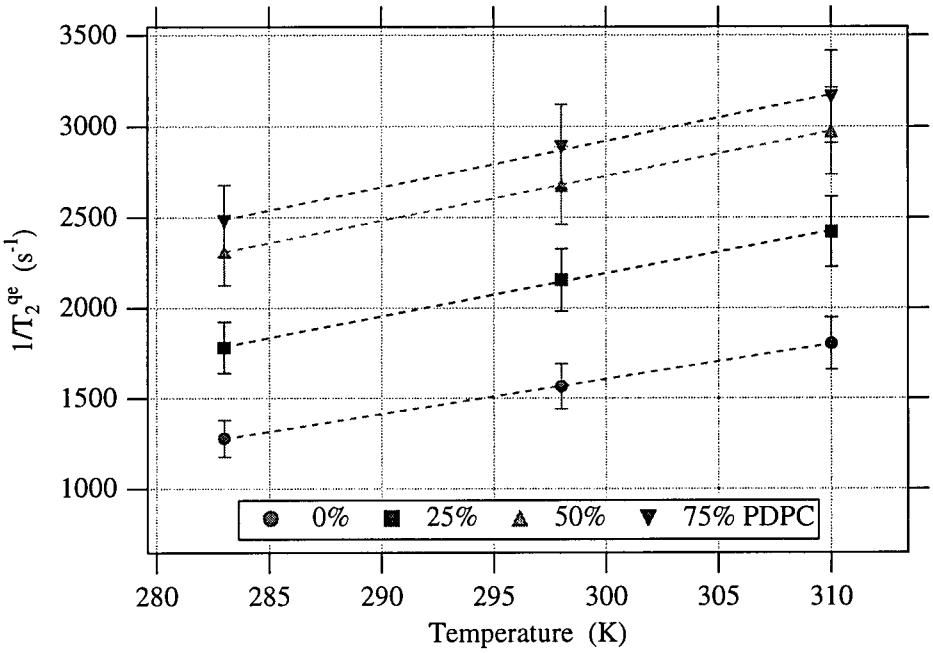

Figure 4.10: Dependence of the mean T_2^{qe} rate on temperature, for the perdeuterated chain of POPC-d_{31} in binary mixtures with PDPC. The linear relation with temperature agrees with the predictions of Equations 2.10 and 2.11 for thermally-activated relaxation mechanisms. Results from least-squares linear fitting are included in Appendix C.

the important mechanisms as described in Section 2.2.2. In principle this could allow us to quantitatively compare membrane parameters (such as the curvature energy or area compressibility) as a function of PDPC content, but this was not possible for the reasons outlined in Section 3.3.4. Instead, to investigate general properties of T_2^{qe} processes in POPC-d_{31}/PDPC binary mixtures, a representative measurement was taken with higher SNR for one sample from the series (25% PDPC at 25° C). Even for this case only qualitative conclusions can be drawn, but these are of great value in interpreting the T_2^{qe} trends described above.

Figure 4.11 shows the representative "T_2^{qe} spectrum". The characteristic signature of the $\sin^2\theta\cos^2\theta$ term in $1/T_2^{qe}$ is immediately evident, as the T_2^{qe} values peak sharply at the shoulders ($\theta = 90^o$) and edges ($\theta = 0^o$) of the spectrum. This behaviour has been reported in all previous studies of angular dependence of T_2^{qe} in MLVs.

Attempts to fit the spectrum were limited to the ranges indicated on the figure (as discussed in Section 3.3.4) and were strictly qualitative in nature. The "best-fit" line, generated from the three-termed $1/T_2$ expression of Equation 2.13, is shown in Figure 4.11. To assess the tolerance of the fit parameters, the coefficients were varied by 10% (yielding acceptable solutions) and 50% (giving poor fits), as also shown[1]. The order-of-magnitude of the best-fit parameters is thus judged to be known with confidence, and their numerical values are probably estimated to within 20-30%. The values of the parameters are shown in Table 4.3.3.

The results presented in Figures 4.9 and 4.10 indicated that the dominant T_2^{qe} mechanisms in this study were likely to be thermally-activated adiabatic modes; the fact that the θ-dependence of T_2^{qe} is described by Equation 2.13 confirms this result. Information

[1]As discussed in Section 3.3.4, the fitting terms were not orthogonal, so variations in the coefficients could partially compensate each other. To obtain the worst-case estimate of uncertainty in the "best-fit" results, the signs of the 10% and 50% variations shown in Table 4.3.3 were adjusted so that the changes would offset.

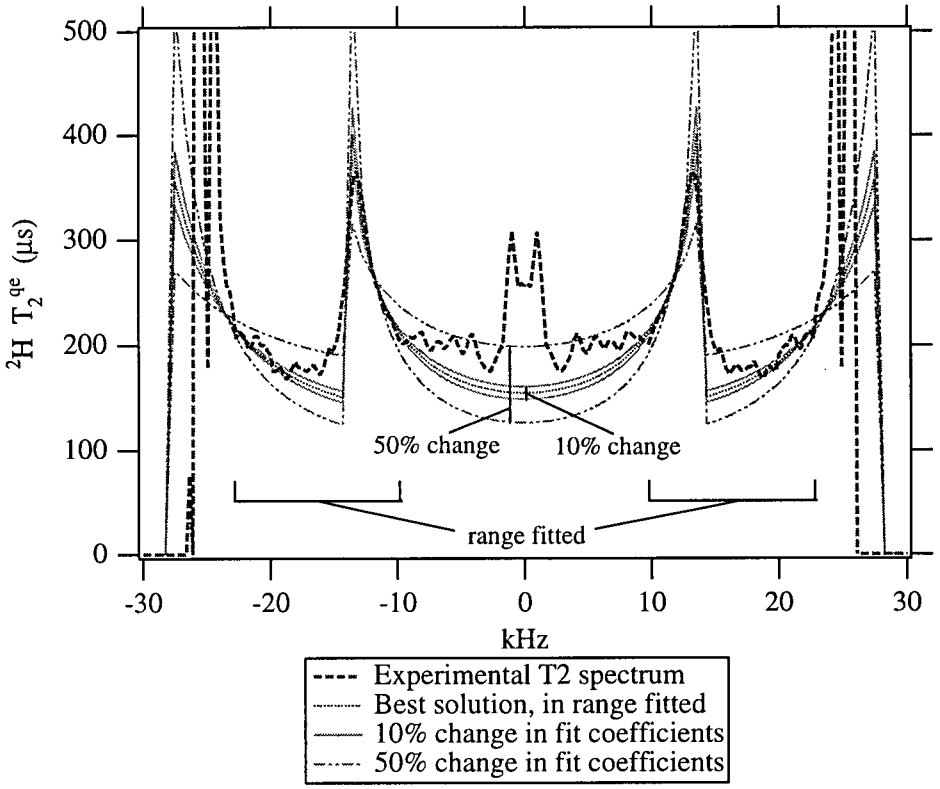

Figure 4.11: Representative T_2^{qe} spectrum, displaying orientation-dependence of T_2^{qe} relaxation mechanisms. The spectrum is dominated by the contributions from the plateau region, and displays characteristic $\sin^2\theta\cos^2\theta$ dependence, featuring peaks at $\theta = 90^o$ (near ± 13 kHz) and $\theta = 0^o$ (near ± 26 kHz). The central peaks are due to the methyl group, and are ignored. The spectrum has been fitted to Equation 2.13, with coefficients as shown in Table 4.3.3. The best-fit line is shown, as well as the lines generated by deliberate variation of the fit parameters, intended to assess the uncertainty on the best-fit values. The spectrum shown is derived from high-SNR measurements of a 25% PDPC sample at 25° C, as described in Section 3.3.4, and is intended to be representative of POPC-d_{31}/PDPC binary mixtures.

Table 4.1: Fit parameters for T_2^{qe} orientation-dependence, from modelling the T_2^{qe} spectrum using Equation 2.13. The 10% and 50% changes impose variations on the best-fit results, in order to assess the tolerance of the coefficients. As described in the text, the signs of these changes were chosen such that they offset and give the worst-case estimate of uncertainty. All coefficients are in units of s^{-1}.

	A	B	C
Best-fit	1800	21000	1000
10% changes	1600	23000	900
	2000	19000	1100
50% changes	900	31500	500
	2700	10500	1500

regarding the nature of these modes can be derived from the relative magnitudes of the fit coefficients, in particular the $\sin^2\theta\cos^2\theta$ and $[P_2(\cos\theta)]^2$ terms (*i.e.* the B and C coefficients). For comparison purposes B must be divided by 4 (since the maximum value obtainable by $\sin^2\theta\cos^2\theta$ is one-fourth that of $[P_2(\cos\theta)]^2$), but clearly it is the larger contribution to the best-fit solution. Further evidence that the $\sin^2\theta\cos^2\theta$ term dominates the orientation-dependence of T_2^{qe} comes from the interdependence of B and C in the fitting process. A two-term function with $C = 0$ was found to fit the data adequately; as C was increased from zero to the maximum value which allowed a reasonable fit (with A and B adjusted freely), B varied by only 20% of its best-fit value. With $B = 0$ no solution could be found.

We thus conclude that $\sin^2\theta\cos^2\theta$ is the critical term in the angular dependence of T_2^{qe} for POPC-d_{31}/PDPC mixtures in MLV form. As discussed in Section 2.2.2, this behaviour is predicted for T_2^{qe} mechanisms arising due to fluctuations in the orientation of the membrane surface normal. Specific interpretations of this result are discussed below, in Section 4.4.2. It must be emphasized, though, that many approximations have been made in analysis of the T_2^{qe} spectra, and that this should be considered to be a possible conclusion rather than a definitive one. It agrees, however, with more in-depth

studies of the θ-dependence of T_2^{qe}, which have found that the $\sin^2\theta\cos^2\theta$ term is clearly dominant in MLV samples [63, 68].

4.4 Synthesis of Moment and Relaxation Results

4.4.1 Fast Motions

Increased values of average T_{1z} were interpreted to mean that correlation times decreased for very fast motions as PDPC was added to the membrane. While the proton results give no indication as to the site of this change, the deuterium measurements show that it certainly does occur in the 16:0-d_{31} chains of the POPC molecules. (Note that this is not an exclusive result – motions could be faster in other regions, as well.) This could be taken to indicate that greater PDPC content decreases the "viscosity" of the membrane, though the meaning of that term on the molecular scale is somewhat vague. In the interest of producing a self-consistent model, we will consider how this result matches the conclusions drawn from the moment and order parameter studies, which also provide information on fast motions in the system. (A deliberate blurring of the distinction between "fast" and "very fast" regimes has occurred here – the important point is that both sets of measurements have been interpreted largely in terms of chain-bending transitions).

In Section 4.2.5 an interpretation is presented in which increasing polyunsaturation frees up space in the middle of the bilayer. Chains like DHA are proposed to spend slightly more time doubled back on themselves, explaining the observed decreases in orientational order of other chains (such as the perdeuterated 16:0 of POPC-d_{31}). This was shown to be consistent with the measured values of M_{2r} for protons and deuterons; we now present a qualitative argument that such a model can account for the observed T_{1z} increases as well.

Acyl chain conformational changes encounter energy barriers due to rotation about the C-C bond (*e.g.* from *trans* to *gauche*) and from steric interactions with neighbouring chains. If, as suggested above, the central region of the bilayer becomes less crowded due to doubling back of the DHA chains, then the steric contribution to the barrier is reduced and the low-lying states become more accessible. At a given temperature, these conformations are thus sampled more freely by random motions, leading to faster loss of spatial correlation and hence smaller values of τ_c.

While admittedly crude, this argument demonstrates that the T_{1z} and order parameter measurements – *i.e.* all results pertaining to "fast" classes of motions – can be explained within the same molecular model. A more quantitative or definitive interpretation is not possible given the current results, however; further work would be required to test this hypothesis and to develop its details.

4.4.2 Slow Motions

The T_2^{qe} results give information on a very different timescale, indicating that spin-spin relaxation in POPC-d_{31}/PDPC samples is dominated by collective modes which slowly modulate the orientation of the membrane surface normal. We suggest that the motions in question are undulations of the membrane.

While other mechanisms, such as diffusion on a curved surface ([61], later argued against in [63]) or "order-director fluctuations" [78], could also give rise to the observed θ-dependence of T_2^{qe}, surface undulations seem the most likely choice. As described in Section 4.3.3, the linear dependence of $1/T_2^{qe}$ with temperature matches the prediction of Equation 2.10 for undulational modes. Undulations also resolve the apparent paradox wherein ^{2}H T_2^{qe} values are almost halved in going from 0% PDPC to 75% PDPC, while $M_{2r,D}$ is virtually constant: $1/T_2^{qe}$ varies linearly with $\langle(\delta\theta)^2\rangle$ (Equation 2.12), while

$M_{2r,D}$ is reduced by a factor $\langle P_2 \cos \delta\theta \rangle^2 \approx \left\langle 1 - \frac{3(\delta\theta)^2}{2} \right\rangle^2$. Since a rough estimate (using values from [66]) gives $\langle (\delta\theta)^2 \rangle \approx 0.02$, then a two-fold decrease in T_2^{qe} due solely to membrane undulations reduces the $M_{2r,D}$ by only 6%.

In addition, the link between acyl chain polyunsaturation and membrane undulations has been demonstrated elsewhere by independent means. In mechanical measurements of membrane area expansion as a function of applied tension, Evans & Rawicz found the *curvature energy* κ_c of di-arachidonoyl-phosphatidylcholine (20:4/20:4-PC) to be roughly half that of 1-stearoyl-2-oleoyl-phosphatidylcholine (18:0/18:1-PC) [79]. That is, polyunsaturation of both chains led to a two-fold decrease in the membrane curvature energy (which from Equation 2.10 would cause the mean-squared amplitude of surface undulations to double). Furthermore, κ_c is predicted to scale linearly with the area compressibility modulus K_a [79, 67]. Koenig *et al.* measured K_a by combining X-ray and NMR techniques (see Section 1.3), and again found an almost two-fold decrease moving from mono-unsaturated SOPC-d35 (18:0-d35/18:1-PC) to polyunsaturated SDPC-d35 (18:0-d35/22:6-PC) [44]. (Note that higher values of K_a correspond to *less* compressible membranes, just as higher values of κ_c indicate less flexibility.)

It thus seems reasonable to attribute the striking decrease in T_2^{qe} values to the effect of increasing PDPC content on membrane surface undulations. If this were the sole cause of the observed changes, then the curvature energy κ_c would diminish by almost 50% in going from 0% PDPC to 75% PDPC. However, since some of the alternate mechanisms discussed earlier (but judged not to be dominant) likely did contribute to some extent, the change in κ_c is probably somewhat smaller. Finally, it should be acknowledged that T_2^{qe} measurements on membrane systems are frequently difficult to reproduce, probably due to effects of preparation and thermal history on adiabatic processes [69].

4.4.3 Relation Between Fast and Slow Motions

Clearly it is desirable to relate the hypothesized decrease in κ_c to the changes in fast chain motions proposed above. However, the task of understanding meso- or macroscopic membrane properties in molecular terms is exceedingly difficult, and comprises a field of research unto itself. Evans concludes that chain-packing irregularities and chain flexibility act to diminish membrane rigidity [67, 79], but it seems unlikely that the subtle order differences measured in this study could be the cause of such a striking increase in undulation amplitudes.

It is possible that the molecular basis for the proposed large changes in κ_c lies in a region where our experiments are not sensitive – the lipid-water interface is an obvious candidate. It is conceivable that changes in the headgroup environment could significantly influence the bending rigidity, and other investigators have proposed effects of lipid polyunsaturation on this region [76, 42, 77]. The greater cross-sectional area of polyunsaturated lipids, as reported in the literature [44] and consistent with our results, would certainly lead to increases in headgroup spacing.

4.5 Suggestions for Further Work

The results discussed above suggest a host of further experiments, which would serve to confirm and expand upon the conclusions drawn in this study. A few are quite obvious and need no explanation, such as field-dependence and T_{1Q} studies to characterize the spectral densities of fast motions, or the $T_2^{qe-cpmg}$ experiment [61] to map the correlation times of very slow motions. A few others will be discussed in slightly greater depth.

The nearly two-fold decrease in membrane curvature energy is the most striking result obtained in this study, but the analysis which led to this conclusion included many uncertainties. The most direct confirmation would be an experiment of the sort performed

by Evans & Rawicz [79]; indeed such work could lead to an in-depth research project, exploring the complementarity of T_2 experiments and micromechanical techniques for the study of membrane mechanical properties. Working within the NMR techniques applied above, a cleaner T_2^{qe} spectrum could be obtained by improving the SNR and by using a specifically-deuterated lipid in place of POPC-d_{31}. This would allow more rigorous fitting of the θ-dependence (expressing the fitting function in orthogonal components), yielding quantitative results for the fit coefficients. It would be of great interest to measure the change in the B term as a function of PDPC content in the membrane – clearly we would expect B to increase proportionally to $1/T_2^{qe}$ if undulations are indeed the cause of the faster relaxation. Finally, a FRAP (fluorescence recovery after photobleaching) experiment could provide an independent assessment of lateral diffusion rates in the membrane, which would aid in quantifying the effective correlation time τ_θ for undulations [66] as well as understanding the origin of the $\sin^2\theta\cos^2\theta$ dependence.

The proposed doubling-back motions of the DHA chains could be tested by a number of NMR approaches. (Recent work by Huster *et al.* has demonstrated the potential of ^1H MAS-NOESY cross-relaxation experiments to yield specific information on the nature of acyl chain disorder, but preliminary experiments did not find evidence for the hypothesis [75].) High resolution/magic angle spinning ^{13}C-NMR is capable of resolving the chemical shifts of the unsaturated carbons on the DHA chain [80]. A site-specific T_{1z} study with and without paramagnetic ions present in the solution should reveal whether the tail end of the DHA chain spends more time near the lipid-water interface. Along similar lines, if the synthetic work were possible one could ^{13}C-label DHA's methyl terminal as well as the headgroup on a mixed lipid such as PDPC, then selectively excite one of them and watch for transfer of the magnetization. Of course, the most direct (and informative) approach would be to specifically deuterate sites on the DHA chain for study using ^{2}H-NMR, but the biochemical synthesis is extremely difficult.

It would also be very interesting to apply the protocol from this study to a number of related systems, using the POPC-d_{31}/PDPC series as a reference. Also, DHA in the free fatty acid form has been found to influence function of several integral membrane proteins (see Section 1.2.3), but it is not known whether this effect is chemical or mechanical in nature. Similarly, cholesterol's interaction with polyunsaturates (or, more precisely, its lack thereof) is a subject of much speculation, and is thought to spur formation of lipid microdomains [48, 35, 47]. Each of these components could be added to a known POPC-d_{31}/PDPC binary mixture, and changes in the parameters discussed above could be interpreted within the existing models. Another potentially valuable spin-off experiment would be to replace PDPC with another polyunsaturated lipid (perhaps 16:0/18:3-PC), to test whether any of the effects reported here could contribute to nature's strong and specific preference for DHA in certain systems. Also (as mentioned in Section 1.4), an analogous series of experiments using PE lipids could yield novel insights into the role of headgroup composition in the properties of polyunsaturated lipids.

Finally, the recent study by Cantor (discussed in Section 1.3.3) presents the tantalizing possibility of comparing our experimental results to a specifically-designed theoretical model. Cantor's technique is readily amenable to predicting "lateral pressure profiles" for binary mixtures of lipids (indeed he presents results for several mixtures in his recent paper [49]), which are natural candidates for comparison with order parameter profiles. It is a promising sign that Cantor's predictions for the effects of polyunsaturation are qualitatively consistent with the $S(n)$ results reported above.

4.6 Relation to Biological Motivation for Study

The results and analysis described above shed considerable light on proposed bases for the functional role of DHA in certain membranes. The notion that polyunsaturated

lipid molecules occupy a wedge-shaped volume in the membrane, and influence protein conformations by exerting lateral pressure through the central portion of the bilayer, has been disproven. Indeed the reverse has been demonstrated to be true, as other membrane species were observed to have slightly greater conformational freedom as the proportion of polyunsaturated lipid was increased. The subtlety of the effect, however, was equally surprising, as average order parameters stayed nearly constant across a huge range of membrane compositions. This could be a result of our deliberate mimicry of the natural lipid composition, analogous to the easy integration of integral membrane proteins into native-like bilayers due to hydrophobic matching [67]. An alternate interpretation is that polyunsaturate-enriched microdomains are formed, isolating the other lipids from DHA's influence on a local scale. Such dynamic lipid clustering has been proposed to underlie polyunsaturated lipids' observed resistance to cholesterol condensation, and is the subject of on-going studies in several prominent research groups [48, 45, 47, 81].

Large-scale surface undulations are unlikely to occur in biological membranes (due to the scaffolding effect of the cytoskeleton), but local fluctuations in bilayer curvature could potentially couple to conformational changes of membrane proteins. Such fluctuations are linked with small density differences between membrane monolayers [79], and the associated changes in lipid packing may transiently favour certain protein transitions or states. Likewise, if the observed change in curvature energy is attributed to increased lateral compressibility of the membrane (since $\kappa_c \propto K_a$, as discussed in Section 4.4.2), then the beneficial role of polyunsaturation may relate to accommodation of changes in protein cross-sectional area [44]. On the cellular scale, the rise in membrane flexibility may facilitate vesicular fusion and budding events, of particular importance in the synaptic terminals where DHA is thought to be concentrated.

The problem of nature's striking specificity for DHA remains, however. There is no

indication of any property imbued by DHA which could not also be achieved by a different polyunsaturated species. The largest effect observed in this study – the marked increase in membrane flexibility as PDPC was added – is thought to be common to all polyunsaturated membranes. (Indeed, this belief was cited in reaching the conclusion, which could be argued to be a poor approach to finding a DHA-specific property. Nevertheless, DHA is a polyunsaturate and thus must be attributed the known or hypothesized properties of that family.)

To conclude on a speculative note, perhaps the specific requirement of certain membranes for DHA is due to a combination of mechanical and chemical roles. Various effects on membrane physical properties have been linked to DHA, but in no instance have these been markedly different for other polyunsaturates. Functional influences of DHA via binding interactions (particularly of the free fatty acid form) have also been reported (see Section 1.2.3); these would be expected to involve greater specificity. It is possible that mechanical properties provide broad selectivity for polyunsaturated lipids, while specific chemical interactions favour lipids bearing DHA chains in particular. Such an explanation is even consistent with Brown's lipid-substitution experiments (the most direct evidence against a chemical role for DHA): the stabilization of metarhodopsin-II selects for physical properties, while an as-yet-undetermined chemical role narrows the choice to DHA. Similar dual roles can certainly be imagined in the complex environment of the synaptic membrane.

While this is undeniably a shot in the dark, one general lesson which emerged in the preliminary stages of this study is that nature tends to use all available degrees of freedom. If a reasonable mechanism can be imagined but has not been observed, it seems often to be the case that we simply haven't found it yet. Both mechanical and chemical roles have been proposed for DHA – it's not inconceivable that nature employs them both.

Chapter 5

Conclusion

The experiments presented here provide an intriguing picture of the effects of DHA on the molecular and mechanical properties of membranes. Interpretation of the results has generated a model which is internally consistent, but cannot be claimed to be definitive. The questions we hoped to address at the outset of this study were outlined in Section 1.4. They are reiterated below, with discussions of what we have learned:

1. *What mechanical effects do polyunsaturated lipids (and particularly those bearing DHA chains) have on other components of the bilayer?* This study presents the first direct evidence that polyunsaturation leads to *inter*-molecular effects between phospholipids, and generated two unexpected insights.

   First, the addition of small or large amounts of PDPC were found to have little net effect on the average orientational order of the membrane, as determined from both proton and deuterium M_{2r} values. This was interpreted to mean that pure PDPC does not differ greatly from POPC in these parameters, so its introduction does not perturb the membrane greatly.

   Second, the order parameter profiles showed that the polyunsaturated lipid does *not* exert lateral pressure on its neighbours in the central region in the bilayer (*i.e.* the PDPC molecule does *not* assume a wedge shape). Instead, the DHA chains are proposed to spend a statistically greater fraction of their time doubled back toward the lipid-water interface.

2. *Does a bilayer with acyl chain composition closer to that found in neural membranes have special properties? Is there a concentration-dependent "magic mixture" effect?* In almost every case, the variation of results with PDPC content was linear to within experimental uncertainty. (The exception was T_2^{qe} times, for which nearly half of the observed change took place in going from 0% to 25% PDPC.) For the proton results alone, this led to ambiguity of interpretation as the results could be attributed either to a concentration-weighted increase in PDPC's contribution or to its influence on the other species. Reporting only from the perdeuterated chain of POPC, however, changes in deuterium results were unequivocally due to inter-species effects.

   No evidence was found for exceptional properties associated with a particular membrane composition, but such a "magic mixture", if it existed, could well involve different headgroups, other lipid classes such as sterols, etc.

3. *Can new insights be gained into the role of DHA in membranes by probing unexplored timescales (and hence distance scales)?* Measurement of the average T_2^{qe} of POPC-d_{31}'s palmitoyl chain revealed a powerful effect of PDPC content on adiabatic collective modes of the systems. These are suggested to be due primarily to increases in the amplitude of membrane surface undulations, indicating a diminishment of up to 50% in the curvature energy, κ_c, of the membrane. This conclusion is in keeping with prior studies of polyunsaturated membranes, though such an effect has not been reported in a binary lipid mixture.

The greater question, of course, is what special property of DHA underlies its remarkable prevalence in certain membrane systems. How can we understand its observed effects on visual and mental function? The above conclusions comment usefully on several leading hypotheses for DHA's role, and bring attention to the hitherto unconsidered

alternative that membrane flexibility be an important factor. It is clear, though, that much further work will be required before the secrets of this enigmatic lipid are revealed. Faced with a dearth of truly unique properties which might explain the striking specificity of nature's preference for DHA, one only wonders whether we're moving in the right direction.

Bibliography

[1] Myer Bloom, Frank Linseisen, James Lloyd-Smith, and Michael Crawford. Insights from NMR on the functional role of polyunsaturated lipids in the brain. In: Bruno Maraviglia, editor, *Magnetic Resonance and Brain Function*, Fermi International School of Physics, Varenna, Italy, 1998. Italian Physical Society.

[2] O.G. Mouritsen. Self-assembly and organization of lipid-protein membranes. *Current Opinion in Colloid and Interface Science*, 3:78–87, 1998.

[3] Myer Bloom. Evolution of membranes from a physics perspective. In: Ole G. Mouritsen and Olaf S. Andersen, editors, *In Search of a New Biomembrane Model*, volume 49, pages 13–17. The Royal Danish Academy of Sciences and Letters, Copenhagen, 1998.

[4] J. M. Bourre, M. Bonneil, J. Chaudiere, M. Clement, O. Dumont, G. Durand, H. Lafont, G. Nalbone, G. Pascal, and M. Piciotti. Structural and functional importance of dietary polyunsaturated fatty acids in the nervous system. In: N.G. Bazan and G. Toffano, editors, *Neurobiology of Essential Fatty Acids*, pages 211–229. Plenum Press, New York, 1992.

[5] N. Salem, H.-Y. Kim, and J.A. Yergey. Docosahexaenoic acid: Membrane function and metabolism. In: A.P. Simopoulos, R.R. Kifer, and R.E. Martin, editors, *Health Effects of Polyunsaturated Fatty Acids in Seafoods*, pages 263–317. Academic Press, New York, 1986.

[6] Michael F. Brown. Modulation of rhodopsin function by properties of the membrane bilayer. *Chemistry and Physics of Lipids*, 73:159–180, 1994.

[7] Bruce Alberts, Dennis Bray, Julian Lewis, Martin Raff, Keith Roberts, and James D. Watson. *Molecular Biology of the Cell.* Garland, 1994.

[8] Harold W. Cook. Fatty acid desaturation and chain elongation in eukaryotes. In: D.E. Vance and J.E. Vance, editors, *Biochemistry of Lipids*, pages 129–152. Elsevier Science B.V., 1996.

[9] M. A. Crawford, N. M. Casperd, and A. J. Sinclair. The long chain metabolites of linoleic and linolenic acids in liver and brain in herbivores and carnivores. *Comp Biochem Physiol [B]*, 54(3):395–401, 1976.

[10] S. A. Keys, E. Boley, and W. F. Zimmerman. A model membrane system to investigate antioxidants in bovine rod outer segments. *Exp Eye Res*, 64:313–21, 1997.

[11] S.-Y. Cho, K. Miyashita, T. Miyazawa, K. Fujimoto, and T. Kaneda. Autoxidation of ethyl eicosapentaenoate and docosahexaenoate. *J Am Oil Chem Soc*, 64:876–879, 1987.

[12] M.A. Crawford and D.E. Marsh. *The Driving Force.* Heineman, London, 1989.

[13] N.G. Bazan, W.C. Gordon, and E.B. Rodriguez de Turco. In: N.G. Bazan and G. Toffano, editors, *Neurobiology of Essential Fatty Acids*, pages 295–306. Plenum Press, New York, 1992.

[14] N. Yamamoto, M. Saitoh, A. Moriuchi, M. Nomura, and H. Okuyama. Effect of dietary alpha-linolenate/linoleate balance on brain lipid compositions and learning ability of rats. *J Lipid Res*, 28:144–51, 1987.

[15] S. Yoshida, M. Miyazaki, M. Takeshita, S. Yuasa, T. Kobayashi, S. Watanabe, and H. Okuyama. Functional changes of rat brain microsomal membrane surface after learning task depending on dietary fatty acids. *J Neurochem*, 68:1269–77, 1997.

[16] J. M. Bourre, M. Francois, A. Youyou, O. Dumont, M. Piciotti, G. Pascal, and G. Durand. The effects of dietary alpha-linolenic acid on the composition of nerve membranes, enzymatic activity, amplitude of electrophysiological parameters, resistance to poisons and performance of learning tasks in rats. *J Nutr*, 119:1880–92, 1989.

[17] M. Neuringer, W. E. Connor, D. S. Lin, L. Barstad, and S. Luck. Biochemical and functional effects of prenatal and postnatal omega 3 fatty acid deficiency on retina and brain in rhesus monkeys. *Proc Natl Acad Sci U S A*, 83:4021–5, 1986.

[18] R. Uauy, P. Peirano, D. Hoffman, P. Mena, D. Birch, and E. Birch. Role of essential fatty acids in the function of the developing nervous system. *Lipids*, 31:S167–76, 1996.

[19] S. E. Carlson, S. H. Werkman, J. M. Peeples, and W. M. Wilson. Long-chain fatty acids and early visual and cognitive development of preterm infants. *Eur J Clin Nutr*, 48:S27–30, 1994.

[20] M. Neuringer, S. Reisbick, and J. Janowsky. The role of n-3 fatty acids in visual and cognitive development: current evidence and methods of assessment. *J Pediatr*, 125:S39–47, 1994.

[21] S. Yoshida, A. Yasuda, H. Kawazato, K. Sakai, T. Shimada, M. Takeshita, S. Yuasa, T. Kobayashi, S. Watanabe, and H. Okuyama. Synaptic vesicle ultrastructural

changes in the rat hippocampus induced by a combination of alpha-linolenate deficiency and a learning task. *J Neurochem*, 68:1261–8, 1997.

[22] M. M. Jensen, T. Skarsfeldt, and C. E. Hoy. Correlation between level of (n - 3) polyunsaturated fatty acids in brain phospholipids and learning ability in rats. a multiple generation study. *Biochim Biophys Acta*, 1300(3):203–9, 1996.

[23] H. Suzuki, S. J. Park, M. Tamura, and S. Ando. Effect of the long-term feeding of dietary lipids on the learning ability, fatty acid composition of brain stem phospholipids and synaptic membrane fluidity in adult mice: a comparison of sardine oil diet with palm oil diet. *Mech Ageing Dev*, 101:119–128, 1998.

[24] M. Martinez. In: N.G. Bazan and G. Toffano, editors, *Neurobiology of Essential Fatty Acids*, pages 347–359. Plenum Press, New York, 1992.

[25] M. Martinez. Polyunsaturated fatty acids in the developing human brain, erythrocytes and plasma in peroxisomal disease: therapeutic implications. *J. Inher. Metab. Dis.*, 18:61–75, 1995.

[26] M. Martinez and E. Vazquez. MRI evidence that docosahexaenoic acid ethyl ester improves myelination in generalized peroxisomal disorders [see comments]. *Neurology*, 51(1):26–32, 1998.

[27] M. Soderberg, C. Edlund, K. Kristensson, and G. Dallner. Fatty acid composition of brain phospholipids in aging and in Alzheimer's disease. *Lipids*, 26:421–5, 1991.

[28] T.D. Lamb and E.N. Pugh. A quantitative account of the activation steps involved in phototransduction in amphibian photoreceptor. *Journal of Physiology*, 449, 1992.

[29] Y. F. Xiao, A. M. Gomez, J. P. Morgan, W. J. Lederer, and A. Leaf. Suppression of voltage-gated L-type Ca^{2+} currents by polyunsaturated fatty acids in adult and neonatal rat ventricular myocytes. *Proc Natl Acad Sci U S A*, 94:4182–7, 1997.

[30] J. S. Poling, S. Vicini, M. A. Rogawski, and Jr. Salem, N. Docosahexaenoic acid block of neuronal voltage-gated K^+ channels: subunit selective antagonism by zinc. *Neuropharmacology*, 35:969–82, 1996.

[31] C. R. Jones, T. Arai, and S. I. Rapoport. Evidence for the involvement of docosahexaenoic acid in cholinergic stimulated signal transduction at the synapse. *Neurochem Res*, 22:663–70, 1997.

[32] S. J. Slater, M. B. Kelly, M. D. Yeager, J. Larkin, C. Ho, and C. D. Stubbs. Polyunsaturation in cell membranes and lipid bilayers and its effects on membrane proteins. *Lipids*, 31:S189–92, 1996.

[33] M. Nishikawa, S. Kimura, and N. Akaike. Facilitatory effect of docosahexaenoic acid on N-methyl-D-aspartate response in pyramidal neurones of rat cerebral cortex. *J Physiol (Lond)*, 475:83–93, 1994.

[34] C. Young, P.-W. Gean, S.-P. Wu, C.-H. Lin, and Y.-Z. Shen. Cancellation of low-frequency stimulation-induced long-term depression by docosahexaenoic acid in rat hippocampus. *Neuroscience Letters*, 247:198–200, 1998.

[35] D. C. Mitchell, K. Gawrisch, B. J. Litman, and Jr. Salem, N. Why is docosahexaenoic acid essential for nervous system function? *Biochem Soc Trans*, 26:365–70, 1998.

[36] C. Nielsen, M. Goulian, and O. S. Andersen. Energetics of inclusion-induced bilayer deformations [published erratum appears in Biophys J 1999 Apr;76(4):2317].

Biophys J, 74:1966–83, 1998.

[37] Kenneth R. Applegate and John A. Glomset. Computer-based modeling of the conformation and packing properties of docosahexaenoic acid. *Journal of Lipid Research*, 27:658–680, 1986.

[38] Kenneth R. Applegate and John A. Glomset. Effect of acyl chain unsaturation on the conformation of model diacylglycerols: a computer modeling study. *Journal of Lipid Research*, 32:1635–1644, 1991.

[39] Kenneth R. Applegate and John A. Glomset. Effect of acyl chain unsaturation on the packing of model diacylglycerols in simulated monolayers. *Journal of Lipid Research*, 32:1645–1655, 1991.

[40] John E. Baenziger, Harold C. Jarrell, Robin J. Hill, and Ian C. P. Smith. Average structural and motional properties of a diunsaturated acyl chain in a lipid bilayer: Effects of two cis-unsaturated double bonds. *Biochemistry*, 30:894–903, 1991.

[41] John E. Baenziger, Harold C. Jarrell, and Ian C. P. Smith. Molecular motions and dynamics of a diunsaturated acyl chain in a lipid bilayer: Implications for the role of polyunsaturation in biological membranes. *Biochemistry*, 31:3377–3385, 1992.

[42] Laura L. Holte, A. Peter Senaka, Teresa M. Sinnwell, and Klaus Gawrisch. ^{2}H nuclear magnetic resonance order parameter profiles suggest a change of molecular shape for phosphatidylcholines containing a polyunsaturated chain. *Biophysical Journal*, 68:2396–2403, 1995.

[43] L. L. Holte, F. Separovic, and K. Gawrisch. Nuclear magnetic resonance investigation of hydrocarbon chain packing in bilayers of polyunsaturated phospholipids. *Lipids*, 31:199–203, 1996.

[44] Bernd W. Koenig, Helmut H. Strey, and Klaus Gawrisch. Membrane lateral compressibility determined by NMR and X-ray diffraction. effect of acyl chain polyunsaturation. *Biophysical Journal*, 73(4):1954, 1997.

[45] D. Huster, K. Arnold, and K. Gawrisch. Influence of docosahexaenoic acid and cholesterol on lateral lipid organization in phospholipid mixtures. *Biochemistry*, 37(49):17299–308, 1998.

[46] Burton J. Litman and Drake C. Mitchell. A role for phospholipid polyunsaturation in modulating membrane protein function. *Lipids*, 31:S193–S197, 1996.

[47] D. C. Mitchell and B. J. Litman. Effect of cholesterol on molecular order and dynamics in highly polyunsaturated phospholipid bilayers. *Biophys J*, 75:896–908, 1998.

[48] J. M. Smaby, M. M. Momsen, H. L. Brockman, and R. E. Brown. Phosphatidylcholine acyl unsaturation modulates the decrease in interfacial elasticity induced by cholesterol. *Biophys J*, 73(3):1492–505, 1997.

[49] R. S. Cantor. Lipid composition and the lateral pressure profile in bilayers. *Biophys J*, 76:2625–39, 1999.

[50] R. S. Cantor. Lateral pressures in cell membranes: a mechanism for modulation of protein function. *J. Phys. Chem B*, 101:1723–1725, 1997.

[51] Michael Crawford, 1998.

[52] A. Abragam. *The Principles of Nuclear Magnetism.* Oxford University Press, Oxford, 1961.

[53] Clare Morrison. *Theory of the General Orientation Dependence of ^{2}H-NMR Spin-Lattice Relaxation and Experiments on Model Membranes.* Ph. D., University of British Columbia, 1993.

[54] B. Klosgen, C. Reichle, S. Kohlsmann, and K. D. Kramer. Dielectric spectroscopy as a sensor of membrane headgroup mobility and hydration. *Biophys J*, 71:3251–60, 1996.

[55] Myer Bloom, Elliott E. Burnell, S. B. W. Roeder, and M. I. Valic. Nuclear magnetic resonance line shapes in lyotropic liquid crystals and related systems. *Journal of Chemical Physics*, 66:3012–3020, 1977.

[56] Myer Bloom, Elliott E. Burnell, Alexander L. MacKay, Christine P. Nichol, Marko I. Valic, and Gerald Weeks. Fatty acyl chain order in lecithin model membranes determined from proton magnetic resonance. *Biochemistry*, 17:5750–5762, 1978.

[57] A. L. MacKay. A proton NMR moment study of the gel and liquid-crystalline phases of dipalmitoyl phosphatidylcholine. *Biophysical Journal*, 35:301–313, 1981.

[58] James H. Davis. The description of membrane lipid conformation, order and dynamics by ^{2}H-NMR. *Biochimica et Biophysica Acta*, 737:117–171, 1983.

[59] M. F. Brown, A. A. Ribeiro, and G. D. Williams. New view of lipid bilayer dynamics from ^{2}H and ^{13}C-NMR relaxation time measurements. *Proceedings of the National Academy of Sciences of the United States of America*, 80:4325–4329, 1983.

[60] K. P. Pauls, A. L. MacKay, O. Soederman, Myer Bloom, A. K. Tanjea, and R. S. Hodges. Dynamic properties of the backbone of an integral membrane polypeptide measured by ^{2}H-NMR. *European Biophysical Journal*, 12:1–11, 1985.

[61] Myer Bloom and Edward Sternin. Transverse nuclear spin relaxation in phospholipid bilayer membranes. *Biochemistry*, 26:2101–2105, 1987.

[62] Clare Morrison and Myer Bloom. Orientation dependence of ^{2}H nuclear magnetic resonance spin-lattice relaxation in phospholipid and phospholipid:cholesterol systems. *Journal of Chemical Physics*, 101:749–763, 1994.

[63] Myer Bloom, Clare Morrison, Edward Sternin, and Jenifer L. Thewalt. Spin echoes and the dynamic properties of membranes. In: D. M. S. Bagguley, editor, *Pulsed Magnetic Resonance: NMR, ESR and Optics*, pages 274–316. Clarendon Press, Oxford, 1992.

[64] A.A. Nevzorov and M.F. Brown. Dynamics of lipid bilayers from comparative analysis of ^{2}H and ^{13}C nuclear magnetic resonance relaxation data as a function of frequency and temperature. *J. Chem. Phys.*, 107:10288–10310, 1997.

[65] Eiichi Fukushima and Stephen B.W. Roeder. *Experimental Pulse NMR; A Nuts and Bolts Approach.* Addison-Wesley Publishing Company, Inc., Reading, Massachusetts, 1 edition, 1981.

[66] Myer Bloom and Evan Evans. Observation of surface undulations on the mesoscopic length scale by NMR. In: L. Peliti, editor, *Biologically Inspired Physics*, pages 137–147. Plenum Press, New York, 1991.

[67] Myer Bloom, Evan Evans, and Ole G. Mouritsen. Physical properties of the fluid lipid-bilayer component of cell membranes: A perspective. *Quarterly Reviews of Biophysics*, 24:293–397, 1991.

[68] Myrna A. Monck. *Studies of the Orientational Order and Bilayer Thickness in Biological Model Membranes.* Ph. D., University of British Columbia, 1993.

[69] Myer Bloom and Thomas Bayerl. Membranes studied using neutron scattering and NMR. *Can. J. Phys.*, 73:687–696, 1995.

[70] Erich Sackmann. Physical foundations of the molecular organization and dynamics of membranes. In: Walter Hoppe, editor, *Biophysics*, pages 425–457. Springer Verlag, Heidelberg, 1983.

[71] A.E. Drobnies, B. Van der Ende, J.L. Thewalt, and R.B. Cornell. CTP:phosphocholine cytidylyltransferase activation by oxidized phosphatidylcholines correlates with a decrease in lipid order: A ^{2}H NMR analysis. *submitted*, 1999.

[72] W. H. Press, B. P. Flannery, S. A. Teukolsky, and W. T. Vetterling. *Numerical recipes*. Cambridge University Press, Cambridge, 1981.

[73] Michel Lafleur, Bernard Fine, Edward Sternin, Pieter R. Cullis, and Myer Bloom. Smoothed orientational order parameter profile of lipid bilayers by ^{2}H-nuclear magnetic resonance. *Biophysical Journal*, 56:1037–1041, 1989.

[74] Frank A. Nezil, Clare Morrison, Kenneth P. Whittall, and Myer Bloom. Relaxation spectra in model membranes by deuterium nuclear magnetic resonance. *Journal of Magnetic Resonance*, 93:279–290, 1991.

[75] Daniel Huster and Klaus Gawrisch. NOESY crosspeaks between lipid headgroups and hydrocarbon chains - spin diffusion or molecular disorder? *Experimental NMR Conference*, Abstract 116, 1999.

[76] William Ehringer, Daniel Belcher, Stephen R. Wassall, and William Stillwell. A comparison of the effects of linolenic (18:3n-3) and docosahexaenoic (22:6n-3) acids on phospholipid bilayers. *Chemistry and Physics of Lipids*, 54:79–88, 1990.

[77] Daniel Huster, Albert J. Jin, Klaus Arnold, and Klaus Gawrisch. Water permeability of polyunsaturated lipid membranes measured by ^{17}O NMR. *Biophysical Journal*, 73:855–864, 1997.

[78] J. Stohrer, G. Groebner, D. Reimer, K. Weisz, C. Mayer, and G. Kothe. Collective lipid motions in bilayer membranes studied by transverse deuteron spin relaxation. *Journal of Chemical Physics*, 95:672–678, 1991.

[79] E. Evans and W. Rawicz. Entropy-driven tension and bending elasticity in condensed-fluid membranes. *Phys. Rev. Letters*, 64:2094–2097, 1990.

[80] F. D. Gunstone. High resolution ^{13}C NMR. a technique for the study of lipid structure and composition. *Prog Lipid Res*, 33:19–28, 1994.

[81] D. C. Mitchell and B. J. Litman. Molecular order and dynamics in bilayers consisting of highly polyunsaturated phospholipids. *Biophys J*, 74:879–91, 1998.

[82] C. P. Slichter. *Principles of Magnetic Resonance.* Springer Verlag, Heidelberg, 3 edition, 1989.

[83] Joachim Seelig. Deuterium magnetic resonance: Theory and application to lipid membranes. *Quarterly Reviews of Biophysics*, 10:353–418, 1977.

[84] Joachim Seelig and Anna Seelig. Lipid conformation in model membranes and biological membranes. *Quarterly Reviews of Biophysics*, 13:19–61, 1980.

[85] Myer Bloom. NMR studies of membranes and whole cells. In: B. Maraviglia, editor, *Physics of NMR Spectroscopy in Biology and Medicine*, pages 293–397. North-Holland, 1988.

[86] R. B. Gennis. *Biomembranes.* Springer-Verlag, New York, 1989.

[87] Myer Bloom and J. Thewalt. Spectroscopic determination of lipid dynamics in membranes. *Chemistry and Physics of Lipids*, 73:27–38, 1994.

[88] Myer Bloom and Jenifer L. Thewalt. Time and distance scales of membrane domain organization. *Mol Membr Biol*, 12(1):9–13, 1995.

[89] E. Sternin, Myer Bloom, and A. L. MacKay. De-pake-ing of NMR spectra. *Journal of Magnetic Resonance*, 55:274–282, 1983.

[90] Frank M. Linseisen, Jenifer L. Thewalt, Myer Bloom, and Thomas M. Bayerl. ^{2}H-NMR and DSC study of SEPC-cholesterol mixtures. *Chemistry and Physics of Lipids*, 65:141–149, 1993.

[91] Michel Lafleur, Pieter R. Cullis, and Myer Bloom. Modulation of the orientational order parameter profile of the lipid acyl chain in the l-alpha phase. *European Biophysical Journal*, 19:55–62, 1990.

[92] A. Seelig and J. Seelig. The dynamic structure of fatty acyl chains in a phospholipid bilayer measured by deuterium magnetic resonance. *Biochemistry*, 13:4839–45, 1974.

[93] H. Schindler and J. Seelig. Deuterium order parameters in relation to thermodynamic properties of a phospholipid bilayer. a statistical mechanical interpretation. *Biochemistry*, 14:2283–7, 1975.

[94] John Hjort Ipsen, Ole G. Mouritsen, and Myer Bloom. Relationships between lipid membrane area, hydrophobic thickness, and acyl-chain orientational order. *Biophysical Journal*, 57:405–412, 1990.

[95] M. B. Sankaram and T. E. Thompson. Deuterium magnetic resonance study of

phase equilibria and membrane thickness in binary phospholipid mixed bilaryers. *Biochemistry*, 31:8258–8268, 1992.

[96] Dalian Lu, Irene Vavasour, and Michael R. Morrow. Smoothed acyl chain orientational order parameter profiles in dimyristoyl-phosphatidylcholine/distearoyl-phosphatidylcholine mixtures: A ^{2}H-NMR study. *Biophysical Journal*, 68:574–583, 1995.

[97] Ole G. Mouritsen and Myer Bloom. Mattress model of lipid-protein interactions in membranes. *Biophysical Journal*, 46:141–153, 1984.

[98] Ole G. Mouritsen and Myer Bloom. Models of lipid-protein interactions in membranes. *Annual Review of Biophysics and Biomolecular Structure*, 22:145–171, 1993.

[99] Myer Bloom and Ole G. Mouritsen. The evolution of membranes. In: R. Lipowsky and Erich Sackmann, editors, *Handbook of Biological Physics*, pages 65–95. Elsevier Science B. V., 1995.

[100] J. Ulmius, H. Wennerstrom, G. Lindblom, and G. Arvidson. Proton NMR band-shape studies of lamellar liquid crystals and gel phases containing lecithins and cholesterol. *Biochim Biophys Acta*, 389:197–202, 1975.

[101] Jeffrey Forbes, John Bowers, Xi Shan, Liam Moran, and Eric Oldfield. Some new developments in solid-state nuclear magnetic resonance spectroscopic studies of lipids and biological membranes, including the effects of cholesterol in model and natural systems. *Journal of the Chemical Society, Faraday Transactions 1*, 84:3821–3849, 1988.

[102] J. H. Davis, M. Auger, and R. S. Hodges. High resolution ^{1}H nuclear magnetic resonance of a transmembrane peptide. *Biophys J*, 69:1917–32, 1995.

Appendix A

Theory: Information on Fluid Membranes from NMR Spectra

(Appendix A has been contributed by Dr. Myer Bloom, and is an excerpt from an earlier paper [1].)

A.1 NMR Background and Goals

We shall assume that the reader has a good background understanding of basic NMR. Many excellent introductory books [52, 82] and articles on NMR are available, including some in which broadline NMR of special importance in the study of biological membranes is emphasized [83, 84, 85]. Our intent is simply to summarize concisely in this section the nature of the information obtainable from NMR [67] on the physical properties of biological membranes.

A.2 Membrane Fluidity and Correlation Times

There is convincing evidence from NMR [83, 84, 85, 67] and a myriad of other physical measurements (see [86] for a large number of references) that biological membranes are invariably fluid under physiological conditions.

At the macroscopic level, *fluidity* in this context implies that membranes do not support shear restoring forces. Model membranes consisting of a single type of lipid (*e.g.* saturated lipids such as DPPC and mono-unsaturated ones such as POPC) have an apparent viscosity of about 1 poise, a typical value for fairly thick oil. Their lipid

molecules have been shown (using standard NMR methods) to diffuse parallel to the membrane surface with an effective diffusion constant D of about $4 \times 10^{-12} m^2 s^{-1}$.

At the molecular level, lipids undergo several types of motion having a hierarchy of correlation times [83, 84, 85, 67, 86, 62, 66, 78]. We list below typical correlation times for various motions studied for representative model membranes. NMR has played an important role in the determination of the correlation times for the motions listed below via standard relaxation time measurements (T_1, T_2, $T_{1\rho}$, *etc.*). Some of these motions may be modified in biological membranes which often consist of many types of lipids, as well as up to about 50% protein (by weight). In addition, large quantities of sterols such as cholesterol [67] are found in the plasma membranes of all eukaryotic cells. Although biological membranes can be complex aggregates of lipids, sterols and proteins (see Figure 1.1), their lipid bilayer cores [67] are invariably fluid and are characterized partially by the following motions and correlation times:

1. The fatty acyl chains and polar head groups of the lipid molecules undergo rapid conformational changes, often referred to as "*trans-gauche* isomerization"[1]. Typical correlation times for conformational changes fall in the range 10^{-10} to 10^{-9} s.

2. The lipid molecules rotate about the local membrane surface normal $\hat{n}$ with correlation times in the range 10^{-9} to 10^{-8} s. Think about a cloud of molecular conformations undergoing rotational diffusion about $\hat{n}$.

3. The membrane surface exhibits highly damped undulations with a spectrum of wavelengths and associated correlation times ranging from microseconds to seconds for vesicles as large as $10\,\mu$m [67, 78]. The lower limit is set by the membrane thickness and the upper limit by the vesicle size.

[1]These conformations refer to rotations about individual C-C bonds. They should not be confused with *trans* or *cis* double bonds

A.3 Time and Distance Scales Associated with NMR Spectra in Membranes

The recording and interpretation of a spectrum of any type implicitly involves a spectroscopic time scale [87, 88]. For membranes, there is an associated length scale which must be kept in mind.

Suppose that the spectral lines associated with different molecular states extend over a range of angular frequencies $\Delta\omega$ and that the rate at which the system undergoes transitions among all these states corresponds to a correlation time τ_c. The spread of frequencies allows us to define a spectroscopic time scale $\tau_s \approx 1/\Delta\omega$. For long correlation times ($\tau_c \gg \tau_s$), the spectrum is an appropriately weighted superposition of spectral lines associated with the individual states and has a width of order $\Delta\omega$. For short correlation times ($\tau_c \ll \tau_s$), the spectrum is a suitably weighted "average spectrum" of all the accessible states. This narrowing effect of the motion is called "motional averaging" or "motional narrowing" [52, 82].

Deuterium (^{2}H-)NMR of acyl chains on lipid molecules in fluid membranes is characterized by a coupling constant $\omega_Q \approx 2\pi \times 125\,\text{kHz}$, giving $\tau_s \approx 10^{-6}\,\text{s}$. The spectrum is motionally narrowed due to conformational and rotational motion of the lipid molecules since $\tau_c \ll \tau_s$ for these motions (see section A.2). As discussed below, the quadrupolar splitting of a given deuteron is decreased by a factor $|S_{CD}|$ called an "orientational order parameter" for that C-D bond. $|S_{CD}|$ can take on values in the range $0 \leq |S_{CD}| \leq 0.5$ for methylene groups in the fluid membrane lamellar phase. Analogous dipolar order parameters, $|S_{HH}|$ and $|S_{CH}|$, may be defined from proton (^{1}H)- and (^{13}C)-NMR spectra, respectively, and are associated with given H-H and C-H vectors in the molecule. NMR has provided major insights into the physical properties of fluid membranes via the measurement of such orientational order parameters, which are quite sensitive to interactions between lipids and molecular components of membranes (lipids, proteins and sterols). In

effect, NMR provides a quantitative measure of the anisotropy of membrane fluidity as a function of position on the acyl chain.

We have tried to illustrate the extremely inhomogeneous nature of biological membranes in Figure 1.1. The question arises as to whether this inhomogeneity manifests itself in a complex NMR spectrum. Suppose, for example, that the difference between the quadrupolar splitting close to and far from a protein corresponds to $\Delta\omega \approx 10^4\,\mathrm{s}^{-1}$ or, equivalently, $\tau_s \approx 10^{-4}\,\mathrm{s}$. Such a change in splitting of $\Delta\nu \approx 10^4\,\mathrm{s}^{-1}/(2\pi) \approx 1.6\,\mathrm{kHz}$ is very easy to measure. Nevertheless, superpositions of NMR spectra reflecting membrane inhomogeneity of the type shown in Figure 1.1 are normally not seen in biological membranes. The reason for this is that the molecules diffuse a distance corresponding to $L_s \approx \sqrt{6D\tau_s} = \sqrt{\frac{6D}{\Delta\omega}} \approx 500\,\text{Å}$ during the spectroscopic time scale required to distinguish different regions – farther if $\Delta\omega$ is smaller. Effectively, NMR averages $|S_{CD}|$ over a large number of lipid, protein and/or sterol interactions. So, contrary to the intuition of most spectroscopists, NMR does not really provide molecular information about membranes. It provides molecular information averaged over a large number of interacting molecules spread over mesoscopic distances [67].

A.4 ^{2}H-NMR of Acyl Chains on Lipid Molecules in Fluid Membranes

Consider a deuteron on a methylene $(CH_2)_k$ group, $k = 2, 3 \ldots (N-1)$, of acyl chain $COO(CH_2)_{N-2}CH_3$. Its NMR spectrum in a fluid membrane, whose surface normal $\hat{n}$ makes an angle θ with the external magnetic field, is a doublet (see Figure A.1a) at angular frequencies $\omega_\pm$ symmetrically displaced from the Larmor frequency ω_0:

$$\omega_\pm = \omega_0 \pm \omega_Q P_2(\mu) S_{CD}(k) \tag{A.1}$$

where $P_2(\mu) = (3\mu^2 - 1)/2$, $\mu = \cos\theta$ and the orientational order parameter $S_{CD}(k) =$

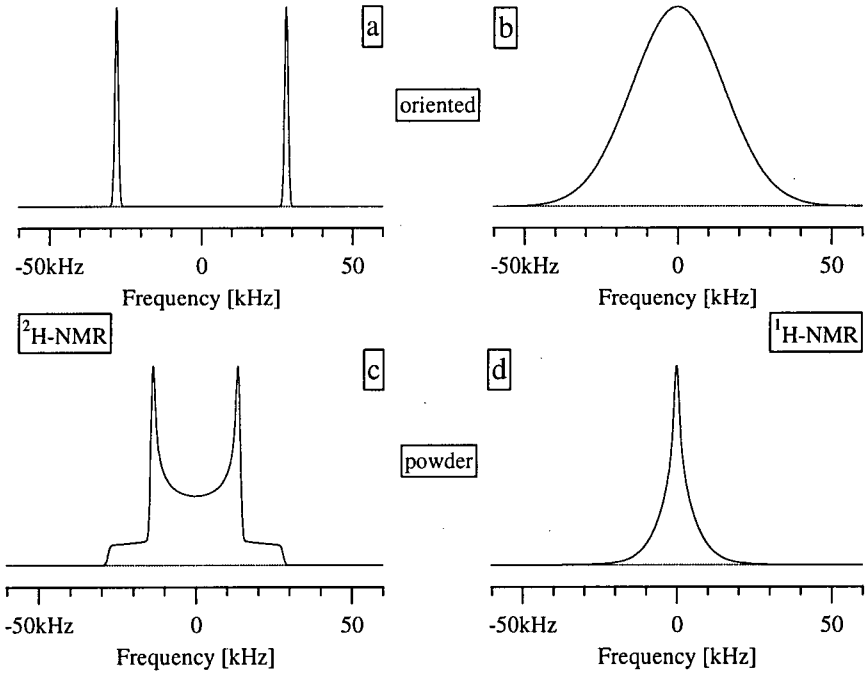

Figure A.1: Simulated broadline ^{1}H- and ^{2}H-NMR spectra. The top row shows the spectra corresponding to samples being oriented with bilayer normal $\hat{n}$ parallel to the magnetic field: **(a)**: Doublet for the case of ^{2}H-NMR; **(b)**: Gaussian lineshape, representing the type of smooth featureless spectra associated with dipolar broadening in ^{1}H-NMR. The bottom row shows the results of calculating the powder spectra (random orientation) from the top row oriented spectra **(c)**: *Pake Doublet* lineshape; **(d)**: "Superlorentzian" lineshape.

$\langle P_2(\mu_k)\rangle$. The average in $S_{CD}(k)$ is taken over the distribution of values of $\mu_k = \cos\chi_k(t)$ implicit in the motional averaging discussed in sections A.2 and A.3 where $\chi_k(t)$ is the instantaneous angle between the C-D bond direction and the symmetry axis $\hat{n}$ for motional averaging.

The superposition of doublets for a uniform distribution of values of μ in the range $\{-1 \leq \mu \leq 1\}$ (isotropic distribution of surface normals) corresponds to the well known *Pake Doublet* lineshape with splittings:

$$|\omega_+ - \omega_-| = 2\omega_Q|S_{CD}(k)||P_2(\mu)| \tag{A.2}$$

as illustrated in Figure A.1c. It exhibits an integrable singularity at $\theta = 90^o$ or $P_2(\mu) = -0.5$ corresponding to $|\delta\omega| = \omega_Q|S_{CD}(k)|$. Because of the singularity, it has proven to be relatively simple to De-Pake the *Pake Doublet*, or even a superposition of *Pake Doublets* [89], in a reliable manner, yielding a spectrum equivalent to that of an oriented sample. From such a complex spectrum (see Figure A.2b) one can use the method of Lafleur *et al.* [73] to extract the superposition of "smoothed values" of $|S_{CD}|$, shown in Figure A.2c.

Various aspects of ^{2}H-NMR spectra of acyl chains in fluid phospholipid membranes (DPPC in this case) are illustrated in Figure A.2. The $|S_{CD}(k)|$ profile varies with temperature, head group (*e.g.* PC, PS, PE – see Figure 1.2) and cholesterol concentration (see Figure A.2d). Increasing cholesterol concentration or PE/PC ratio and decreasing temperature all lead to an increase in the $|S_{CD}(k)|$ values along the entire acyl chain, leaving the shape of $|S_{CD}(k)|$ basically unchanged. The reasons for these increases in $|S_{CD}|$ values can be stated in very simple physical and geometrical terms:

- Cholesterol has a smooth ring structure so that lipid-cholesterol interactions favour the all-*trans* chain conformations.

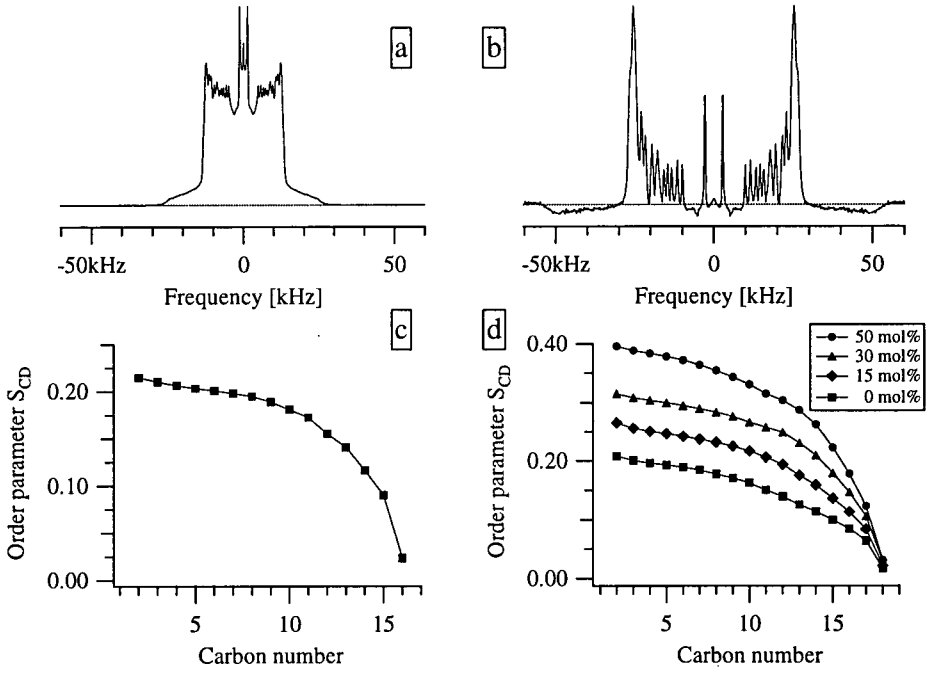

Figure A.2: Typical ^{2}H-NMR spectra and smoothed order parameter profiles. Figures **(a)**, **(b)** and **(c)** show results for chain perdeuterated DPPC (16:0-d_{31}/16:0-d_{31}-PC) at $T = 50°$C: **(a)**: Superposition of *Pake Doublets*, produced by multi-lamellar vesicles; **(b)**: Result of "De-Paking" the spectrum shown in (a); **(c)**: smoothed order parameter profile, as calculated from Figure (b). **(d)**: Smoothed order parameter profiles for a number of different mixtures of SEPC (16:0-d_{31}/18:1-PC) and cholesterol (cholesterol percentage given) at $T = 50°$C [90]. Note that the carbon number in (c) and (d) represents the ordering of the magnitudes of the quadrupolar splitting and not necessarily the chain position [73].

- The PE head group has a smaller area than that of PC so that more crowding of lipids in the presence of PE also causes the acyl chains to stretch out.
- Lower temperatures favour the lowest energy all-*trans* conformations.

A remarkable feature of the $|S_{CD}(k)|$ profiles is that, even though these three perturbations of orientational order involve different parts of the POPC molecules, the shapes of the $|S_{CD}(k)|$ profiles are virtually identical [91]. It is as though only a single parameter is required to specify changes of $|S_{CD}(k)|$ for the entire acyl chain in the case of a simple model membrane in the fluid phase. For convenience in what follows, we choose this parameter to be the chain averaged magnitude of $S_{CD}(k)$, *i.e.* $S = \langle |S_{CD}(k)| \rangle$.

A.5 Orientational Order of Acyl Chains and Hydrophobic Thickness of Fluid Membranes

Seelig and other researchers [84, 92, 93, 94] have shown that the hydrophobic bilayer thickness d is linearly related to the average order parameter as follows:

$$d = d_{max}(\alpha S + \beta) \tag{A.3}$$

This was derived by approximating the conformational states of the acyl chain by positions on a diamond lattice, and identifying the hydrophobic thickness of a monolayer, $d/2$, as the average projection of the end-to-end vector of the acyl chain along the bilayer normal $\hat{n}$. In eq. A.3, $d_{max} \approx 2.5\,\text{Å} \times (N-1)$ is the maximum hydrophobic bilayer thickness corresponding to acyl chains in their all-*trans* conformation. In this fully extended conformation the C-D bonds are perpendicular to the axis of reorientation and give a value of $|S_{CD}| = 0.5$ for all chain positions. The value of $S_{max} = 0.5$ for an all-*trans* acyl chain rotating about its long axis leads to the following relation between α and β: $\alpha/2 + \beta = 1$ (*e.g.* consistent with $\alpha = 1.0$ and $\beta = 0.5$).

The use of NMR to determine membrane hydrophobic thickness via eq. A.3 should be regarded as a semi-empirical, secondary method and its application to mixtures of lipids requires further work [95, 96], both theoretical and experimental. A recent comparison with X-ray diffraction [44] has demonstrated the relative sensitivity, reliability and ease of use of the NMR method for pure lipid bilayer membranes, even for lipids consisting of one unsaturated and one saturated chain.

The success of Seelig's method of determining membrane thickness has allowed NMR spectroscopists to explore mechanical properties of fluid membranes [94, 44, 74, 90]. Furthermore, it has generated a major advance in the quantitative description of lipid-protein interactions, namely that integral membrane proteins invariably have hydrophobic regions that are matched to the hydrophobic regions of the lipid bilayer membrane in which they are located [97, 98, 99, 2]. We believe that this hydrophobic matching comes about as a result of the optimization of the physical properties of membranes via evolution [99]. A schematic illustration of hydrophobic matching and how lipid-protein interactions couple proteins to mechanical aspects of membranes is given in Figure A.3.

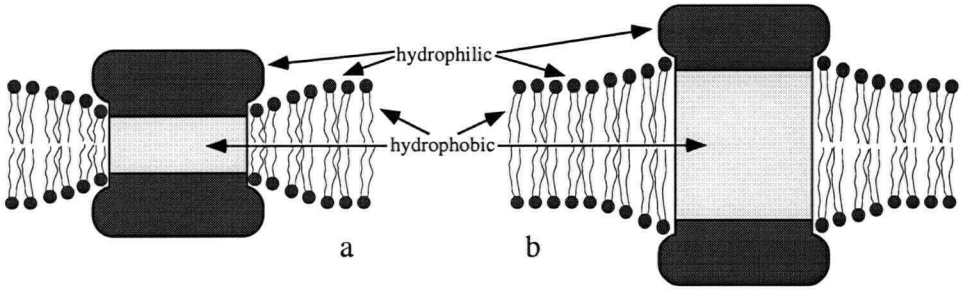

Figure A.3: Schematic illustration of hydrophobic matching. The dark parts of the lipids and the integral membrane proteins are hydrophilic, the lipid chains and the light regions of the proteins are hydrophobic. Figure **(a)** shows the case of a protein having a smaller hydrophobic thickness than the membrane, leading to local positive curvature of each lipid monolayer and possible mechanical strain; Figure **(b)** shows the opposite case.

A.6 Dipolar Broadened ^{1}H- and ^{13}C- NMR in Membranes

The motionally averaged dipolar interaction between a pair of spins, A and B, is governed by a dipolar pseudo-order parameter $S_{AB} = \langle P_2(\mu_{AB})/r_{AB}^3 \rangle$ [55, 56], where the vector joining A and B has the instantaneous length R_{AB} and length R_{AB}^0 in the all-*trans* conformation, such that $r_{AB} = R_{AB}/R_{AB}^0$. μ_{AB} is given by $\mu_{AB} = \cos\theta_{AB}$ (in analogy with μ_k in section A.4) with θ_{AB} being the polar angle between the dipole-dipole vector and the surface normal $\hat{n}$.

Because dipolar interactions only fall off with distance as R^{-3}, many pairs of spins normally contribute to the spectrum. As a consequence, the NMR spectrum in fluid membranes is usually a broad featureless lump (see Figure A.1b and d) and the potential of ^{1}H- and ^{13}C- NMR for investigating basic physical properties of fluid membranes has not been explored to the same degree as ^{2}H-NMR. In view of the discussion in section A.5, however, one wonders whether measurements of dipolar second moments [52, 82] in membranes, which would provide quantitative measures of $\left\langle |S_{AB}|^2 \right\rangle$, might be useful in the same spirit as is the determination of S using ^{2}H-NMR.

In common with ^{2}H-NMR, the dipolar-broadened spectrum scales with orientation as $P_2(\mu)$ (with $\mu = \cos\theta$ and θ being the angle between the membrane surface normal $\hat{n}$ and the magnetic field). This scaling property has several profound consequences:

1. The spectrum $f_\theta(\omega)$ of a sample being oriented at an angle θ between its surface normal $\hat{n}$ and the external magnetic field, can easily be calculated from the spectrum $f_0(\omega)$ of a sample, oriented at 0^o:

$$f_\theta(\omega) = \frac{f_0(\omega/P_2(\mu))}{|P_2(\mu)|} \tag{A.4}$$

2. The powder spectrum $f_p(\omega)$ can be easily calculated from the oriented spectrum

$f_0(\omega)$ (see Figure A.1 for example spectra) as:

$$f_p(\omega) = \int_{-1}^{1} \frac{f_0(\omega/P_2(\mu))}{|P_2(\mu)|}\, d\mu \tag{A.5}$$

3. Regardless of the detailed shape of the oriented spectrum $f_0(\omega)$ (with the exception of spectra having sharp features, as for quadrupolar splittings in ^{2}H-NMR and anisotropic chemical shifts in ^{31}P-NMR and ^{13}C-NMR) the powder spectrum, $f_p(\omega)$ has a "super-Lorentzian" shape $f_p(\omega) = f_{sl}(\omega) \approx a + b\ln(\omega)$ [55, 100] (see Figure A.1d). The approximation $f_{sl}(\omega) \approx a + b\ln(\omega)$ is only valid for $\omega_{min} \ll \omega \ll \omega_{max}$, where $\omega_{min} = 1/T_2$ and $\omega_{max} \approx \sqrt{M_2}$. The powder spectrum has a rapid cut-off near $\omega \approx \omega_{max}$ and a finite peak amplitude at $\omega = 0$. The "superlorentzian" $f_{sl}(\omega)$ falls off more slowly in the wings than a Lorentzian, except for $\omega \geq \omega_{max}$, but has a finite second moment because of the cut-off.

4. The isotropic, motionally averaged spectrum in small vesicles [56] is an unusual superposition of Lorentzians weighted by $f_0(\omega)$, leading to subtleties in the interpretation of the line-width.

5. Magic angle spinning (MAS) is very effective in producing high resolution spectra for dipolar broadened spectra in membranes [101]. This has already given rise to interesting studies of peptide structure in membranes [102]. We anticipate that MAS studies will become increasingly important in the study of fluid membranes.

Appendix B

Preparatory NMR Experiments

B.1 ^{1}H-NMR – Buffer Contribution and Water Suppression

Unless otherwise noted, all samples were prepared in buffers made with deuterium-depleted H_2O. The ^{1}H-NMR signal thus contains a small contribution from the buffer molecules and an overwhelming contribution from the water, in addition to that of the lipid. To assess the effects of the buffer protons, free induction decays (FIDs) were measured for pure deuterium-depleted water and for buffer solution, as well as for POPC samples prepared (as above) in pure water and in buffer solution. The presence of buffer led to no observable differences in the FIDs (or the corresponding spectra); in particular, there was no fast-relaxing component (or broadened line) in the absence of lipid. This finding was verified by measuring the proton FID of a D_2O buffer solution, which showed only a low-amplitude, slow-relaxing component with T_2^* roughly that of water ($\sim 0.5\,\mathrm{s}$). The signal from the buffer protons is thus shown to be indistinguishable from that of the water for the purposes of our broadline experiments.

The more difficult problem in the ^{1}H-NMR experiments pertains to separating the relatively small lipid signal from the much larger signal due to the water and buffer. Since the dispersions were prepared in excess buffer solution, typically less than 20% of the protons in a sample were found on lipid molecules. Add to this that the T_2^* of lipid is tens of microseconds while that of water is often hundreds of milliseconds, and extracting quantitative information from the lipid proton signal becomes a significant

challenge. The unaltered FID resulting from a single 90^o pulse is shown in Figure B.1.

The first approach to this problem made use of the differing T_{1z}'s of the two proton pools ($T_{1z,H_2O} \approx 3\,\text{s}$; $T_{1z,lipid} \approx 400$ ms), by adding a "pre-inversion" (180^o) pulse before the excitation (90^o) pulse. The pulses are spaced such that the excitation pulse coincides with the zero-crossing of the water signal, *i.e.* after a time $\frac{T_{1z,H_2O}}{\sqrt{2}} \approx 2\,\text{s}$. As a result, only the lipid signal – which has almost fully relaxed by this time – is excited. This works very well for a single-scan experiment, cleanly eliminating the slow-relaxing component and isolating the solid-like lipid signal. However, if the water signal is not allowed to relax fully between scans, then the delay between the pre-inversion and excitation pulses must be reduced (in essence because the water signal has a "head start" towards its zero-crossing). Given the need to minimize the duration of the NMR protocols (due to concerns about sample integrity), the water could not be allowed to come to equilibrium (a $\sim 15\,\text{s}$ wait) before each scan. As a result, the pulse spacing required to fully eliminate the water signal was so short that much of the lipid signal would have been lost as well – clearly an unacceptable result.

An alternative solution employed the Carr-Purcell-Meiboom-Gill (CPMG) pulse sequence to refocus the slow-relaxing signal into a series of echoes following the FID. The echo maxima were fitted to a line (higher-order fits did not differ significantly for these data), which was extrapolated to $t = 0$ and subtracted from the FID. This technique isolates the lipid signal quickly and easily, but has two drawbacks. The first is that the FID is "scarred" by the CPMG pulses, and cannot be Fourier transformed to yield a meaningful spectrum; this is not a concern for our purposes, since as described in Section 2.1.2 the desired information can be derived from the proton FID. The second disadvantage is that since the full amplitude of the water signal is collected in this technique, only a small portion of the dynamic range of the receiver is devoted to the lipid signal. This could lead to inaccurate representation of the data and decreased signal-to-noise ratio,

due to coarser binning of the lipid signal by the analogue-to-digital converter.

Motivated by the dynamic range consideration, a combination of the two approaches was used in the final proton protocol, since even a partially effective pre-inversion pulse allowed greater dynamic range for the lipid signal. The effectiveness of water suppression by the pre-inversion technique increased with inter-scan repetition time, such that gains in dynamic range were offset by increased experiment duration. A compromise was selected in which the relative contribution of lipid to the FID was doubled, but so was the data-collection time. This gain in signal-to-noise significantly exceeds the usual factor of $\sqrt{t}$ derived from signal-averaging with random noise. A sample FID obtained in this way is shown in Figure B.1.

B.2 ^{2}H-NMR – Spectrometer Validation

The Bruker CXP spectrometer used for these experiments had not previously been used for ^{2}H-NMR measurements with this spectral width (we required $\sim 100\,\text{kHz}$), and some doubt existed regarding whether it would distort higher-frequency components of the spectra. To investigate this possibility, comparative measurements were performed on the CXP (at 30.7 MHz) and on a dedicated deuterium spectrometer (custom-built, operating at 46.7 MHz; details in [71]) with established capabilities. Quadrupolar echo data were collected (with identical parameters, except for Larmor frequency) for the same DPPC-d_{62} sample above and below the main transition temperature, and the lineshapes were compared. The normalized fluid phase spectra are shown in Figure B.2.

The reference spectrum was found to have greater intensity towards its outer edge than that of the CXP, which can be attributed to the higher field strength of that spectrometer. (The stronger field causes the vesicles to be more ellipsoidal in shape, aligning with their long axes parallel to the field. This results in a higher proportion of molecules

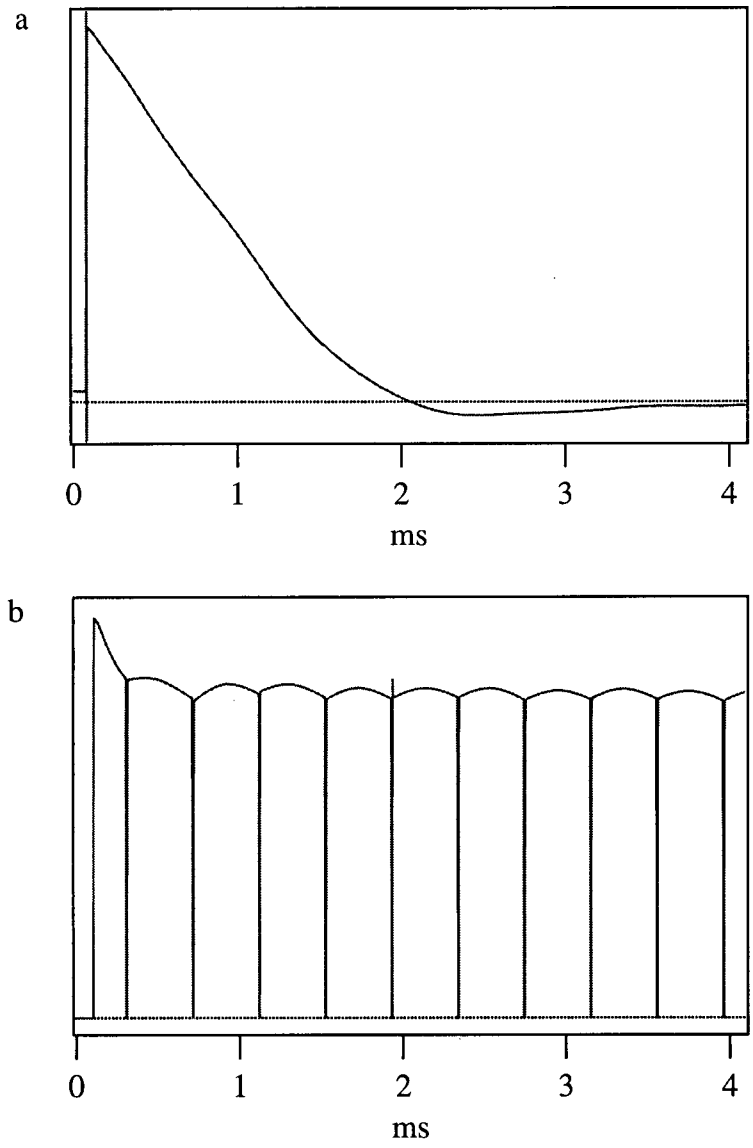

Figure B.1: Comparison of proton FIDs collected with and without water suppression techniques. Figure (a) shows the FID signal collected using a standard $(90°)_x$ pulse-and-collect sequence. The lipid contribution is lost in the large water signal. Figure (b) shows an FID collected using the pulse sequence shown in Section 3.2.2, using a pre-inversion 180^o pulse and CPMG train to suppress and quantify the water signal. The lipid contribution is the small, fast-decaying component at the far left of the CPMG echo-train.

with their membrane normal oriented near $\theta = 90^o$, so that the Pake doublet arising from each deuterated site is distorted to have greater amplitude near its peaks. When the distorted doublets for all sites on the perdeuterated chain are superposed, the plateau region dominates and leads to relatively higher amplitudes near the outer edge of a normalized spectrum.) This effect will lead to quantitative differences in spectral moments, order parameter profiles, and even relaxation times measured using the different instruments, but no particular field strength is inherently preferable. Rigorous comparisons can be made safely between measurements taken on a given spectrometer, as in this study.

Figure B.2 also shows a slight difference in the width of the powder patterns, equivalent to a constant scaling factor. This was found to be corrected by a small adjustment in temperature, and prompted a new temperature calibration for the deuterium probe of the CXP before the main series of experiments was begun.

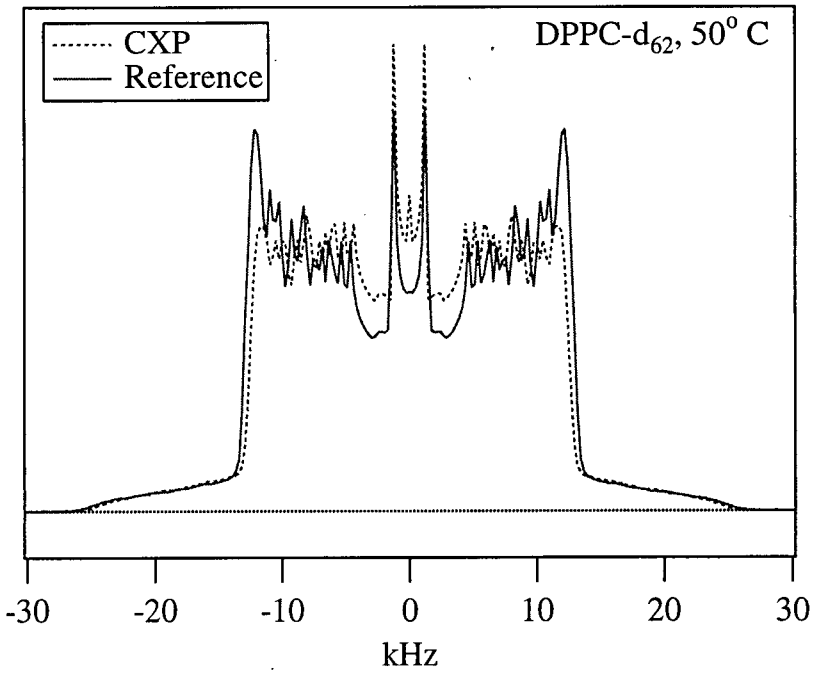

Figure B.2: Validation of the spectrometer for ^{2} NMR work. Powder pattern spectra are shown for DPPC-d_{62} in the fluid phase, as measured by the Bruker CXP spectrometer used for these studies and by a dedicated deuterium spectrometer (SFU) known to be reliable. The difference in peak amplitudes across the edges of the spectrum is explained in the text; the slight difference in width of the spectra was corrected by re-calibration of the CXP temperature control system.

Appendix C

Supplemental Results

Table C.1: Fit parameters for proton residual second moments, $M_{2r,H}$, as a function of PDPC content; results shown graphically in Figure 4.1. Units: s^{-2}/mol% PDPC.

Temperature	Slope ± Uncertainty
10^o C	$(+1.0 \pm 1.2) \times 10^5$
25^o C	$(+3.1 \pm 1.4) \times 10^5$
37^o C	$(+1.1 \pm 1.6) \times 10^5$

Table C.2: Fit parameters for deuterium residual second moments, $M_{2r,D}$, as a function of PDPC content; results shown graphically in Figure 4.2. Units: s^{-2}/mol% PDPC.

Temperature	Slope ± Uncertainty
10^o C	$(-2.7 \pm 3.0) \times 10^6$
25^o C	$(+0.5 \pm 3.7) \times 10^6$
37^o C	$(-0.1 \pm 5.2) \times 10^6$

Table C.3: Fit parameters for the average length of the perdeuterated chain,$\langle L \rangle$, as a function of PDPC content; results shown graphically in Figure 4.4. Units: Å/mol% PDPC.

Temperature	Slope ± Uncertainty
10^o C	$(-14.3 \pm 6.0) \times 10^{-4}$
25^o C	$(-7.6 \pm 5.8) \times 10^{-4}$
37^o C	$(-9.9 \pm 5.7) \times 10^{-4}$

Table C.4: Fit parameters for the average proton T_{1z}, as a function of PDPC content; results shown graphically in Figure 4.5. Units: ms/mol% PDPC.

Temperature	Slope ± Uncertainty
10^o C	$+0.62 \pm 0.12$
25^o C	$+0.95 \pm 0.16$
37^o C	$+0.75 \pm 0.19$

Table C.5: Fit parameters for the average deuterium T_{1z}, as a function of PDPC content; results shown graphically in Figure 4.6.

Temperature	Slope ± Uncertainty
10^o C	$(+3.9 \pm 1.0) \times 10^{-2}$
25^o C	$(+8.3 \pm 1.3) \times 10^{-2}$
37^o C	$(+9.2 \pm 1.7) \times 10^{-2}$

Table C.6: Fit parameters for the average deuterium T_2^{qe} rate, as a function of temperature; results shown graphically in Figure 4.10. Units: $s^{-1}\,K^{-1}$

PDPC content	Slope ± Uncertainty
0 mol%	$+19.5 \pm 0.2$
25 mol%	$+23.7 \pm 0.8$
50 mol%	$+24.6 \pm 0.2$
75 mol%	$+25.4 \pm 1.3$

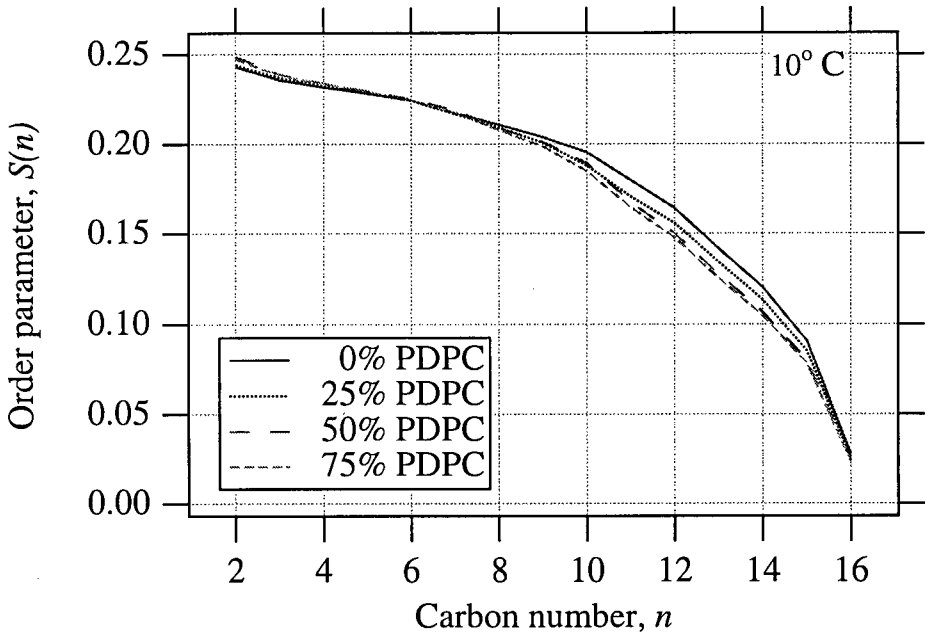

Figure C.1: Smoothed order parameter profiles, $S(n)$, for POPC-d_{31}/PDPC mixtures, measured at 10° C. Note the qualitative similarity to the results from 25° C, shown in Figure 4.3 and discussed in Section 4.2.3.

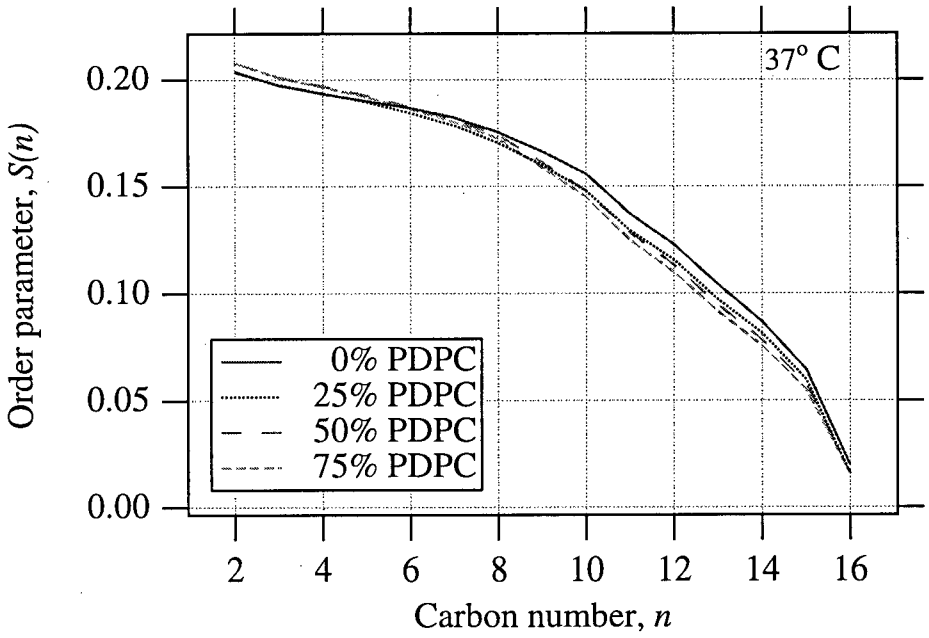

Figure C.2: Smoothed order parameter profiles, $S(n)$, for POPC-d_{31}/PDPC mixtures, measured at 37° C. Again, note the similarity to the results from 25° C, shown in Figure 4.3 and discussed in Section 4.2.3.